Dissertation

On

THERMAL MODELLING OF SOLAR STILL

Submitted in partial fulfillment of the requirement for

the award of degree of

MASTER OF ENGINEERING

IN

THERMAL

Submitted By

AMRIK SINGH

Roll No. 801083002

Under the Guidance of

Dr. MADHUP KUMAR MITTAL

Assistant Professor

Mechanical Engineering Department

ThaparUniversity, Patiala

DEPARTMENT OF MECHANICAL ENGINEERING

THAPAR UNIVERSITY

PATIALA-147004, INDIA

ACKNOWLEDGEMENT

Words are often less to revels one's deep regards. With an understanding that work like this can never be the outcome of a single person, I take this opportunity to express my profound sense of gratitude and respect to all those who directly or indirectly helped methrough the duration of this work.

I take the opportunity to express my heartfelt adulation and gratitude to my supervisors, ***Madhup Kumar Mittal****for his unreserved guidance, constructive suggestions, thought provoking discussions and unabashed inspiration in the nurturing work. It has been a benediction for me to spend many opportune moments under the guidance of the perfectionist at the acme of professionalism. The present work is testimony to their activity, inspiration and ardent personal interest, taken by them during the course of this work in its present form. I am grateful to* ***Dr. Ajay Batish****, Prof. & Head, MED for providing the facilities for the completion of the work.*

No words acknowledge the support I received from my friends for their valorous help and co-operation.

I take pride of myself being son of ideal parents for their everlasting desire, sacrifice, affectionate blessings, and help, without which it would not have been possible for me to complete my studies.

I would like to thank to all the members and employees of Mechanical Engineering Department, Thapar University Patiala for their everlasting support. Above all, I express my indebtedness to the "ALMIGHTY" for all His blessing and kindness.

Amrik Singh

Roll no: 801083002

DECLARATION

I hereby declare that the thesis entitled **Thermal Modelling of Solar Still** is an authentic record of my study carried out as requirement for the award of degree of **Master of Engineering in Mechanical (THERMAL) Engineering** at **Thapar University, Patiala,** under the guidance of **Dr. MADHUP KUMAR MITTAL**, Assistant Professor Department of Mechanical Engineering, Thapar University, Patiala during **July 2011 to June 2012.** The matter embodied in this report has not been submitted in part or full to any other university or institute for the award of any other degree.

Amrik Singh

(Amrik Singh)

Reg. No. 801083002

This is to certify that above declaration made by the student concerned is correct to the best of my knowledge & belief.

Madhup

Dr. MADHUP MITTAL

Assistant Professor

Mechanical Engineering Department

Thapar University, Patiala

Countersigned by:

Dr. AJAY BATISH

Professor and Head

Mechanical Engineering Department,

Thapar University,

Patiala-147004

Dr. S.K MOHAPATRA

Dean of Academic Affairs,

Thapar University,

Patiala-147004

ABSTRACT

Supply of drinking water is a major problem in under-developed and in some developing countries. The use of solar energy for desalination purpose was one of the first processes developed for producing fresh water from salt water. The process is based on the use of solar thermal energy to evaporate water thus separating pure water from brine water. The solar stills are used as a good method for obtaining the fresh water for even small scale demand because of economical and technical advantages as it uses the inexpensive technology including the material prices and manufacturing. Hence for increasing the performance of solar still it is necessary to model and investigate the effect of different parameters as condensing cover. Present work aimed at modeling of single slope solar still using ANSYS CFX 13.0 to investigate the effect of different slopes on the yield. Three dimensional two phase model is developed for evaporation and condensation process to simulate the temperature distribution of water and gas phase and also the amount of fresh water productivity. Two condensing covers at inclination 15^0 and 30^0 slope studied to analyse the effect on rate of evaporation. Simulation is carried out from 40-60^0C with 2^0C interval. For 15^0 and 30^0 inclination various contours have been plotted and studied for each simulation. Simulation results have been compared with the available experimental data it was observed that fresh water production rate and water temperature are in good agreement. Simulation results are also used to calculate the convective and evaporative heat transfer coefficient based on two models and there results are compared with experimental data they are in good agreement with certain error. It was concluded that condensing cover at inclination 30^0 obtain the higher yield and high convective and evaporative heat transfer coefficient as compared to 15^0 slope.The condensing cover at 30^0inclination gives about 29.4% higher yield than 15^0 inclination. Hence CFD is powerful tool in design of solar still and studying effective parameters on the performance.

LIST OF FIGURES

Figure No.	Title	Page No.
1.1	Working of Solar Still	2
1.2	A simple Solar Still design	7
1.3	Single-basin type solar still	8
1.4	Tilted-tray solar still	9
1.5	Multiple-effect diffusion solar still	10
2.1	One dimensional heat conduction across a slab at T1>T2	24
2.2	Formation of laminar and turbulent boundary layers when a fluid flows over a flat surface. The velocity of the fluid increases with the distance from the surface and the edge	26
2.3	Reflection of radiation on a) specular and b) diffuse surfaces	27
2.4	Heat transfer modes in a conventional solar still	30
3.1	A schematic diagram of experimental setup of solar still	36
3.2	3-D model of condensing cover for 15^0 inclination	37
3.3	3-D model of condensing cover for 30^0 inclination	37
3.4	3D Unstructured mesh for 15^0inclination	38
3.5	3D Unstructured mesh for 30^0inclination	38
3.6	Domain in CFX pre	40
3.7	Temperature variation of different components of solar still for 15^0 inclination	40
3.8	Temperature variation of different components of solar still for 30^0 inclination	41
3.9	Convergence graph of fluid flow simulation	43
3.10	Photograph of experimental setup of Kumar and Tiwari	44
4.1	a) Gas mixture temperature on a plane inside the solar still when bath temperature is 40^0 C for 15^0inclination. b) Temperature Plot.	46
4.2	a) Gas mixture temperature on a plane inside the solar still when bath temperature is 42^0 C for 15^0inclination. b) Temperature Plot.	47
4.3	a) Gas mixture temperature on a plane inside the solar still when bath temperature is 44^0 C for 15^0inclination. b) Temperature Plot.	48

4.4	a) Gas mixture temperature on a plane inside the solar still when bath temperature is 46^0 C for 15^0inclination. b) Temperature Plot.	49
4.5	a) Gas mixture temperature on a plane inside the solar still when bath temperature is 48^0 C for 15^0inclination. b) Temperature Plot.	50
4.6	a) Gas mixture temperature on a plane inside the solar still when bath temperature is 50^0 C for 15^0inclination. b) Temperature Plot.	51
4.7	a) Gas mixture temperature on a plane inside the solar still when bath temperature is 52^0 C for 15^0inclination. b) Temperature Plot.	52
4.8	a) Gas mixture temperature on a plane inside the solar still when bath temperature is 54^0 C for 15^0inclination. b) Temperature Plot.	52
4.9	a) Gas mixture temperature on a plane inside the solar still when bath temperature is 56^0 C for 15^0inclination. b) Temperature Plot.	52
4.10	a) Gas mixture temperature on a plane inside the solar still when bath temperature is 58^0 C for 15^0inclination. b) Temperature Plot.	53
4.11	a) Gas mixture temperature on a plane inside the solar still when bath temperature is 60^0 C for 15^0inclination. b) Temperature Plot.	53
4.12	a) Gas mixture temperature on a plane inside the solar still when bath temperature is 40^0 C for 30^0inclination. b) Temperature Plot.	54
4.13	a) Gas mixture temperature on a plane inside the solar still when bath temperature is 42^0 C for 30^0inclination. b) Temperature Plot.	55
4.14	Temperature Plot and Gas mixture temperature on a plane inside the solar still when bath temperature is (i) 44^0 (ii) 46^0 and (iii) 48^0C respectively for 30^0 inclination.	56
4.15	Temperature Plot and Gas mixture temperature on a plane inside the solar still when the bath temperature is (i) 50^0 (ii) 52^0 (iii) 54^0 C for 30^0 inclination.	57
4.16	Temperature Plot and Gas mixture temperature on a plane inside the solar still when bath temperature is (i) 56^0 (ii) 58^0 and (iii) 60^0 C for 30^0inclination.	58
4.17	Temperature Plot and Water temperature contours when bath temperature is (i) 40^0 and (ii) 50^0 C for 15^0inclination.	59
4.18	Temperature Plot and Water temperature contours when bath temperature is (i) 60^0 for 15^0inclination (ii) 40^0 C and (iii) 50^0 C	60

	for 30^0 inclination.	
4.19	Temperature Plot and Water temperature contour when bath temperature is 60^0 C for 30^0inclination.	61
4.20	Water temperature predicted by the CFD simulation and experimental data for i) 15^0 inclination ii) 30^0 inclination	61
4.21	Water mass flow predicted by CFD simulation.	62
4.22	The rate of fresh water production from experimental data and simulation result for 15^0inclination.	63
4.23	The rate of fresh water production from experimental data and simulation result for 30^0inclination.	63
4.24	Water volume fraction on the glass for (i) 15^0 inclination and (ii) 30^0 inclination.	64
4.25	Water volume fraction contour from the side view for (i) 15^0 inclination and (ii) 30^0 inclination.	64
4.26	Water volume fraction contour on distillate collector for (i) 15^0 inclination and (ii) 30^0 inclination.	65
4.27	Gas mixture velocity on a plane inside the solar still for 15^0 inclination	66
4.28	Gas mixture velocity on a plane inside the solar still for 30^0inclination.	66
4.29	Variation of convective heat transfer coefficient (h_{cw}) within temperature range of 40-60^0C for 15^0slope of the condensing cover by using CFD data.	67
4.30	Variation of evaporative heat transfer coefficient (h_{ew}) within temperature range of 40-60^0C for 15^0slope of the condensing cover by using CFD data.	68
4.31	Variation of convective heat transfer coefficient (h_{cw}) within temperature range of 50-60^0C for 15^0 slope of the condensing cover by using CFD data.	69
4.32	Variation of evaporative heat transfer coefficient (h_{ew}) within temperature range of 50-60^0C for 15^0slope of the condensing cover.	69
4.33	Variation of convective heat transfer coefficient (h_{cw}) within	70

	temperature range of 40^0- 60^0C for 30^0slope of the condensing cover.	
4.34	Variation of evaporative heat transfer coefficient (h_{ew}) within temperature range of 40^0-60^0C for 30^0slope of the condensing cover.	71
4.35	Variation of convective heat transfer coefficient (h_{cw}) within temperature range of 50^0- 60^0C for 30^0slope of the condensing cover.	71
4.36	Variation of evaporative heat transfer coefficient (h_{ew}) within temperature range of 50^0- 60^0C for 30^0slope of the condensing cover.	72
4.37	Variation of convective heat transfer coefficient (h_{cw}) within temperature range of 40^0- 60^0C for 15^0slope of the condensing cover.	73
4.38	Variation of evaporative heat transfer coefficient (h_{ew}) within temperature range of 40^0- 60^0C for 15^0 slope of the condensing cover.	73
4.39	Variation of evaporative heat transfer coefficient (h_{cw}) within temperature range of 40^0- 60^0C for 30^0 slope of the condensing cover.	74
4.40	Variation of evaporative heat transfer coefficient (h_{ew}) within temperature range of 40^0- 60^0C for 30^0 slope of the condensing cover.	75
4.41	Variation of convective heat transfer coefficient (h_{cw}) within temperature range of 40-60^0C for $15^0$and 30^0 slope of the condensing cover by CFD data.	76
4.42	Variation of evaporative heat transfer coefficient (h_{ew}) within temperature range of 40-60^0C for 15^0 and 30^0 slope of the condensing cover by CFD data.	76
4.43	Variation of convective heat transfer coefficient (h_{cw}) within temperature range of 40-60^0C for 15^0 and 30^0 slope of the condensing cover by CFD data.	77
4.44	Variation of evaporative heat transfer coefficient (h_{ew}) within	77

temperature range of 40-60^{0}C for 15^0 and 30^0 slope of the condensing cover by CFD data.

4.45 Fresh water production rate for different inclination for bath temperature from 40-60^{0}C by CFD data. 78

LIST OF TABLES

Sr. No.	Title	Page No.
3.1	Temperature dependent physical properties of vapour	34
3.2	Specification of two condensing covers	36
3.3	Mesh statistics	39
3.4	The boundary conditions	41
3.5	Thermal properties of water	42
3.6	Thermal properties of air	42
3.7	Thermal properties of water vapour	42

C	Unknown constant in the nusselt number expression
Gr	Grashof number
h_{cw}	Convective heat Transfer coefficient from water to condensing cover (W/m^2 K)
h_{ew}	Evaporative heat Transfer coefficient(W/m^2 K)
K_v	Thermal conductivity of humid air (W/m K)
L	Latent heat of vaporization of water, J/Kg
L_v	Characteristic dimension of condensing cover, m or it is the average spacing between water surface and glass cover, m
n	Unknown constant in the nusselt number expression
$\dot{m}_{ew}$	Distillate output kg/m^2 sec
Nu	Nusselt number
P_g	Partial saturated vapour pressure at condensing cover temperature N/m^2
Pr	Prandtl number
P_w	Partial saturated vapour pressure at water temperature, N/m^2
$\dot{q}_{ew}$	Rate of evaporative heat transfer W/m^2
T_g	Inner temperature of condensing cover, ^0C
T_w	Water temperature, ^0C
t	Time interval in sec
A_w	Evaporative surface area
V	Velocity vector, m/s
F_{LG}	Rate of interphase mass transfer, kg/m^3s
K	Thermal conductivity
r	Volume fraction, dimensionless
CFD	Computational fluid dynamics
TDS	total dissolved solids
RO	Reverse osmosis

Subscripts

L	Liquid
G	Gas

v	Vapour
w	Water

Greek symbols

α'	thermal diffusivity ($m^2\ s^{-1}$)
β	coefficient of thermal expansivity (K^{-1})
Δ	Change in
∇^2	Laplacian (a scalar differential operator)
μ	dynamic viscosity (kg $m^{-1}\ s^{-1}$)
λ	wavelength (m)

INDEX

TITLE	PAGE NO.
ACKNOWLEDGEMENT	**i**
DECLARATION	**ii**
ABSTRACT	**iii**
LIST OF FIGURES	**iv**
LIST OF TABLES	**ix**
ABBREVIATIONS AND SYMBOLS	**x**
CHAPTER 1 INTRODUCTION	**1-12**
1.1 Introduction	1
1.2 Distillation by Solar Still	2
1.3 Desalination Techniques	2
1.3.1 Reverse Osmosis method	3
1.3.2 Evaporative Process	3
1.4 Evaporation Behaviour	4
1.4.1 Evaporation Theory	4
1.5 Condensation Behaviour	5
1.5.1 Condensation	5
1.6 Historical Background	5
1.7 Principle of a Solar Still	6
1.8 Types of Solar Still	7
1.8.1 Active & Passive Solar Still	7

1.8.2 Solar still design 8

1.8.2.1 Single basin type solar still 8

1.8.2.2 Tilted tray solar still 8

1.8.2.3 Tilted wick solar still 9

1.8.2.4 Multiple effect diffusion solar still 9

1.9 Modeling of Solar Still 10

1.10 Solar Collectors 10

1.10.1 Types of Solar Energy Collectors 11

1.11 Modeling procedure in CFD 11

1.12 Objective of present work 12

1.13 Organization of thesis 12

CHAPTER 2 LITERATURE REVIEW 13-30

2.1 Introduction 13

2.2 Categorization of literature 13

2.2.1 Conventional or Passive solar still 13

2.2.2 Advanced or Active solar still 18

2.2.3 Heat and mass transfer 22

2.2.3.1 Conduction 22

2.2.3.2 Convection 24

2.2.3.3 Radiative heat transfer 26

2.2.3.4 Thermal resistance 28

2.2.3.5 Heat & mass transfer as applied to solar distillation 29

2.3 Gap in literature 30

CHAPTER 3 METHODOLOGY **31- 44**

3.1 Simulation methodology 31

3.1.1 Assumptions 31

3.1.2 Mathematical model 31

3.1.2.1 Governing equations 31

3.1.3 Heat transfer coefficient analysis 32

3.2 Simulation 35

3.2.1 Simulation of evaporation and condensation

inside distillation unit 35

3.2.2 Geometric modeling 36

3.2.2.1 Methodology 37

3.2.2.2 Meshing details 38

3.2.2.3 Boundary conditions 39

3.2.2.4 Material Defination 41

3.2.2.5 CFX Solver 42

3.2.2.6 CFX Post 43

3.3 Experimental methodology 44

CHAPTER 4RESULTS AND DISCUSSIONS **45-78**

4.1 Computational fluid dynamic simulation 45

4.1.1 Evaporation simulation through condensing covers 45

at different inclinations

4.1.2 Temperature distribution 45

4.1.2.1 Simulation for 15^0 inclination 45

4.1.2.2 Simulation for 30^0 inclination 53

4.1.2.3 Simulation result for 15^0 and 30^0 inclination for water temperature 59

4.2 Experimental validation 61

4.2.1 Water temperature 61

4.2.2 Production rate of water 62

4.2.3 Heat transfer coefficient analysis 66

4.2.3.1 Heat transfer coefficient for 15^0 inclination 67

4.2.3.2 Heat transfer coefficient for 30^0 inclination 70

4.2.4 Comparison of experimental and simulation results for heat transfer coefficient 72

4.3 Optimization 75

CHAPTER 5CONCLUSION AND FUTURE SCOPE **79-80**

5.1 Flow of work done 79

5.2 Future scope 80

REFERENCES **81-82**

CHAPTER 1

INTRODUCTION

1.1 INTRODUCTION

Distillation is a process which is used to obtain fresh water from salty, brackish or contaminated water. Without fresh water human life is not possible even industries and agriculture also need fresh water. Earlier fresh water is easily available from rivers, lakes and ponds in plenty. Now it's becoming scarce because of industrialization. Sunlight is one of several forms of heat energy that can be used to power the process of water purification. Sunlight has the advantage of zero fuel cost but it requires more space (for its collection) and generally more costly equipment to get high temperature. It is not necessary to boil water to distill it. Simply elevating its temperature, at values lower than its boiling point, will adequately increase the evaporation rate. Although vigorous boiling accelerates the distillation process it can also force unwanted residue into the distillate, leading impurification. Many levels of purification can be achieved with solar distillation process, depending upon the application. The cost of solar-distilled drinking water is more than that of water provided by most municipal utilities, but its cost is very less energy wise. On the other hand, solar-distilled water is much less expensive than bottled water. Solar distillation of potable water from saline water has been practiced for many years in tropical and sub-tropical regions where fresh water is not sufficient.

Solar still is a distillation system which can be small or large. It is designed either to serve the needs of a single family, producing from ½ to 3 gallons of drinking water a day on the average, or to produce much greater amounts for an entire neighborhood or village. In some parts of the world the scarcity of fresh water is partially overcome by covering shallow salt water basins with glass in greenhouse-like structures. These solar energy distilling plants are relatively inexpensive, low technology systems, especially useful where the need for small plants exists. Arid lands generally have great solar energy potential. This potential may be developed by solar desalination concepts and methods specifically suited to supply dry regions with freshwater. Direct solar desalination systems have low operating and maintenance costs but require large installation areas and high initial investment. However, solar distillation is an appropriate solution for remote areas and small communities in arid and semi-arid regions lacking water. Most studies in the last decade have considered small

scale solar desalination systems for application in remote areas. Some of them have proposed medium and large scale systems which already are, or could be, effective in the near future.

1.2 DISTILLATION BY SOLAR STILL

Desalination in this method brackish or saline water is evaporated using thermal energy and resulting steam is collected and condensed as final product. It is a simple device to get fresh distilled water from impure water, using solar energy as fuel, for its various applications in domestic and industrial sectors shown in Fig 1.1. The basic concept of using solar energy to obtain drinkable fresh water from salty, brackish or contaminated water is really quite simple. Water left in an open container in an open area will evaporate into the air. The purpose of a solar still is to capture this evaporated water by condensing it onto a cool surface.

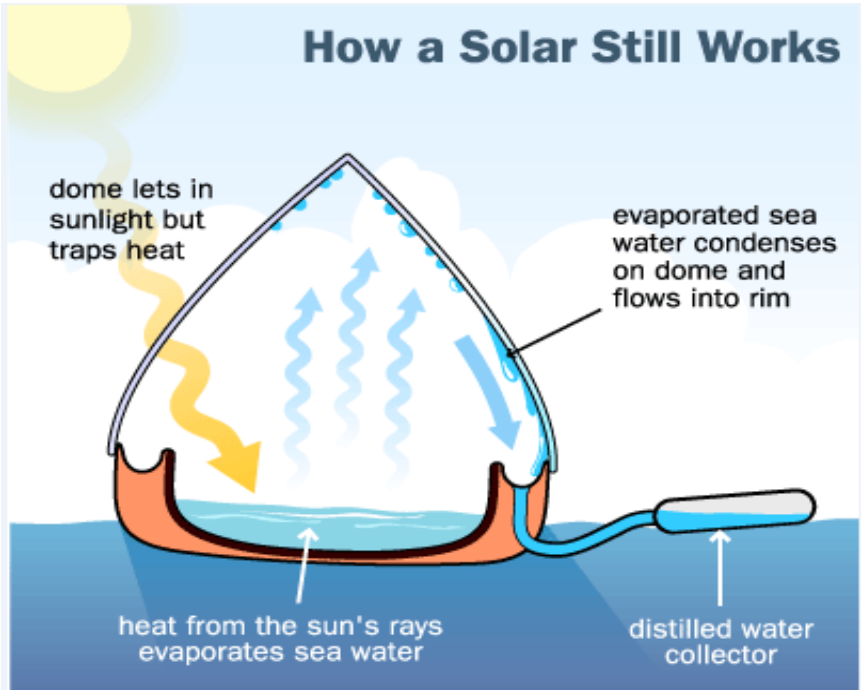

Fig1.1: Working of Solar Still

1.3 DESALINATION TECHNIQUES

Desalination is a process by which dissolved minerals can be removed from seawater or brackish water, to produce potable water. The potable water can be used for agricultural uses or it can also be further treated to yield pure water which can be used for human consumption. The dissolved minerals can be removed through different ways such as by

evaporating water, or by reverse osmosis process in which dissolved minerals are extracted by passing water through membranes. The two most commonly used methods worldwide for commercial water desalination are:

i. The Reverse Osmosis method
ii. The Evaporative method

1.3.1 Reverse Osmosis Method

Reverse osmosis is a distillation process used to desalinate water with the help of membrane. In normal osmosis, the solvent moves from the lower solute concentration to a region of higher solute concentration through a semi-permeable membrane to reach equilibrium. In case of the reverse osmosis process, high pressure which is above the osmotic pressure, is applied to the higher solute concentration region, forcing the solvent to move opposite the normal direction of osmotic flow. Therefore, high pressure is applied to the saline water to desaline it. So potable water with lower saline concentration passes through the semi-permeable membrane to obtain fresh water. As the osmotic pressure is proportional with the solute concentration, higher pressure is needed to generate fresh water from seawater as opposed to brackish water, and hence higher electrical energy is needed to desalinate seawater by reverse osmosis.

1.3.2 Evaporative Processes

Evaporative processes is a technique by which fresh water vapour are separated from the dissolved minerals in a manner similar to the earth's natural water cycle. When the salinated water is evaporated, water gets converted into water vapour which is condensed to obtain potable water in liquid state. The evaporative process can be enhanced by using multistage flash distillation or multiple-effect distillation for commercial purpose. In a multistage flash distillation, the feedwater is heated up and pressurised to the plant's maximum allowable temperature, and is then discharged to a chamber which is maintained at a pressure slightly below the saturation vapour pressure of water. This will then cause some of the water to 'flash' into steam and condensed to obtain fresh water. The average energy requirement for a multistage flash distillation is significantly higher than the reverse osmosis process. Moreover, multiple-effect distillation is another energy-efficient method for water desalination as it uses the heat energy from the water vapour when it condenses to preheat the subsequent water. The high latent heat of water which is transferred to preheat the next

stage of water does significantly reduce the overall system's energy requirement for water evaporation. Currently, the average energy requirements for a multistage flash distillation are about 47.5-52kWh/kL [1]. This is significantly higher compared to the reverse osmosis process.

The advantages of using an evaporative process are

- Large water desalination capacities
- Low mineral content water obtained with high quality

1.4 EVAPORATION BEHAVIOUR

To successfully model and optimize the evaporation process for water desalination, research was undertaken to determine the causes of evaporation, the factors affecting evaporation rates and also previous mathematical models which will be used determine evaporation rates.

1.4.1 Evaporation Theory

In the evaporation process water gets converted into water vapour, when the molecules on the surface of the liquid gains sufficient kinetic energy to overcome the liquid phase intermolecular forces. The rate of evaporation increases with high overall kinetic energy of the molecule. Evaporation can also be determined through observing the equilibrium vapour pressure. Evaporation occurs when the equilibrium vapour pressure, which is proportional to temperature, is equivalent or higher than the atmospheric pressure. Evaporation highly depends upon the kinetic energy of the molecules.

The factors influencing the evaporation are as below:

(a) Surface area

The evaporation increases with the increase in surface area as there will be more amounts of surface water molecules available that could overcome the intermolecular forces.

(b) Liquid temperature

With increase in temperature of liquid, the liquid particle gains the kinetic energy that overcome the intermolecular forces.

(c) Velocity of air

The higher air velocity decreases the humidity of the air surrounding the liquid. With less water vapour in the surrounding air, water is more likely to evaporate.

(d) Pressure

A lower atmospheric pressure will cause the liquid to evaporate easier because it will be easier for the vapour pressure to equalize the atmospheric pressure.

1.5 CONDENSATION BEHAVIOUR

As the solar desalination system was intended to reduce electrical energy requirements, passive cooling methods for condensation were researched into. The suggested condensation method was hot vapour condensing on a cool surface to collect liquid water. This phenomenon was modeled as film condensation. A film condensation analysis is applicable to saturated vapour condensing on a cool surface in which the liquid formed is drained off the surface by the action of gravity [2].

1.5.1 Condensation

In the condensation process the latent energy is removed to cause a phase change from the gas phase to the liquid phase. It is the reverse of the evaporation process. In this project the film condensation is modeled. When the vapour is cooled down below the saturation temperature of the vapour the film condensation take place on the condensing cover whose temperature is below the saturation temperature of vapour. A film of liquid will be produced at the wall due to condensation of the vapour. The heat transfer coefficient of a laminar film condensation is mainly dependant on the difference between the wall temperature and the saturated vapour temperature. Dew point temperature is temperature corresponding to partial pressure of vapour where first drop forms. So to improve the condensation process we determine the parameter which affect the dew point temperature and it was found that that the increase in humidity or a reduction in condenser wall temperature could make the dew point temperature closer to the vapour temperature and hence further facilitate the condensation process.

1.6 HISTORICAL BACKGROUND

The first conventional solar still plant was built in 1872 by the Swedish engineer Charles Wilson in the mining community of Las Salinas in Northern Chile. This still was a large basin-type still used to supply fresh water from brackish feed water to a nitrate mining community. The plant had wooden basins with bottoms blackened using logwood dye and alum. The total capacity of the distillation plant was about 23 m^3/ day. This first stills was in

operation for 40 years until the mines were exhausted. During World War II, efforts were increased to produce a solar still that could be utilized on life rafts, for ships and aircraft. Telkes [3] invented a small inflatable plastic unit for this purpose and hundreds of thousands of these units were produced. Most stills built and studied since then have been based on the same concept, though with many variations in geometry, materials, methods of construction and operation.

From 1958 to 1965 the Office of Saline Water (OSW) at the Research Station in Florida tested a number of different types of solar stills and concluded that high fixed charges associated with still construction would not be offset by the savings resulting from free solar energy. Past research work has been focused on the construction cost obstacle of the solar still. For example, to this aim, various plastic films have been used instead of the more durable but also more expensive glass coverings. The next stage was to improve the operating efficiency of the various types of solar distillation devices. Several researchers have attempted to enhance the vapour condensation rate by forcing air circulation in stills, and to increase the output of the stills by using latent heat of condensation/vaporization in either multi-effect systems or for preheating the brine.

1.7 PRINCIPLE OF A SOLAR STILL

A wide, shallow pan painted black is used as an ideal vessel for the water distillation. It is made wide and shallow to increase the surface area so that it can trap maximum solar energy. The painted surface is baked in the sun to free volatile toxicants which might otherwise evaporate and condense along with the drinking water. The pan is painted black or with some other dark color, to maximize the amount of solar energy absorbed and to increase water temperature so that rate of evaporation can be accelerated. To capture and condense the evaporated water, we need some kind of surface close to the heated salt water, which are several degrees cooler than the water. The evaporating pan is usually covered by a sheet of clear glass or translucent plastic (to allow sunlight to reach the water) which is tilted to a slight angle to let the fresh water that condenses on its underside trickle down to a collecting trough [4]. The glass creates a cavity and also holds the heat inside. Figure 1.2 combines all these components in a simple solar still design.

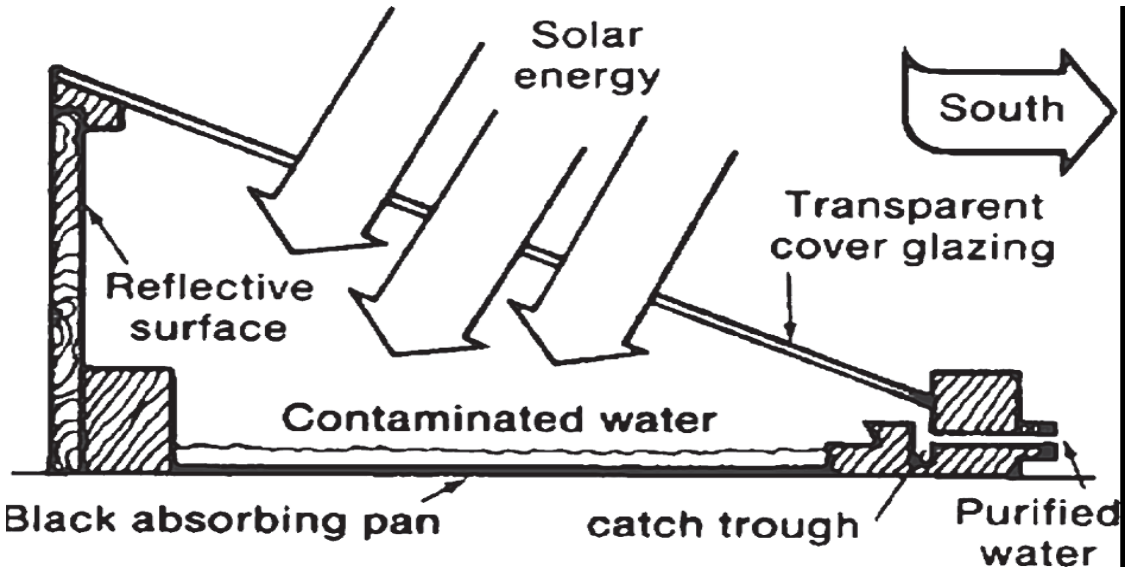

Fig 1.2: A simple Solar Still design [4]

1.8 TYPES OF SOLAR STILL:

Solar distillation systems are classified as follows:

1. In terms of energy supply
    I. Active solar still
    II. Passive solar still
2. In terms of structure of the conventional solar still
    I. Single basin solar still
    II. Single-slope double-basin solar still
    III. Single-slope triple-basin solar still
    IV. Pyramid- shaped solar still
    V. Conventional solar still with sponge cubes in basin
    VI. Double-slope single-basin solar still.

1.8.1 Active and passive solar still

The active solar stills are modern solar stills in which extra thermal energy is given to the passive solar still for faster evaporation. This extra thermal energy may be obtained from a solar collector, or any available waste thermal energy from any industrial plant, such as a power plant. But the passive solar still systems are conventional solar still systems which use solar energy as the only source of thermal energy.

1.8.2 Solar still design

Solar still designs are range from the simple to high-tech design. The simplest and most practical design for a solar still is the single-basin type.

1.8.2.1 Single basin type solar still

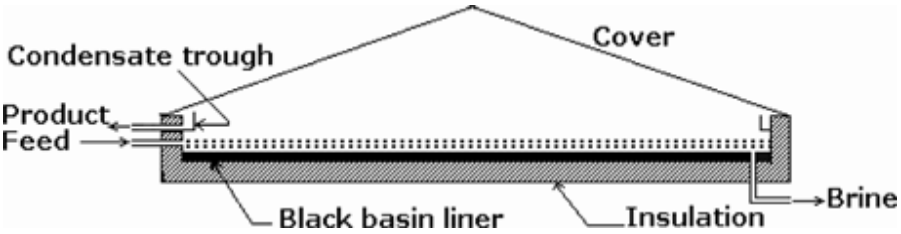

Fig 1.3: Single-basin type solar still [6, 7]

The still consists of an air tight basin, usually made of galvanized iron sheet which contains the salt water. It has a top cover made of a transparent material, e.g. glass, and the interior surface of its base is blackened to enable absorption of solar energy to the maximum possible extent. The glass cover allows solar radiation to pass into the still. Here the radiation is mostly absorbed by the blackened base. The water begins to heat up and the moisture content of the air, trapped between the water surface and the glass cover, increases. The base also radiates energy in the infra-red region, which is reflected back into the still by the glass cover, so trapping the solar energy inside the still. Heated water vapour evaporates from the basin and condenses on the inside of the glass cover. Condensed water trickles down the inclined glass cover to an interior collection trough, placed at the lower edges of the cover to collect the distillate.

1.8.2.2 Tilted-tray solar still

It operates in a cascade formation and the rate of the continuous feed just compensates the rate of evaporation. This type of construction results in higher efficiency than the simple basin type. However, the additional costs of construction are not compensated for by increased performance.

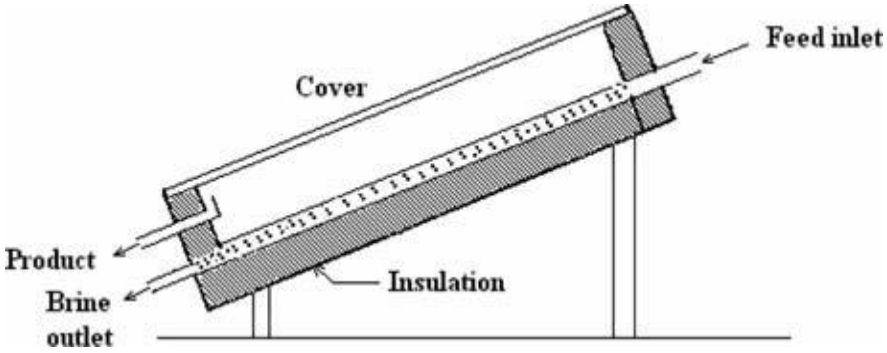

Fig 1.4: Tilted-tray solar still [5]

1.8.2.3 Tilted-wick still

Another type of solar still that is designed to operate with a very low heat capacity is the tilted-wick still. It consists of a tilted solar still in which the water basin is replaced by a porous wick through which water flows down by gravity. Wick type solar still confirmed an increase in productivity of 20–50% over the basin type, and however, the difficulties in keeping the wick wet and clean, and the cost of the construction, prevent its use on a large scale [5]. A multiple-wick solar still in which blackened jute cloth pieces, of different lengths, are layered one upon the other and separated by polythene sheets.

1.8.2.4 Multiple-effect diffusion solar still

The process consists of a number of parallel plates in contact with saline soaked wicks, with narrow air gaps between the plates. The evaporation and condensation processes occur in all gaps between the plates. The hot water is applied to the first plate, in order to heat it up and to cause evaporation from the plate. The latent heat of condensation is recovered to induce evaporation from the parallel plate. The process is repeated for all plates to increase the production of distillate (Fig. 1.5). The average daily productivity of this proposed solar still was found to be 14.8– 18.7 l/day distillate per unit effective area of glass, under an incident solar radiation range of 20.9–22.4MJ/m^2/day [6]. The process yields are doubled when coupling the unit with a flat plate collector to preheat feed water and with wheels attached to the still bottom for manual azimuth tracking. This equipment, required in addition to the vertical still, contributes to increase solar absorption at the proper angle on the first partition of the unit.

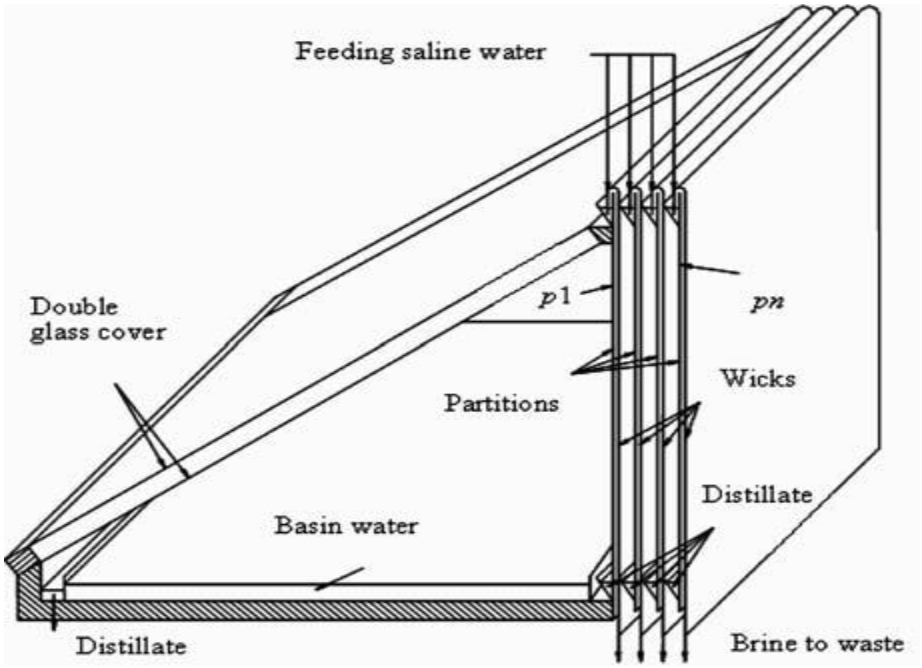

Fig 1.5: Multiple-effect diffusion solar still [8,9]

1.9 MODELING OF SOLAR STILL

Any type of solar still system can be modeled using energy balance and mass balance equations for the system. Since the main energy source is solar intensity which depends on the time of day, the basic energy and mass balance equations must be time dependent. In the modeling of the solar still, the most important parameters are convection heat transfer coefficients to estimate heat transfer from the glass, heat losses from the bottom and sides of the cavity, evaporation rate (or evaporation coefficient), and condensation rate (or condensation coefficient).

1.10 SOLAR COLLECTORS

Solar energy collectors are special kind of heat exchangers that transform solar radiation energy to internal energy of the transport medium. The major component of any solar system is the solar collector. This is a device which absorbs the incoming solar radiation, converts it into heat, and transfers this heat to a fluid (usually air, water, or oil) flowing through the collector. The solar energy thus collected is carried from the circulating fluid either directly to the hot water or space conditioning equipment or to a thermal energy storage tank from which can be drawn for use at night and/or cloudy days.

1.10.1 Types of Solar Energy Collectors

1) Non-concentrating or flat plate type solar collector.
2) Concentrating (focusing) type solar collector.

A non-concentrating collector has the same area for intercepting and for absorbing solar radiation, whereas a sun-tracking concentrating solar collector usually has concave reflecting surfaces to intercept and focus the sun's beam radiation to a smaller receiving area, thereby increasing the radiation flux. A large number of solar collectors are available in the market. In this section a review of the various types of collectors currently available will be presented. This includes FPC, ETC, and concentrating collectors.

1.11 MODELING PROCEDURE IN CFD

Computational fluid dynamics (CFD) is one of the branch of Engineering, Finding numerical solutions of governing equations, using high-speed digital computers. The concept of Computational fluid dynamics model is based upon dividing the solution domain into very large number of sub-zones. For each node boundary condition is given at the domain and for each node mass, momentum, and energy conservation equations are solved, The fluid temperature and velocity at each node are determined. Small change in the properties of the fluid at a node is used as input to next node point. The above procedure is repeated for all grid points, to know all the properties, like temperature, velocities etc at all the points in the domain. This procedure is best done using the computation power of modern digital computers because it involves solution of very large number of equations iteratively. The quick calculations of large number of equations can be performed using computer giving detailed results in a relatively short time. The temperature, pressure and velocity at each point in the domain can be easily estimated using computational fluid dynamic software. The results are obtained in the visual form. Earlier CFD modeling was used for industrial application. Today it is used in research work, product development, and in almost all sphere of activity which involve heat transfer and fluid flow. A number of software based on CFD codes have been developed, some of them are: Fluent, Flovent, Phoenics, and CFX. Each software is usually supported by supplementary software for different applications, such as domain model preparation, mesh generation etc. Presently CFD techniques are increasingly used to model flow through solar collectors and solar distillation units.

1.12 OBJECTIVE OF PRESENT WORK

The proposed study has been carried out to theoretically investigate the performance of single basin type solar still with the following objective:

Simulation work

1) To determine temperature distribution of the water and gas mixture in the single slope solar still at different inclination (15^o, 30^o) by using CFD.
2) To predict convective heat transfer coefficient and evaporative heat transfer coefficient.
3) To predict the distillate water production rate.

Experimental Validation

To validate simulation results with available experimental data of Kumar and Tiwari [7].

1.13 ORGANIZATION OF THESIS

Chapter1 covers brief introduction about solar distillation unit and distillation techniques, principle of solar still, Heat transfer in solar still and solar collector.

Chapter 2 presents the extensive literature review of research work which has been done by different researchers in the past .This literature is divided into two categories: Active and passive solar still and their experimental validation

Chapter 3 covers problem formulation for the thesis work. It presents the simulation methodology and experimental methodology to be adopted.

CHAPTER 2
LITERATURE REVIEW

2.1 INTRODUCTION

Substantial amount of work has been done on different types of active and passive solar still. Various correlations are proposed to calculate heat and mass transfer inside the solar still. This chapter covers the literature on thermal analysis and methods to increase the efficiency, heat and mass transfer of solar still. To increase heat and mass transfer in solar still different models are given. Using concentrator on simple solar still efficiency can be increased. One more method used to increase performance by using phase change material and various thermal analysis are done to calculate various loses to improve efficiency of simple solar still.

2.2 CATEGORIZATION OF LITERATURE

Literature is divided into following two main categories in terms of energy supplied**.**

1. Conventional or passive solar still.
2. Advanced solar still or Active solar still.
3. Heat and mass transfer inside solar still.

2.2.1 Conventional or passive solar still

AK Tiwari and GN Tiwari [7] conducted an experiment using three condensing surfaces inclined at 15^0, 30^0 and 45^0 to determine the relation for calculating convective and evaporative heat transfer coefficient under indoor conditions. The experiment was maintained at steady state by using a constant temperature bath and the operating temperature range is from 40^0 C to 80^0 C. The temperature and mass of the distillate is collected in a time interval of 10 minutes which is used to determine the value of constant C & n and convective & heat transfer coefficient. It was concluded that the distillation still with 30^0 inclination of condensing cover obtained highest convective and evaporative heat transfer coefficient and yield. The values of convective and evaporative heat transfer coefficient obtained at higher temperature by Dunkle's model do not agree with Kumar and Tiwari's model due to various assumptions and limitations of the Dunkle's model at higher temperature.

J Madhav [8] studied the effect of using two different basin materials in solar still and to increase the productivity of water. Single-basin solar stills can be used for water

desalination. They are considered the best solution for water production in remote, arid to semi-arid, small communities, where fresh water is unavailable. The amount of distilled water produced per unit area is somewhat low which makes the single basin solar still unacceptable. The experimental results showed that the productivity of the distilled water was enhanced for black granite basin solar still as compared to iron steel basin solar still. The productivity of the granite basin solar still through the period is averaging 3.784 L/m2.day, whereas iron steel basin still is 2.358 L/m2.day which is nearly 38 % higher than the iron steel basin still. Basin water temperature in the granite basin still increased up to 87^{o} C compared with iron steel basin still water temperature of about 79^{o} C .the productivity of granite basin still is always greater than the productivity of iron steel basin still throughout the day. The granite basin solar still is capable of enhancing the productivity. There are many designs for solar stills. 95 percent of functioning solar stills are of the basin type solar still. The performance of basin still depends on the basin, transparent glazing cover, evaporation surface, insulation material and climatic condition. The granite solar still has given more yield than iron steel solar still, this may because of higher water temperature of granite solar still than iron steel solar still. An overall result shows that, the productivity of modified still is 15% higher than the conventional still. The increase in either ambient temperature or the solar intensity can lead to the increase of productivity.

S Kumar and GN Tiwari [9] developed thermal model to determine the convective mass transferfor different Grashof number range in solar distillation process. The values of C and n have been calculated by using linear regression analysis. Dunkle formulated a semi empirical relation for internal heat and mass transfer. He proposed the values of C = 0.075 and n = 0.333 for Grashof number Gr > $3.2 * 10^{5}$. Due to some limitations the Dunkle's relation is not valid for high temperature ranges. So Kumar and Tiwari developed model for high temperature ranges. The values of C and n are calculated from experimental data. These values of C and n obtained from experimental data used to find out the theoretical output of heat and mass transfer coefficient. They concluded that it is very necessary to modify the values of C and n to predict the exact performance of solar still for different ranges of Grashof number.

AK Tiwari and GN Tiwari [10] conducted an experiment for different five water depths from 0.04m to 0.18m for five days. They observed the effect of water depth on evaporative mass transfer coefficient. The hourly average values of h_{cw} , h_{ew} , $h_{cw\ dunk}$, $h_{ew\ dunk}$ calculated by using experimental data. Fluctuation in water temperature were higher at low water

depth, with increase in water depth the fluctuation in water temperature decreased due to storage effect. Higher the water depth, the more time water will take to exceed the glass temperature and ultimately the glass temperature will be more due to solar radiation. Therefore negative value of ΔT . For higher depth of water once ΔT became positive it remained positive till next sunrise. For lower water depth ΔT became positive very soon at 12 noon. Whereas for higher water depth ΔT became positive at 3 pm, 3 hours later. Higher the water depth, the more energy stored within the water in the form of sensible heat and lesser rise in temperature of water surface. They finally concluded that heat transfer coefficient depends significantly on water depth.

MS Tarawneh [11] constructed and operated a small scale solar powered desalination system to improve the solar still performance and to increase its productivity. Two symmetrical greenhouse solar stills were constructed. The effect of water depth on the still productivity was studied experimentally. The greenhouse solar stills were used as a good method for obtaining the fresh water even for a small scale demands, because of economic and technical advantages as it uses the inexpensive technology including the material prices and manufacturing. Also the effect of the design and operational parameters was studied. Different depths of brackish water with TDS of 5000 ppm were tested under same conditions. Distillate output decreases significantly with the increase of water depth in the basin of the solar still, also with the same solar irradiance the evaporation rate increases with the reduced mass of water on the absorber plate. The increased productivity from the lower depth is directly related to the increased evaporation rate as well as the faster condensation which is due to the cooling effect. The fastest condensation rate was achieved by applying the method of cooling the glass cover. The significant effect of cooling the system is strongly observed on the increased productivity. The efficient utilization of solar energy with a percentage of 70% was reached and demonstrated by the good agreement between the obtained productivity of 6.7 lit/day and the theoretical productivity of 9.5 lit/day that could be obtained under the available climatic conditions. It was found that the geographical location may have a significant positive effect on the increased water productivity, especially for those locations with an abundant solar irradiation and situated at higher elevations above the sea level, where the reduced boiling point of water and the corresponded saturation pressure are below the standard atmosphere.

O Badran and M Khader [12] conducted an experimental work on a single slope solar still. Different effective parameters should be taken into account to increase the still

productivity. A mathematical model was presented and compared with experimental results. The model gave good match with experimental values. The thermal performance of the single slope solar still was examined and evaluated through by implementing the various parameters. To increase the productivity various parameters were taken: (a) different insulation thicknesses of 1, 2.5 and 5 cm; (b) water depth of 2 and 3.5 cm; (c) solar intensity; (d) Overall heat loss coefficient (e) effective absorptivity and transmissivity; and (f) ambient, water and vapor temperatures. The theoretical analyses were performed by energy balance on various components of the still with the help of MATLAB software.

RV Dunkle [13] has given a semi empirical relation for internal heat and mass transfer coefficient to predict the hourly and daily yield for different solar still design. It is the oldest empirical relation. He proposed the values of C = 0.075 and n = 1/3 on the basis of simulation studies for Gr >3.2 $*10^5$ .Dunkle (1961) has derived the expression for hcw which is written in chapter 3. However this relation has following limitations. (i) It is only valid for a mean operating temperature range of 120^0F and equivalent temperature difference of 30^0F. (ii) It is independent of cavity volume, i.e. the average distance between the condensing and evaporating surfaces. (iii) It holds good for heat flow upwards in horizontally enclosed air space.

N Sctoodeh, R Rahimi, A Ameri [14] developed 3-dimensional 2-phase model for condensation and evaporation process in solar still using CFD. The recorded experimental data is 14 hours, as 14 hours simulation is difficult to run on computer so it is divided into 14 stages of 1 hour interval. In a time period of 1 hour it was assumed that glass temperature and received radiation are almost constant. Solar radiation are based upon absorption factor, emissivity of glass and water at the bottom. The value of convective and evaporative heat transfer coefficient was predicted using CFD. It was observed that due to the solar radiation water vaporised and condensed on the glass surface. The condensed drops slip down and collected in the downcomer. The amount of water collected in CFD were compared with the water produced by the experimental set up, there is good agreement. The values of C and n calculated according to Kumar and Tiwari model and consequently evaluated convective and evaporative heat transfer coefficient. It was found that the convective and evaporative heat transfer coefficient were in good agreement with experimental data with certain error. Therefore CFD is powerful tool for design, parameter analysis and difficulties removal in solar still construction.

AJ Khalifa [15] developed four correlations to illustrate the effect of solar radiation, dyes, cover slope and brine depth on the productivity of the basin type solar still using the available data given by the different investigators.

Solar radiation

The productivity of the still as a function of the solar radiation.

$$y = 0.0036(I)^2 + 0.070(I) + 0.2475 \quad , R^2 = 0.762 \tag{2.1}$$

Where (y) is the productivity in (l/m^2 day) and (I) is the solar radiation in (MJ/m^2 day). Root Mean square value R^2

Brine depth:

It was evident that the shallower the basin layer, the higher the efficiency. A thin layer of water attained higher temperatures as compared to a deep layer because of its lower capacity.

$$y = 3.884e^{-0.0458\,(d)} \quad , \quad R^2 = 0.832 \tag{2.2}$$

Where (y) is the productivity in (l/m^2 day), (d) is the brine depth in cm and (R^2) is root mean square value.

Cover tilt angle:

The amount of radiation reflected by the cover may vary with season, which might be explained by the fact that the sun's declination angle has negative values in the winter and positive values in the summer.

$$y = -0.225 + (a)^2 + 0.1562(a) + 0.843 \quad , R^2 = 0.734 \tag{2.3}$$

Where (y) is the productivity in (l/m^2 day) and (a) is the cover tilt angle (degree).

The correlations developed illustrated that the still productivity could be influenced by the brine depth alone by up to 33% and by the tilt angle alone by up to 63%. A cover tilt angle of about 30° gave the highest productivity. The still productivity could be enhanced by adding dark soluble dye to the brine by up to 20%. The still productivity increased with the increase of insulation, thickness of the still and with more solar radiation received. The productivity of the still is directly related to the intensity of the solar radiation received.

S Abdallaha, M Khaderb, O Badran [16] examined the effect of using different types of absorbing materials in order to enhance the yield of solar still through improvement in the thermal conductivity. These absorbing materials are of two types: coated and uncoated porous media (called metallic wiry sponges) and black volcanic rocks. Four identical solar stills were manufactured using locally available materials. The first three solar stills contain black coated and uncoated metallic wiry sponges made from steel quality AISI 430 type,

and black rocks collected from Mafraq Area in north-eastern Jordan. The fourth still is used as reference still which contains no absorbing materials (only black painted basin). It was noticed that all three stills that contain the absorbing materials gave much better water collection than the reference still. During day collection, the uncoated metallic sponge gave the highest water collections then the black rock comes second and finally the coated metallic wiry sponges. Black rocks gave around 60% gain with no corrosion problems. Also, there is no cost endured for using these rocks which make them an interesting and very viable option to consider as an absorbing and heat storage material. So, it may be concluded that the black rocks absorb, store and release the incident solar energy better than the coated and uncoated metallic wiry sponges and can enhance the productivity by nearly 20%. Also it is a very cheap and non corrosive material.

V Belessiotis, K Voropoulos, E Delyarmis [17] examined the thermal behavior of a typical solar still experimentally and theoretically and analyzed its basic characteristics. The large number of experimental measurements were conducted and concluded that the operation of such stills during daytime is characterized by three phases: (1) starting, (2) pseudo steady-state, and (3) saturation. A mathematical equation is formed for the instantaneous simulation of the solar still during the pseudo steady-state phase. From this the equation in its integrated form determines satisfactorily the daily output by the daily solar radiation (solar energy input), the average ambient air temperature during the day, $T_{a(av)}$ and the temperature of the water in the basin at the beginning of the day, T_{win} as parameters. This method is called the "input-output" method. The I/O method is simple and can be used as a standard method for the characterization of solar distillation systems by measuring M_{out}, H_d , T_{ad}, and T_{wd} for a period from 6 h before the solar noon to 6 h after the solar noon for a number of days with radiation levels from 5-25 M J/ m 2. Subsequently, the characteristic parameters of the still F_1, F_2 and F_3 can be determined by regression analysis. The determination of F_1, F_2 and F_3, which express efficiency, losses and inertia of the still, respectively, gives the ability ofiong-term (annual) prediction of the output with minimum computational effort, as long as the daily climatic conditions H_d and T_a of the area where the still is located are known. The arithmetic calculation of F_1, F_2 and F_3 can be used for the technical and economical design optimization of similar systems using minimum computational effort.

2.2.2 Advanced solar still or Active solar still.

AA Sebaii [18] built the still of basin area $1m^2$, and painted it with black galvanized iron sheet, leaving a gap under the horizontal portion of the basin liner. This gap can be loaded

or unloaded with the PCM (phase change material) via a pipe that will take care of the volume expansion of the PCM upon melting. Stearic acid had been used as a latent heat storage material because of its low cost and large availability of heat. PCM will act as a heat source for the basin water during low intensity solar radiation periods as well as during the night. Consequently the still continues to produce fresh water after sunset even with thin layers of basin water. A.A. El-Sebaii gave the transient mathematical models for a single slope-single basin solar still with and without phase change material (PCM) under the basin liner of the still. Analytical expressions for temperature of the still elements and the PCM had been obtained. The still performance was investigated by computer simulation and found that PCM store heat during the noon time and release heat in the night. Effect of mass of the PCM (m_{pcm}) on the daylight Pdl, overnight P_{on} and daily productivity P_d and efficiency g_d of the still for different masses of basin water mw had been investigated. It was found that P_{dl} decreases as m_{pcm} increases; but P_{on} and P_d increase. During discharging of the PCM, the convective heat transfer coefficient from the basin liner to basin water was doubled; thus, the evaporative heat transfer coefficient was increased by 27% on using 3.3 cm of stearic acid beneath the basin liner. Therefore, on a summer day, a value of Pd of 9.005 (kg/m2 day) with a daily efficiency of 85.3% was obtained compared to 4.998 (kg/m2 day) when the still was used without the PCM. The PCM is more effective for lower masses of basin water on winter season.

H Tanaka, Y Nakatake [19] investigated the effect of the vertical flat plate external reflector on the distillate productivity of the tilted wick solar still. The still consisted of a glass cover, evaporating wick and a vertical flat plate external reflector of highly reflective materials such as a mirror finished metal plate. Saline water was fed to the wick constantly. The direct and diffuse solar radiation and also the reflected solar radiation from external reflector are transmitted through the glass cover and absorbed onto the wick. To simplify the following calculation to determine the absorption of solar radiation on the wick, the walls of the still are disregarded, since the height of the walls (10 mm) was negligible in relation to the still's length (1 m) and width (1 m). They performed numerical analysis of heat and mass transfer in the still to predict the distillate productivity on four days (spring and autumn equinox and summer and winter solstice days) at 30EN latitude. They found that the external reflector can increase the distillate productivity in all but the summer seasons, and the increase in the daily amount of distillate averaged over the four days is predicted to be about 9%.

B Chaouchi, A Zrelli, S Gabsi [20] built the experimental device which was composed of a solar parabolic collector. To evaluate the performance of this unit, they developed a theoretical model to calculate the absorber average temperature as well as the distillate flow rate as a function of solar flux. The experimental results were compared with those calculated theoretically. The parabolic concentrator was supported by molded fiberglass with 1.8 m in dish aperture diameter. This dish surface was covered with rectangular stainless steel sheet segments with a thickness of 1 mm. It shows that the experimental and theoretical flow rates were approximately the same. It increased in the beginning of the day to reach their maximum toward 14 h and decrease thereafter. This evolution was closely linked to solar lightening, which was responsible for this production and therefore has a similar rate. The obtained results showed the variations of the distilled water flow rate, the average temperature of the absorber enlightened face, the instantaneous global efficiency and solar irradiation according to the local time. A comparison of theoretical and experimental results showed that the difference between them was small concerning the temperature but can reach an average relative error of 42% for the distillate flow rate. This was due to the imperfections in paraboloid geometry, the sun manual follow-up and especially to the system's tilt variation during the day, which does not make it possible always to keep the absorber surface covered with salted water. This phenomenon is remarkable, especially the morning when the tilt is significant.

O Badran [21] experimentally investigated the effect of coupling a flat plate solar collector on the productivity of solar still. This experiment was carried out on single slope solar still with mirrors fixed to its interior sides was coupled with a flat plate collector. The present solar still consists of asymmetric-green house type solar still coupled with solar collector. It has a black painted basin of $1m^2$ area filled with brackish water supplied to it from a collector which preheats the water to act as an enhancer to the solar still. The evaporating basin was covered by a sheet of clear glass (to allow sunlight to reach the water) which was tilted at a slight angle (35^0) to let the fresh water that condenses on its underside trickle down to a collecting trough. A trough running along the bottom side of the glass cover ensures the collection of the distilled water towards the collecting vessel. The glass also holds the heat inside the still. It had been found that coupling of a solar collector with a still had increased the productivity by 36%. Also the increase of water depth decreased the productivity, while the still productivity is found to be proportional to the solar radiation intensity.

K Sampathkumar, T Arjunan, P Pitchandi and P Senthilkumar [22] reviewed different active solar distillation systems. Thermal modeling was done for various types of active single slope solar distillation system. Solar distillation process is considered as both economical and ecofriendly technique particularly in rural areas. Many active distillation systems have been developed to overcome the problem of lower distillate output in passive solar stills. The performance of a solar still could neither be predicted nor improved by some of the uncontrollable parameters like intensity of solar radiation, ambient temperature and wind velocity. But, there are certain parameters such as depth of water, glass cover angle, fabrication materials, temperature of water in the basin and insulation thickness, which affects the performance of the solar still that could be modified for improving the performance. The still performance can be increased by reducing the water depth and thereby increasing the evaporation rate. The temperature difference between water in the basin and condensing glass cover also has a direct effect in the performance of the still. The increased temperature of the water in basin can increase the temperature difference between the evaporating and condensing surfaces. To achieve better evaporation and condensation rate, the temperature of water in the basin could be raised by feeding thermal energy from some external sources. It was concluded that the annual yield is at its maximum when the condensing glass cover inclination is equal to the latitude of the place. The yield is directly related to thermal conductivity of condensing cover materials; copper gives a greater yield compared to glass and plastic due to higher thermal conductivity. Solar still coupled with FPC with forced circulation mode gives higher yield than that of the thermosyphon mode. Double slope active solar still under natural circulation mode gives higher yield in comparison with the double slope passive solar still. The thermal efficiency of double slope active solar still is lower than the thermal efficiency of double slope passive solar still. In active double effect solar still, a higher yield from the lower basin at noon is due to the high water temperature at that time. The concentrator assisted regenerative solar still has much higher thermal efficiency than the flat plate collector assisted regenerative still at all water depths and they inferred that there is less thermal loss in the concentrator compared to the flat plate collector panel. The yield was high in hybrid photovoltaic/thermal (PV/T) active solar still compared to the passive solar still. The multistage solar desalination system with heat recovery system produces higher yield than the simple solar still. The length of solar still, depth of water in basin, inlet water temperature and solar radiation are the major parameters which affects the performance of the still. Kumar and Tiwari model is most suitable for evaluating the internal heat transfer coefficients and hourly yield accurately

except in extreme cases. The values of 'C' and 'n' differ for each design of the solar still and for the operating water temperature range. Therefore, it is recommended that before predicting the performance theoretically, experiments must be carried out for given climatic conditions to evaluate the values of 'C' and 'n' for a particular design of solar still.

R Dev and GN Tiwari [23] developed an inverted absorber solar still (IASS) in which the heat is supplied both from bottom and top by using the curved reflector at the bottom. Because of this, the high water temperature can be obtained in the IASS in comparison to that of the single slope solar still (SS). The IASS is a concentrating type of solar distillation system. It consists of a conventional SS and a curved reflector under its metallic basin. The IASS receives solar radiation from both the top and bottom sides unlike the conventional SS. The addition of a reflector under the basin concentrates solar radiation on the lower surface of the metallic basin. Because of this additional heat, the temperature of the water in the IASS increases at a faster rate in comparison to conventional SS. An increased temperature difference between the water and condensing glass cover enhances the distillate production rate. The IASS can be said an improved design of conventional SS. The linear and non-linear characteristic equations of the IASS were developed based on derived analytical expressions of instantaneous gain (ηi) and loss (ηiL) efficiencies by using experimental data for the climatic condition of Muscat, Oman. The results showed that the behaviour of the IASS is non-linear as expected. It was concluded that the non-linear characteristic curves are found to be more suitable to show the behaviour of the IASS and SS under the quasi-steady state. It is because of non-linearity in the climatic parameters. The non-linear characteristic curves are obtained on the experimental results. The values of ηi are higher for the SS in comparison to that of the IASS at the same water depth and climatic conditions. The values of ηi decreases as the water depth increases whereas the values of ηiL decreases due to the thermal storage effect of the water . The lower water depth 0.01 m has been found with better values of ηi, ηiL and ṁew over other water depths hence 0.01 m water depth can be recommended for solar stills. The annual cost of distilled water per kg-m2 has been found to be Rs. 0.95/- and Rs. 0.54/- when the life and rate of interest of the IASS and SS have been considered 15 years and 15% respectively.

2.2.3 Heat And Mass Transfer

Heat is a form of energy which is being transported from one point to another due to temperature differences between the points, greater the temperature difference faster is the heat transport and it can take place through conduction, convection and radiation. In a solar desalination thermal system, heat is distributed from the absorber to other components of

the system through one or a combination of these modes of heat transfer. Heat transmission in solar desalination unit there are various loses energy and a reduction in the system efficiency. Consequently, the design, construction, testing and operation of desalination unit require knowledge about heat transmission mechanisms.

2.2.3.1 Conduction

Conduction is the mode of heat transfer which is supposed to occur generally in the solid due to temperature difference by molecular lattice vibration energy transfer and also by free electron transfer among the molecules or heat conduction is the rate of energy transfer between two points in a medium where by kinetic energy is transferred between particles or groups of particles. This mode of heat transfer can take place in gaseous, liquid and solid phases of a substance. In addition heat is conducted in the direction of decreasing temperature. The temperatures may vary (transient) or remain constant (steady-state) with time.

For transient heat conduction in three dimensions, heat flow is based on the

Theory proposed by Fourier [24].

$$\nabla^2 T + \frac{\dot{q}}{k} = \frac{1}{\alpha'}\frac{\partial T}{\partial t} \tag{2.4}$$

Where ∇^2 is the Laplacian

In Cartesian coordinates, Eq (2.4) is given as:

$$\frac{\partial^2 T}{\partial x^2} + \frac{\partial^2 T}{\partial y^2} + \frac{\partial^2 T}{\partial z^2} + \frac{\dot{q}}{k} = \frac{1}{\alpha'}\frac{\partial T}{\partial t} \tag{2.5}$$

Eq (2.4) can also be expressed in cylindrical or spherical coordinates, depending on the geometry of the conductor. It is possible to solve this equation analytically to obtain an accurate spatial distribution of temperature at a given time. Some mathematical models involve systems of differential equations which cannot be solved analytically. In such cases, numerical methods can be used to obtain an approximate solution. In one dimension, Eq (2.5) reduces to

$$\frac{\partial^2 T}{\partial x^2} + \frac{\dot{q}}{k} = \frac{1}{\alpha'}\frac{\partial T}{\partial t} \tag{2.6}$$

The heat flux in three dimensions can be given by:

$$\bar{q} = -k\nabla T \tag{2.7}$$

Where ∇T is the temperature gradient (a vector quantity).

In one dimension, heat flux (q) can be calculated from:

$$q = -k\frac{dT}{dx} \tag{2.8}$$

Conductivity:

Thermal conductivity (k) is the property of the material which tells about the ability of the material to allow the heat to get the heat conducted through it. It is noted from Eq (2.8) that the rate of heat transfer increases with the coefficient of heat conduction (k) and temperature gradient. Material with relatively high values of k (such as copper; aluminium, stainless steel and galvanized steel) are suitable for the fabrication of solar absorber plates while those with low values of k (such as plywood, polystyrene, sawdust and cork) are appropriate for insulation to reduce heat loss from a given system to the environment. In addition, k varies with the direction of heat flow and temperature of the conductor. The rate of heat flow (Q) across the slab without heat source (Fig 2.1) can be given by

$$Q = \frac{kA(\Delta T)}{x} \tag{2.9}$$

$$\Delta T = T_1 - T_2 \tag{2.10}$$

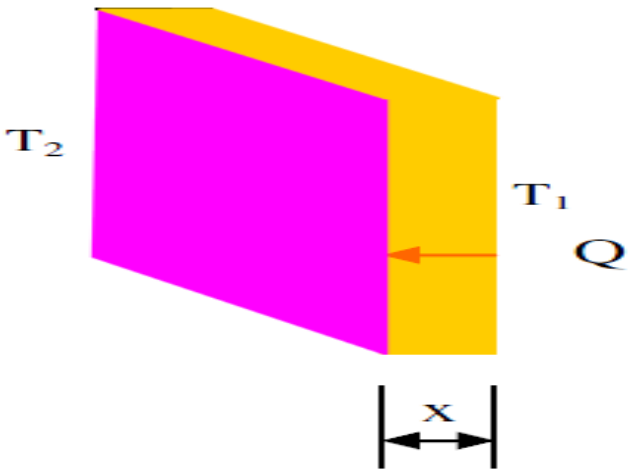

Fig 2.1: One dimensional heat conduction across a slab at T1>T2.

2.2.3.2 Convection

Convection is a mode of heat transfer which generally occur between a hot solid body and the surrounding fluid due to temperature difference associated with macroscopic bulk transport of the fluid over the solid which is provided by an external agency like fan or blower in the case of forced convection on which may happen naturally due to buoyancy

force arising out of density changes due to temperature changes or heat convection is the rate of energy transfer between two points in a fluid which involves mixing of the fluid by natural or forced mechanisms. In natural convection, the fluid moves due to the density gradient arising from temperature differences. Forced convection occurs when a moving fluid absorbs heat and transports it away by means of an external pump such as a fan. At the fluid-solid boundary, heat is transferred by means of conduction. Heat may be transferred from a hot solid surface to a cold fluid or from a hot fluid to a cold surface. The rate of heat transfer by natural convection can be given by [26]

$$q = h_c(T_2 - T_1) \tag{2.11}$$

where $h_c = Nu\ k/L_v$, $Nu = C(Gr.Pr)^n$, and C and n are dimensionless parameters.

It should be noted that the Nusselt number (Nu) is a ratio of convective(h_c) to conductive (k/L_v) heat transfer coefficients within a fluid. This parameter is dimensionless and it can be calculated from the product of the Grashof (Gr) and Prandtl (Pr) numbers. The Grashof number is a ratio of buoyancy to viscous force in a fluid while the Prandtl number is a ratio of kinematic viscosity (v) to thermal diffusivity (α'). Both of these parameters are also dimensionless and they can be given by

$$Pr = \frac{v}{\alpha'} \tag{2.12}$$

$$Gr = \frac{\beta g L_v^3 \rho^2 \Delta T}{\mu^2} \tag{2.13}$$

Eqs. (2.12) and (2.13) show that the product (GrPr) is influenced by fluid properties, the difference between the surface and fluid temperatures, and the geometry of the surface in contact with the fluid. Consequently, the coefficient of convective heat transfer is also affected by the same factors.

Natural convection can be divided into three regions, depending on the value of the dimensionless parameter n. a) turbulent natural convection (n=1/3), b) laminar natural convection (n=1/4), and c) a region with n<1/4. When a fluid flows under forced convention, a boundary layer is created between the fluid and the surface (say a flat surface) in contact with the fluid (Fig 2.2). Flow within the boundary layer close to the leading edge of the surface is laminar forced convection. As flow continues along the surface, there is a rise in the thickness of the boundary layer to a critical level. Thereafter, turbulent forced convection sets in. So, forced convection can be laminar or turbulent. At a very low fluid velocity, flow remains laminar in long tubes or channels with small hydraulic diameter and

it is said to be fully developed laminar flow. At a high fluid velocity or in a tube with large diameter, transition to turbulent flow takes place and flow is fully developed turbulent. These flow regions are employed in the computation of the coefficient of convective heat transfer (hc), Incropera [24] provide a summary of models used for this computation. For example, h_c for natural convection can be given by:

$$h_c = C\frac{k}{L_v}\left(\frac{\beta g L_v^3 \rho^2 \Delta T}{\mu^2}\right)^n \left(\frac{\mu C_p}{k}\right)^n \tag{2.14}$$

Where L_v=height, length, diameter and 0.5x diameter for vertical plates or pipes, horizontal plates, horizontal pipes and spheres respectively.

For forced convection, h_c can be calculated from:

$$h_c = C\frac{k}{L_v}\left(\frac{L_v \dot{m}''}{\mu}\right)^n \left(\frac{\mu C_p}{k}\right)^n \tag{2.15}$$

It is noted from Eq (2.15) that the coefficient of natural convection is independent of the characteristic length (L_v) when n=1/3. For forced convection, hc is independent of the geometry of a cavity when the exponent e=1 in Eq.(2.15).

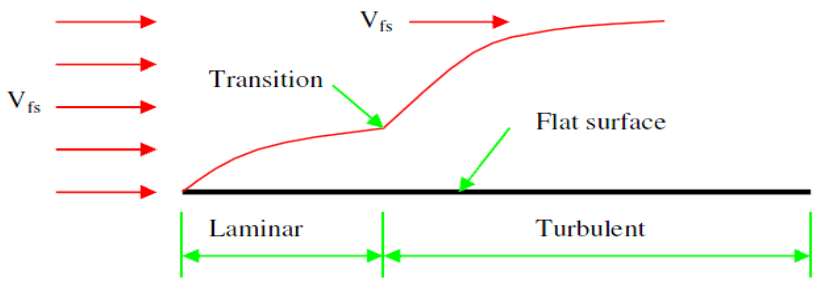

Fig 2.2: Formation of laminar and turbulent boundary layers when a fluid flows over a flat surface. The velocity of the fluid increases with the distance from the surface and the edge.

2.2.3.3 Radiative heat transfer

Thermal radiation is the mode of heat transfer which does not require any material medium and hence occur electromagnetic wave propagation travelling with the speed of light. It can be defined in another way also. Heat radiation is the transfer of thermal energy through electromagnetic waves. This mode of heat transfer does not require a medium for propagation, unlike heat conduction and convection. Consequently, the use of a vacuum to reduce heat loss only eliminates convective and conductive heat losses. In fact, the presence of a medium between a radiator and receiver provides impedance to radiative heat transfer. The amount of energy emitted by a radiator depends on the nature of the material,

microscopic structure and temperature of the radiator and its surroundings. A blackbody absorbs all the radiation incident on it. Its emissive power to a hemispherical region above it is given by (Boltzmann). For instance all the bodies at all temperature emit thermal radiation, the rate of emission from the surface of any body is directly proportional to forth power of the absolute temperature of body.

$$\acute{E}_{bb} = \sigma T^4 \tag{2.16}$$

$$\acute{E}_{bb,\lambda} = \frac{c_1 \lambda^{-5}}{e^{c2/(\lambda T)} - 1} \tag{2.17}$$

where c_1 =3.742x10-16 Wm2 and c_2=0.014388 m K are respectively the first and second Planck's constants. A real surface absorbs part of the radiant energy which it receives. So, its emissive power to a hemispherical surface above it is given by:

$$\acute{E} = \varepsilon\sigma\left(T_i^4 - T_j^4\right) \tag{2.18}$$

$$\acute{E}_{\lambda} = \varepsilon_{\lambda}\acute{E}_{bb,\lambda} \tag{2.19}$$

$$\varepsilon = \frac{1}{\sigma T^4}\int_0^{\infty} \varepsilon_{\lambda}\acute{E}_{bb,\lambda}\, d\lambda \tag{2.20}$$

If ε_λ is independent of λ, then $\varepsilon=\varepsilon_\lambda$, and a surface with such a characteristic is known as a gray body. In practical calculations, surfaces are usually assumed to be gray because of the unavailability of information about the relationship between el and l. It should also be mentioned that the energy from a non-black surface comprises the radiant and reflected components, and this energy may leave the surface specularly or diffusely. The reflected radiation follows one direction from a specular reflector but it goes in different directions from a diffuse reflector (Fig 2.3).

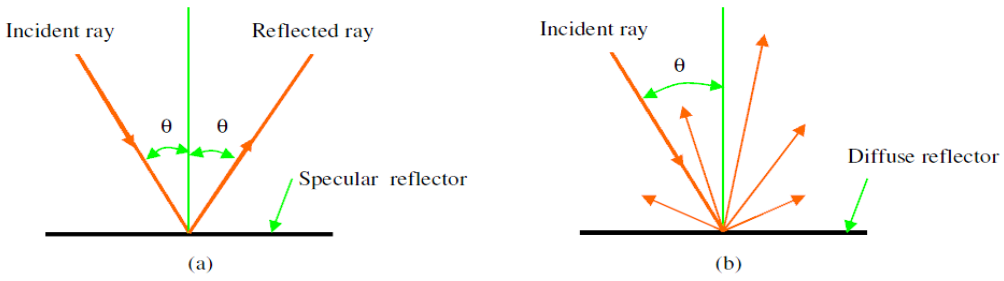

Fig 2.3: Reflection of radiation on a) specular and b) diffuse surfaces.

If solar irradiance on surface (i) is G_{gp}, then the amount of solar power reflected diffusely from surface (i) to surface (j) can be given by

$$G_{i\text{-}j} = W_{i\text{-}j}\, \rho_i G_{gp} \tag{2.21}$$

Eq (2.21) shows that the amount of solar radiation reflected to a receiver is influenced by both the reflectance and view factor of the surfaces. To calculate the amount of radiation energy transferred between two surface, the following assumptions are often made. a) surfaces are gray or black, b) radiation and reflection are diffuse, c) α=ε, and α does not depend on the temperature of the source of the incident radiation and d) surfaces are separated by a non-absorbing medium. For two given surfaces, the net radiative heat transfer can be given as

$$Q = \frac{\sigma\left(T_i^4 - T_j^4\right)}{\frac{1-\varepsilon_i}{A_i\varepsilon_i} + \frac{1-\varepsilon_j}{A_j\varepsilon_j} + \frac{1}{A_i W_{i,j}}} \tag{2.22}$$

The net radiative heat transfer between two surfaces can also be expressed in a linear form by defining a coefficient of radiative heat transfer:

$$Q = A_i h_{r,i-j}\left(T_i - T_j\right) \tag{2.23}$$

$$h_{r,i-j} = \frac{\sigma\left(T_i^2 + T_j^2\right)\left(T_i + T_j\right)}{\frac{1-\varepsilon_i}{\varepsilon_i} + \frac{A_i\left(1-\varepsilon_j\right)}{A_j\varepsilon_j} + \frac{1}{W_{i,j}}} \tag{2.24}$$

If the two surfaces are rectangular and parallel to each other, then $W_{i-j} \approx 1$ and $A_i = A_j$. Consequently, Eq. (2.24) reduces to:

$$h_{r,i-j} = \sigma\varepsilon_{i,j}\left(T_i^2 + T_j^2\right)\left(T_i + T_j\right) \tag{2.25}$$

$$\varepsilon_{i,j} = \frac{1}{\varepsilon_i} + \frac{1}{\varepsilon_j} - 1 \tag{2.26}$$

2.2.3.4 Thermal resistance

The flow of heat is similar to that of an electric current. Thermal energy flows from a point at higher temperature to another point at lower temperature, encountering resistance in the process. For conductive, convective and radiative heat transfers, the corresponding resistances are given as. [24]

$$R_{cd} = \frac{x}{kA} \quad (2.27)$$

$$R_c = \frac{1}{h_c A} \quad (2.28)$$

$$R_r = \frac{1}{h_r A} \quad (2.29)$$

It is observed that R_{cd} increases with decreasing k for given values of A and x, which is useful in thermal insulation. A material with a low value of k is used as an insulator to curtail heat loss from a thermal system. Similarly, convective and radiative resistances increase with decreasing their corresponding coefficients of heat transfer for a constant value of A.

Thermal resistance due to evaporative heat transfer (Re) is computed by replacing h_c with h_e in Eq (2.28).

The effective resistance for series or parallel connections is.

$$R_{ef} = R_1 + R_2 + \cdots + R_r, \text{ for series connection} \quad (2.30)$$

$$\frac{1}{R_{ef}} = \frac{1}{R_1} + \frac{1}{R_2} + \ ... + \frac{1}{R_r}, \text{ for parallel connection} \quad (2.31)$$

Eqs (2.30) and (2.31) are useful in the analysis of a real thermal system with multiple resistances. For instance, a solar still has composite resistances. Consequently, this system can also be analyzed by using the resistance method.

2.2.3.5 Heat and mass transfer as applied to solar distillation process

Saline water in the basin of a solar still is heated by solar radiation that passes through the transparent cover and is absorbed by the water and bottom part of the basin liner. Vapour rises from the hot water and condenses when it gets into contact with the inner surface of the transparent cover at or below dew point. The condensate is collected through a channel fitted along the lower edge of the transparent cover. The solar distillation process involves all the three modes of heat transfer (Fig 2.6). There is heat conduction through the transparent cover, bottom and side walls, which results in a loss of heat from the still. This loss can be reduced by using a thick insulation layer with a relatively low k-value. Heat from the basin liner is transferred to the saline water by convection while thermal energy from the hot water is transferred by vaporization, convection and radiation, onto the condensing cover. Water vapour condenses on the cover, yielding latent heat of

condensation and distilled water. In turn, the cover dissipates heat to the environment by convective and radiative heat transfer modes. It should be noted that internal heat transfer in a solar still also includes mass transfer. Consequently, special correlations are used to estimate the coefficients of convective and evaporative heat transfers from hot water to the transparent cover surface. Dunkle proposed the first empirical relation for heat and mass transfer and later various models are developed these are explained in literature review.

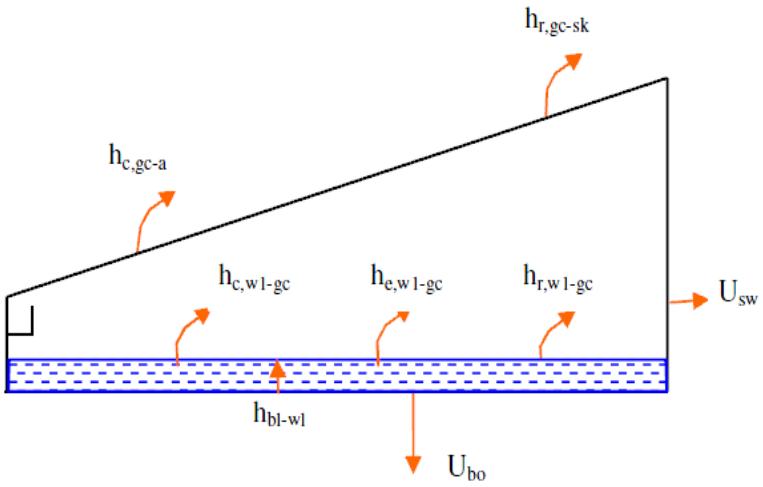

Fig 2.4: Heat transfer modes in a conventional solar still.

2.3 GAP IN LITERATURE

A lot of work has been done on Solar still; few researchers have worked on the thermal modeling of solar still and various loses from the solar still. Literature review shows that there has been less attention to solar still modeling by means of CFD.

CHAPTER 3
METHODOLOGY

3.1 SIMULATION METHODOLOGY

Here in this chapter starting from the development of two phase three dimensional model of solar still with assumptions each step for carrying out simulation is explained. Size of geometry, meshing, boundary condition applied on the simulation model and simulation procedure has been discussed here with an enhanced contrast.

3.1.1 Assumptions

1) There is no vapour leakage from the solar still.
2) All the walls are adiabatic, hence no heat loss.
3) There is no temperature gradient across the glass cover of solar still.

3.1.2 Mathematical model

A two-phase model was developed in the volume of fluid (VOF) for liquid water and mixture of air and water vapor system at quasi steady state condition and adaptive time step has taken. So only surface evaporation of liquid occurs and their interface should be considered for modeling. For each phase the time and volume-average continuity, energy and mass equations are numerically solved.

3.1.2.1 Governing equations

CFD solve the continuity, momentum, energy and mass transfer conservation principles at steady state condition as are given below.

i) Continuity equation

Vapour phase

$$\nabla \cdot (r_G \rho_G V_G) + F_{LG} = 0 \tag{3.1}$$

Liquid phase

$$\nabla \cdot (r_L \rho_L V_L) - F_{LG} = 0 \tag{3.2}$$

F_{LG} is the rate of mass transfer from liquid phase to vapor phase and from vapour phase to liquid phase. Mass transfer between phases must satisfy the local balance condition, so $F_{LG} = -F_{GL}$.

ii) Momentum equation

Vapour phase

$$\nabla \cdot (r_G(\rho_G V_G V_G)) = -r_G \nabla \mathrm{P_G} + \nabla \cdot \left(\mathrm{r_G}\,\mu_{\mathrm{laminar\ ,G}}(\nabla \mathrm{V_G} + (\nabla \mathrm{V_G})^{\mathrm{T}})\right) + r_G \rho_G g - M_{GL} \quad (3.3)$$

Liquid phase

$$\nabla \cdot (r_L(\rho_L V_L V_L)) = -r_L \nabla \mathrm{P_L} + \nabla \cdot \left(\mathrm{r_L}\,\mu_{\mathrm{laminar\ ,L}}(\nabla \mathrm{V_L} + (\nabla \mathrm{V_L})^{\mathrm{T}})\right) + r_L \rho_L g + M_{GL} \quad (3.4)$$

M_{GL} describes the interfacial forces acting on each phase. The required drag coefficient in CFX due to high interfacial area was assumed to be 0.44.

iii) Energy equation

Vapour phase

$$\nabla \cdot (r_G \rho_G V_G h_G) = -\nabla \cdot \mathrm{q} + (\mathrm{Q_{LG}} + \mathrm{S_{LG}}\,\mathrm{h_{LG}}) \quad (3.5)$$

Liquid phase

$$\nabla \cdot (r_L \rho_L V_L h_L) = -\nabla \cdot \mathrm{q} - (\mathrm{Q_{LG}} + \mathrm{S_{LG}}\,\mathrm{h_{LG}}) \quad (3.6)$$

Heat transfer between phases must satisfy the local balance equation.

$$\mathrm{Q_{LG}} = -\mathrm{Q_{GL}} \quad (3.7)$$

Dunkle's [13] relation for convective heat transfer coefficient from water to glass, h_{CW} is used. Dunkle relation used for the temperature range of 40-60^{0}C. Dunkle's relation is given by

$$h_{cw} = 0.884\left[T_w - T_g + \frac{(P_w - P_g)(T_w + 273)}{268.9\times10^3 - P_w}\right]^{1/3} \quad (3.8)$$

The evaporative heat transfer coefficient, h_{ew} from water to glass is given by Eq. 3.9

$$h_{ew} = 0.01623 \times h_{cw} \times \left(\frac{P_w - P_g}{T_w - T_g}\right) \quad (3.9)$$

For mass transfer model, interfacial mass flux is used. It was assumed that the rate of water evaporation is equal to the rate of fresh water production. Therefore mass flux equation between the two phases is

$$\dot{\mathrm{m}}_{ew} = \frac{q_{ew} \times A_w \times t}{L} \quad (3.10)$$

Where

$$\dot{q}_{\mathrm{ew}} = h_{ew}(T_w - T_g) \quad (3.11)$$

3.1.3 Heat transfer coefficient analysis

In solar distillation system, the heat transfer can be classified in terms of external and internal modes. In this case convective heat transfer occurs simultaneously with evaporative heat transfer and these two heat transfer processes are independent of radiative heat transfer.

The gas phase above the liquid water is convected to the condensing cover by the action of buoyancy force caused by density variation due to temperature difference between water surface and condensing cover temperature. Heat transfer occurs across humid air inside enclosure of distillation unit by free convection.

Therefore the rate of heat transfer from the water surface to the glass cover by convection in the upward direction through humid fluid can be estimated by

$$\dot{q}_{\text{cw}} = h_{cw}\,(T_w - T_g) \tag{3.12}$$

h_{cw} is the convective heat transfer coefficient .From the we see that it depends upon the

- Operating range of temperature ΔT
- Geometry of the condensing cover A(Length of condensing cover)
- Physical properties of the fluid within the operating temperature

h_{cw} can also be calculated from non dimensional Nusselt number.

The accurate estimation of internal heat transfer coefficients is a critical step for the prediction of a solar still performance. The convective heat transfer coefficient is given by the Nusselt number, which is the ratio of convective to conductive heat transfer across a boundary.

$$Nu = \frac{h_{cw}}{k_v} * L_v = C(Gr.Pr)^n \tag{3.13}$$

hence

$$h_{cw} = \frac{K_v}{L_v} * C(Gr.Pr)^n \tag{3.14}$$

Where Gr and Pr are the Grashof and Prandtl numbers respectively and are given by the expressions shown below.

$$Gr = \frac{\beta g\, L_v^3 \rho^2 \Delta T}{\mu^2} \tag{3.15}$$

The Grashof number Gr approximates the ratio of the buoyancy force to the viscous force acting on a fluid.

$$Pr = \frac{\mu \cdot C_p}{K_v} \tag{3.16}$$

Prandtl number Pr expresses the ratio of viscous to thermal diffusion rates and is only a function of the fluid and the fluid state. The variables on right hand side of expressions are temperature dependent physical properties of vapour and are given in Table 3.1. In order to calculate vapour physical properties which are required in equations (3.13) – (3.16), T_w and

T_g were averaged over volume and glass surface respectively. So the Nu number and heat transfer coefficient obtained are average values.

$$T_v = (T_w + T_g)/2 \tag{3.17}$$

Table 3.1: Temperature dependent physical properties of vapour.

Quantity	Symbol	Expression
Specific heat	C_p	$C_p = 999.2 + 0.1434 \times T_i + 1.101 \times 10^{-4} \times T_i^2 - 6.7581 \times 10^{-8} \times T_i^3$
Density	ρ	$353.44/(T_i + 273.15)$
Thermal conductivity	K_v	$0.0244 + 0.7673 \times 10^{-4} \times T_i$
Viscosity	μ	$1.718 \times 10^{-5} + 4.620 \times 10^{-8} \times T_i$
Latent heat of vaporization of water	L	$3.1615 \times 10^6 \times [1 - (7.616 \times 10^{-4} \times T_i)]$; for $T_i > 70^0C$ $2.4935 \times 10^6 \times [1 - 9.4779 \times 10^{-4} T_i + 1.3132 \times 10^{-7} \times T_i^2 - 4.7974 \times 10^{-9} \times T_i^3]$; for $T_i < 70^0C$
Partial saturated vapour pressure at condensing cover temperature	P_g	$Exp[25.317 - 5144/(T_g + 273)]$
Partial saturated vapour pressure at water temperature	P_w	$Exp[25.317 - 5144/(T_w + 273)]$
Expansion factor	β	$1/(T_i + 273.15)$

Calculation of constants C and n in equation (3.14) were based on regression analysis of the predicted results of CFD using Kumar and Tiwari [7] method. The convective heat transfer coefficient is evaluated from Eq.3.14 using the values of obtained C and n. The evaporative heat transfer coefficient in the system and condensed water rate are obtained from Eqs. (3.9) and (3.10)

By substituting h_{cw} from Eq. (3.14) into Eq (3.9) we have

$$h_{ew} = 0.01623 \times \frac{K_v}{L_v} \times C(GrPr)^n \times \left(\frac{P_w - P_g}{T_w - T_g}\right) \tag{3.18}$$

Further substituting h_{ew} into Eq. (3.11) and then $\dot{q}_{ew}$ into Eq. (3.10) we get

$$\dot{m}_{ew} = \frac{0.01623}{L} \times \frac{K_v}{L_v} \times A_w \times t \times (P_w - P_g) \times C(GrPr)^n \tag{3.19}$$

Therefore

$$\dot{m}_{ew} = R \cdot C(GrPr)^n \tag{3.20}$$

$$\frac{\dot{m}_{ew}}{R} = C(GrPr)^n \tag{3.21}$$

Where

$$R = \frac{0.01623}{L} \times \frac{K_v}{L_v} \times A_w \times t \times \left(P_w - P_g\right) \tag{3.22}$$

$$y = mx + C_\circ \tag{3.23}$$

Taking the logarithms of both sides of Eq. (3.21)

$$y = ln\left(\frac{\dot{m}_{ew}}{R}\right)\ C_\circ = ln\ C, x = ln(GrPr)\ and\ m = n \tag{3.24}$$

using linear regression analysis the constants C and n evaluated.

$$m = \frac{N(\sum XY) - (\sum X)(\sum Y)}{N(\sum X^2) - (\sum X)^2} \tag{3.25}$$

$$C_\circ = \frac{(\sum Y)(\sum X^2) - (\sum X)(\sum XY)}{N(\sum X^2) - (\sum X)^2} \tag{3.26}$$

$$C = exp(C_\circ) \tag{3.27}$$

$$n = m \tag{3.28}$$

3.2 SIMULATION

For the simulation of condensation and evaporation process inside the distillation unit, CFD simulation software ANSYS CFX 13 is used. ANSYS CFX 13 is a fluid analysis and simulation software which combines CAD automatic Meshing and fast solution algorithms, which include Pre-processing, solving, Post processing.

Pre processor include modeling (CAD), meshing, applying boundary conditions,

Solver which is based on finite volume method Include applying the solution algorithms and iterating and forming the results.

Post processor includes displaying the results, forming temperature diagrams, contours graphs on display screen.

3.2.1 Simulation of evaporation and condensation inside distillation unit

In the distillation unit when heat is supplied to the basin. The water in the basin starts evaporating by leaving behind the contaminants; the resulting steam is collected and condensed. Evaporation rate depends upon the convective and evaporative heat transfer coefficient greater the convective heat transfer coefficient greater will be the final product. For this purpose the condensing covers at different inclination are simulated and evaluated

the inclination at which maximum yield is obtained is discussed in chapter 4. ANSYS version CFX 13.0 (workbench mode) has been used to simulate the condensation and evaporation process in solar still. Volume of fluid (VOF model) in ANSYS has very good capabilities to simulate temperature distribution.

3.2.2 Geometric Modeling

The schematic diagram of experimental set up of Anil Kr. Tiwari, G. N. Tiwari are shown in Fig 3.1. Evaporative surface area of the condensing cover is 250mm*365mm. For simulation purpose two condensing covers are taken at inclination 15^0 and 30^0 dimensions are shown in the table 3.2.

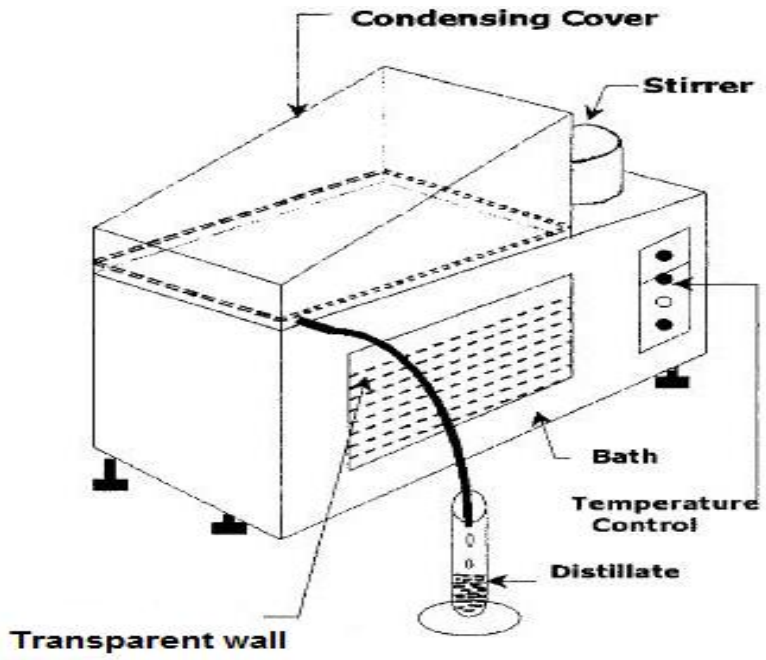

Fig 3.1: A schematic diagram of experimental setup of solar still [7].

Table 3.2: Specification of two condensing covers

Sr.no	Dimensions	Inclination,mm	
		15°	30°
01	Length	365	365
02	Lower height	70	70
03	Higher height	185	295
04	Width	250	250

3.2.2.1 Methodology

Geometric modal of solar still is created using ANSYS CAD module and this geometric modal is imported to the ANSYS meshing module to generate the meshing of the solar still. And a mesh file (.msh) is saved in working directory. Geometry is shown in figures 3.2 and 3.3 for 15^0 and 30^0 inclinations respectively.

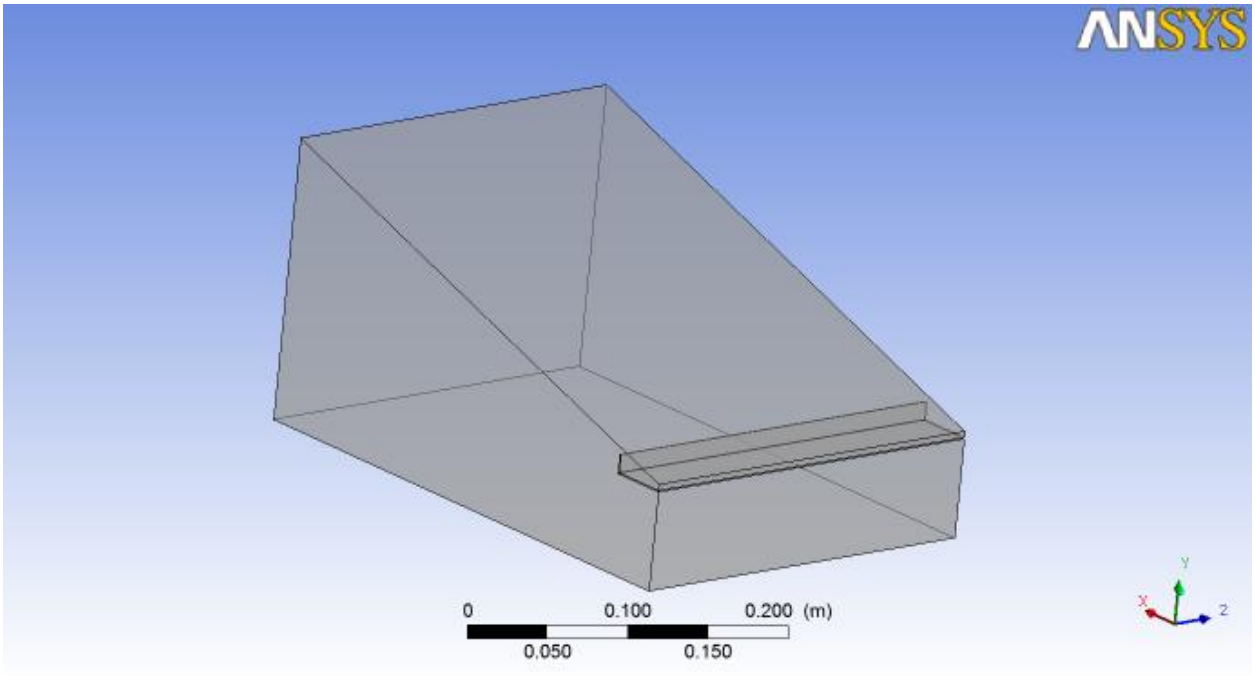

Fig. 3.2: 3-D model of condensing cover for 15^0 inclination

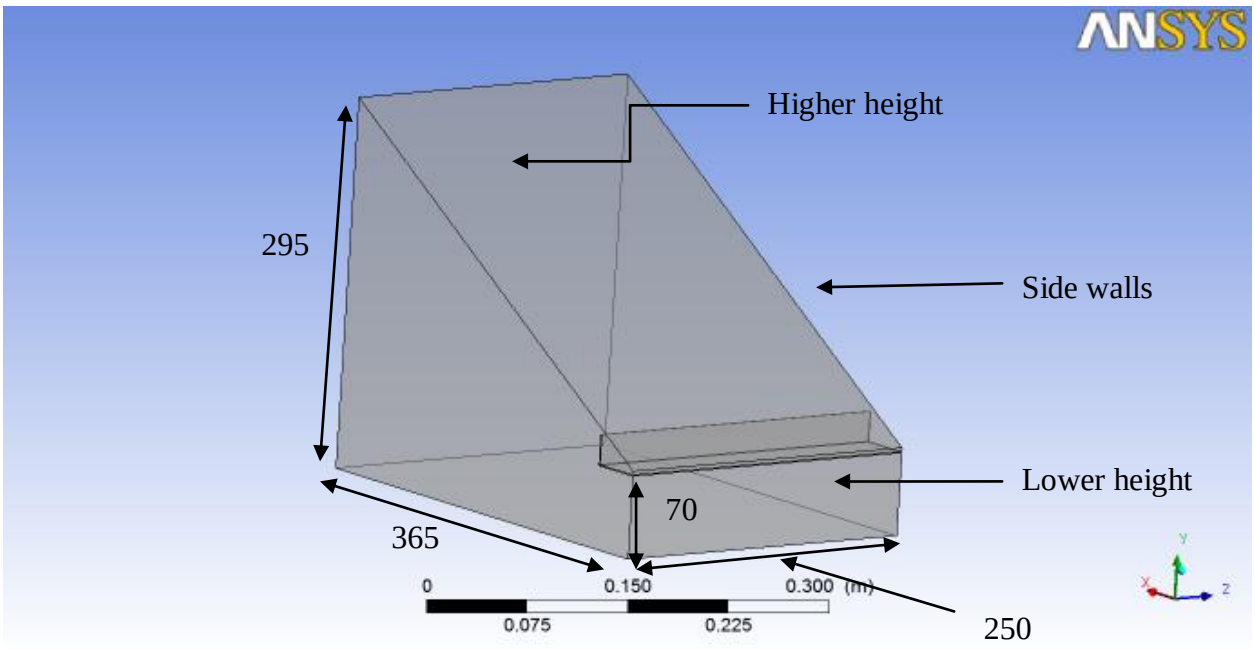

Fig 3.3: 3-D model of condensing cover for 30^0 inclination

3.2.2.2 Meshing Details

Geometry is imported to ansys meshing module and meshing is done. Unstructured mesh of type tetrahedral is used. A mesh independence test was conducted to ensure the results obtained are accurate and reliable. Test for grid independence is done and jacobian for meshing is taken 0.8. Fig 3.4 and 3.5 show meshing details.

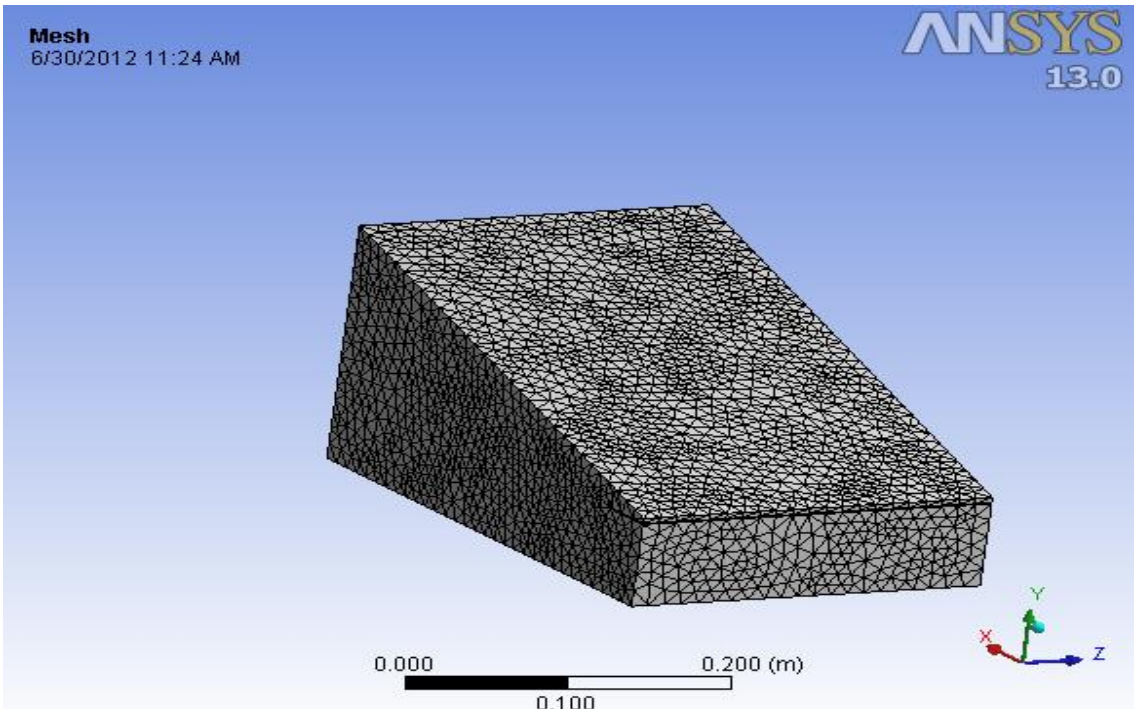

Fig 3.4: 3D Unstructured mesh for 15^0 inclination.

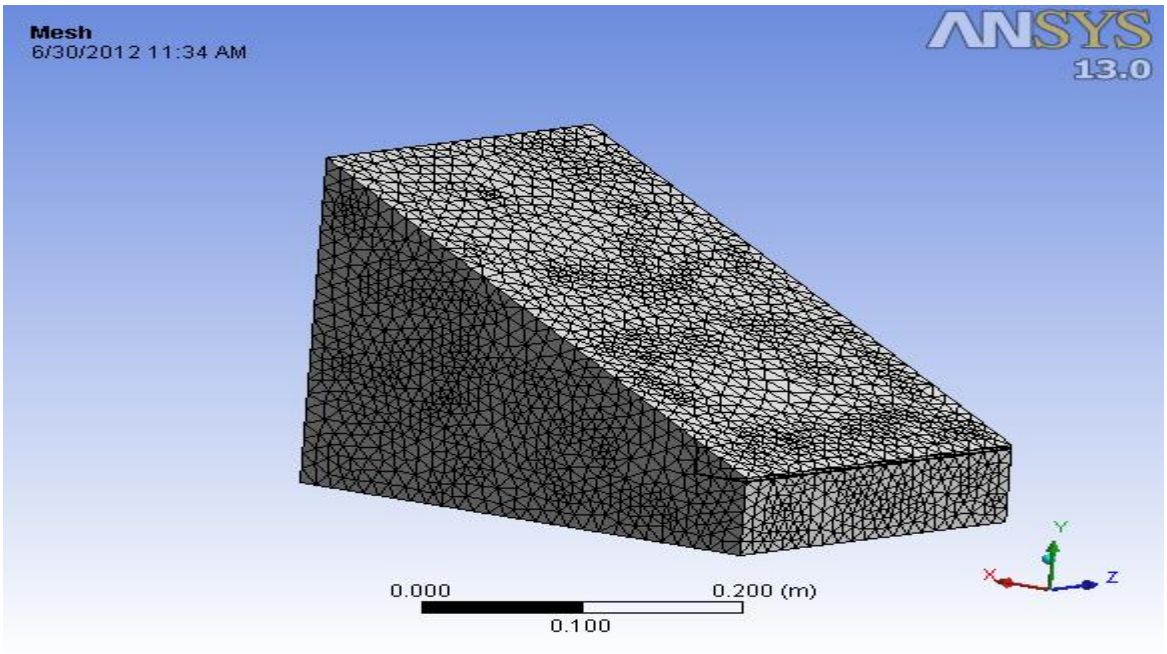

Fig 3.5: 3D Unstructured mesh for 30^0 inclination.

Table 3.3: Mesh statistics

Domain	Nodes	Elements
15^0 inclination	13619	69174
30^0 inclination	15248	77941

3.2.2.3 Boundary Conditions

Mesh files of solar still are then imported to the CFX Pre. In CFX pre physics and boundary conditions are applied on the domain is explained to solve the continuity and momentum equation. A two phase domain is created in the (VOF) framework for liquid water and mixture of water vapour and air. Evaporation process is modeled as laminar at quasi steady, accounting for thermal energy heat transfer while considering the effects of buoyancy. A distinct interface between vapor and liquid phases exists, hence both phases are continuous. To transfer heat, two resistance model is taken zero resistance model is taken for gas phase and heat transfer coefficient for water phase. It was assumed that bottom temperature is equal to water bath temperature. Distillate collector temperature is equal to glass temperature. For drop formation on the condensing cover adhesion forces are taken. All sides are assumed adiabatic so there is no heat loss to surrounding. No slip boundary condition is specified for liquid phase and free slip boundary condition is specified for Vapour phase.

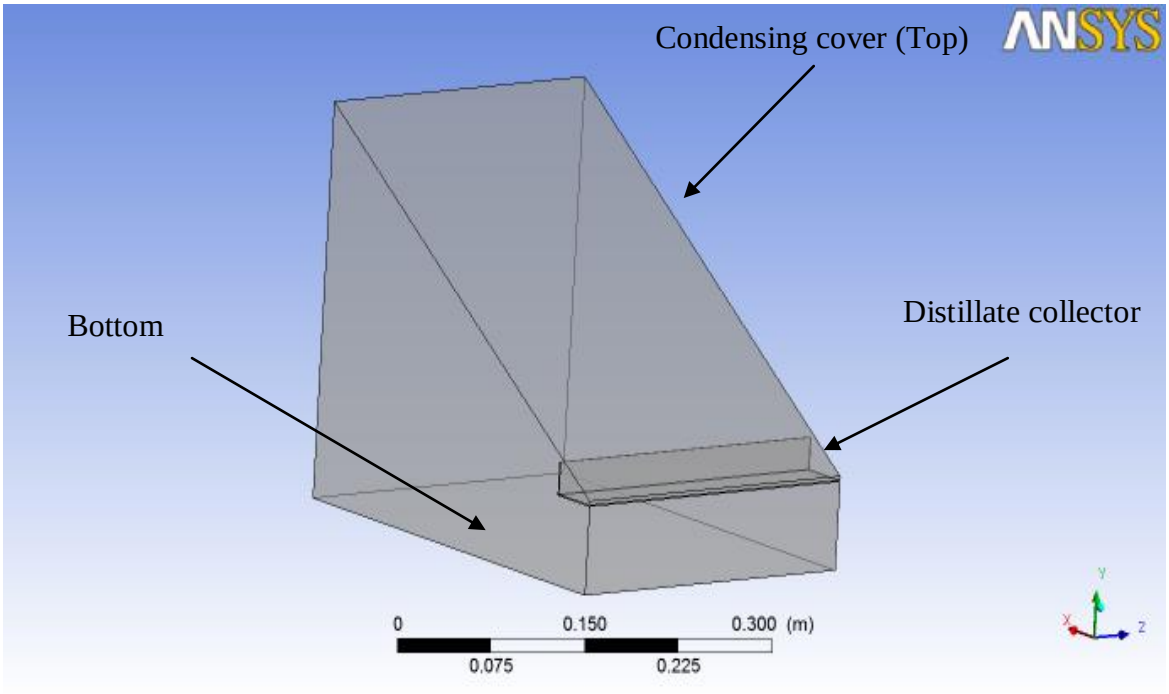

Fig 3.6: Domain in CFX pre.

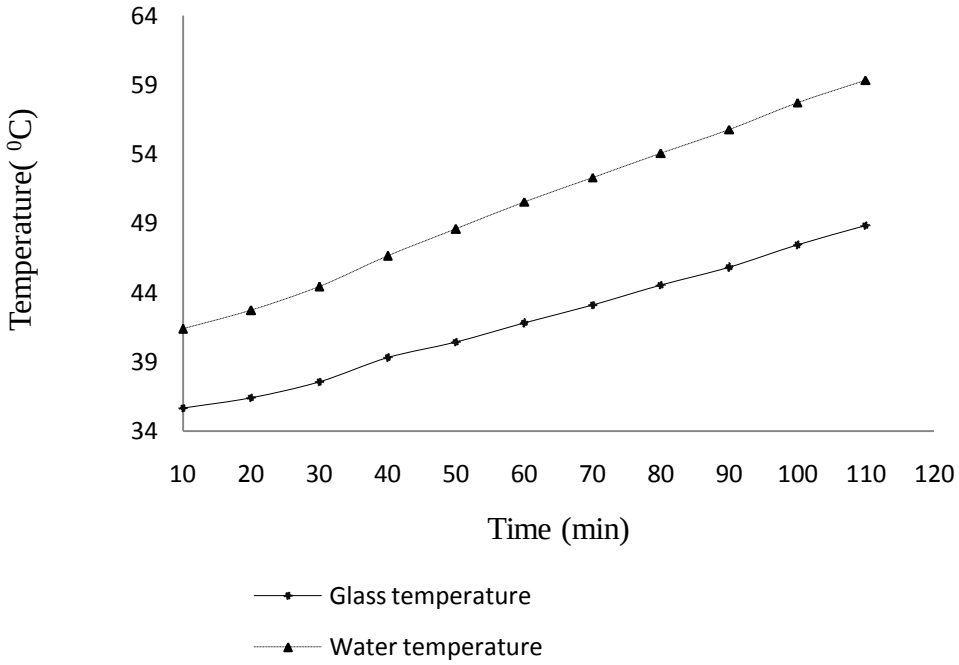

Fig 3.7: Temperature variation of different components of solar still for 15^0 inclination [7].

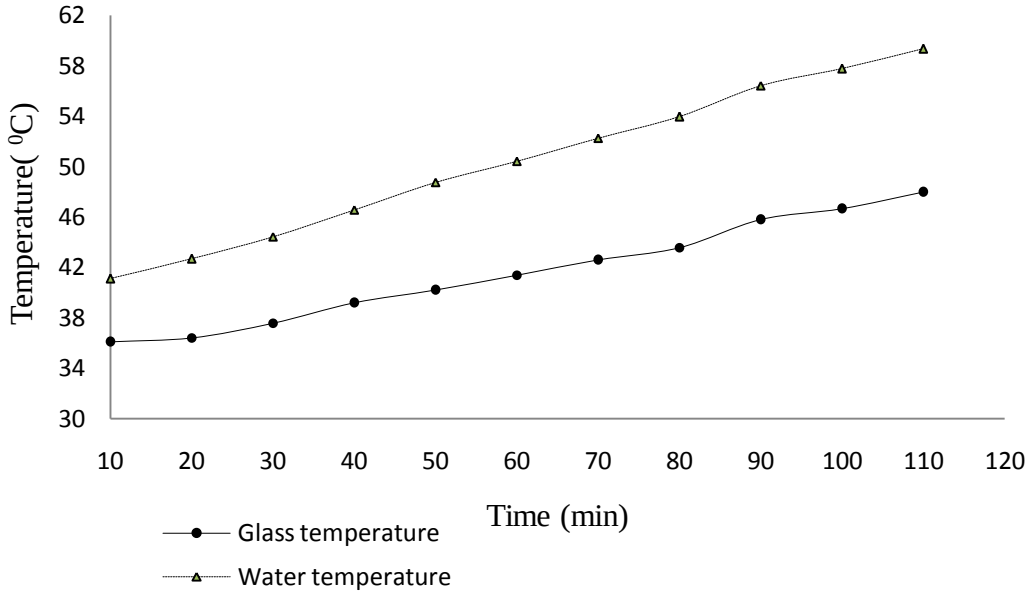

Fig 3.8: Temperature variation of different components of solar still for 30^0 inclination [7].

Figs 3.7 and 3.8 shows glass and water temperature based on the experimental data. Glass temperature and bottom temperature are taken according to experimental data. Water level in the basin is taken as 30mm so the water and mixture volume fraction are taken as 0.23 and 0.77 for 15^0 slope. For 30^0 slope water level is 30mm and water and mixture volume fraction is taken as 0.16 and 0.74.

Table 3.4: The boundary conditions

Location	**Boundary Type**	**Boundary Details**	**Comments**
Top (condensing cover)	Wall	Fixed temperature wall	Condensing wall for drop formation adhesion forces were taken into account
Bottom	Wall	Temperature = 40^0 C to 60^0 C with 2^0C interval	Bottom temperature is equal to the bath temperature from which heat is given to the water
All four Sides Long wall Small wall Front	Wall	Adiabatic	No slip boundary condition specified for liquid phase and free slip for gas phase and all walls

Back			are also set to be adiabatic so that there is no heat loss to the surrounding
Distillate Collector	Wall	Distillate collector temperature = Glass cover temperature	To collect condensed water

3.2.2.4 Material Defination.

To set up the domain for 2-phase fluid (Multiphase) analysis. First of all fluid material have defined

Three types of material are as follows:

1. Liquid water
2. Water vapour
3. Air as an ideal gas

In ANSYS CFX 13 material named gas mixture was prepared by combining the water vapour and air. They are defined by using the variable composition mixture. The thermal properties of air and water vapour mixture are given in table

Table 3.5: Thermal properties of water

Density	958.37 [kg/m^3]
Molar Mass	18.02 [kg kmol^-1]
Specific Heat Capacity	4215.6 [J/kg/K]
Specific Heat Type	Constant Pressure
Dynamic Viscosity	0.00028182 [Pa s]
Thermal Conductivity	0.67908 [W m^-1 K^-1]
Thermal Expansivity	0.000257 [K^-1]

Table 3.6: Thermal properties of air

Molar Mass of air	28.96 [kg kmol^-1]
Specific Heat Capacity	1.0044E+03 [J kg^-1 K^-1]
Specific Heat Type	Constant Pressure
Dynamic Viscosity	1.831E-05 [kg m^-1 s^-1]
Thermal Conductivity	2.61E-2 [W m^-1 K^-1]

Table 3.7: Thermal properties of water vapour

Molar Mass	18.02 [kg kmol^-1]
SPECIFIC HEAT CAPACITY	NASA Format
TEMPERATURE LIMITS	Lower Temperature = 300 [K] Midpoint Temperature = 340 [K] Upper Temperature = 373 [K]
Dynamic Viscosity	9.4E-06 [kg m^-1 s^-1]
Thermal Conductivity	193E-04 [W m^-1 K^-1]

3.2.2.5 CFX Solver

CFX Solver performs the iteration process when the iteration process comes to the end of convergence as shown in Fig 3.9 it provides the results to the CFX Post Processor.

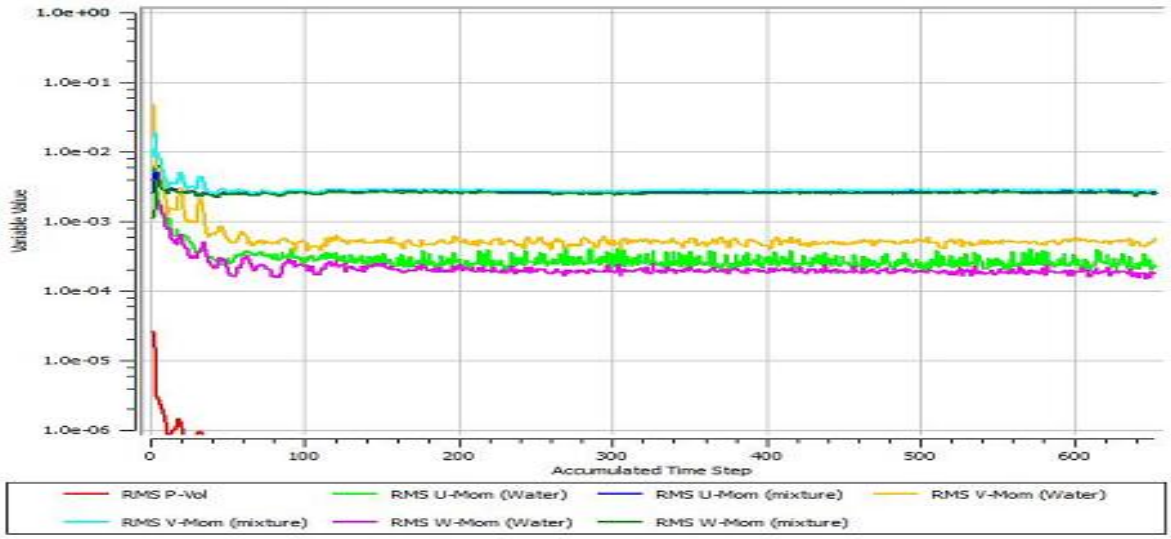

Fig 3.9: Convergence graph of fluid flow simulation

3.2.2.6 CFX Post

CFX Post Processor provides the results contours and temperature distribution diagrams of fluid flowing in the solar still. Results are shown in chapter 4.

3.3 EXPERIMENTAL METHODOLOGY

The experiments were conducted by Kumar and Tiwari [7]. The experimental set-up includes a constant temperature bath, condensing covers at different inclinations, digital temperature indicator, well calibrated thermocouples and a measuring jar. The water is

heated by bath heating coils and the stirrer maintains a uniform temperature and a proportional control facilitates setting a desired temperature. All these are seen through two transparent sides of the bath. The schematic diagram of a system is given in Fig 3.1 and a photograph of the same is shown in Fig. 3.10. There were five thermocouples attached to a digital temperature indicator having the least count of 0.1 °C. Two thermocouples show outside and inside surface temperatures of the condensing covers, respectively, and three others record vapor, water, and ambient room temperature. The experiments were conducted from 40°C to 80°C at intervals of 2°C under natural mode. The distillate output was collected in a transparent measuring jar and was weighed on a scale with an accuracy of 0.1 g.

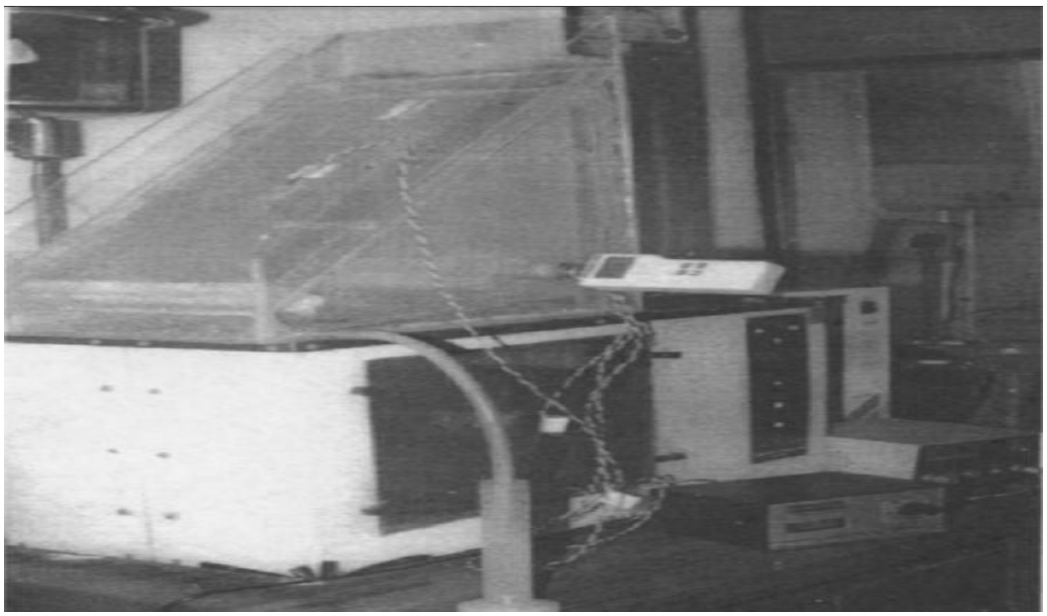

Fig 3.10: Photograph of experimental setup of Kumar and Tiwari [7]

CHAPTER 4
RESULTS AND DISCUSSIONS

4.1 COMPUTATIONAL FLUID DYNAMIC SIMULATIONS

The performance of a solar still depends upon the glass cover angle, depth of water, fabrication materials, temperature of water in the basin and insulation thickness which could be modified for improving the performance. So Computational fluid dynamic (CFD) simulation approach is adopted to analyse the effect of different glass cover angles on the rate of evaporation to obtain the maximum yield. In evaporation water phase change takes place which is very difficult to model mathematically. The complicated thermal relationship involved in the phase change of water from liquid to gas phase is accurately solved by using CFD. The numerical analysis using CFD CFX 13.0 is used to determine the temperature distribution and behavior of buoyant flow. In the present work, following the simulation methodology and utilizing the boundary conditions as mentioned in detail in Chapter 3, simulations were completed to obtain the following sets of results:

1. Water temperature distribution inside the solar still.
2. Vapour temperature distribution inside the solar still.
3. Determination of heat transfer coefficient by Kumar and Tiwari and Dunkle models using CFD simulated data.

4.1.1 Evaporation Simulation Through Condensing Covers At Different Inclinations.

The evaporation process is simulated for two condensing covers at inclinations 15^0 and 30^0. The evaporative area is same for both the condensing covers. The solar still selected for the simulation is the single slope solar still. Slope of inclination is varied by changing the higher height where as the lower height is kept constant. Simulations through different inclination are shown bellow.

4.1.2 Temperature Distribution

4.1.2.1 Simulation for 15^0 inclination.

Fig4.1-4.11 shows the results of simulation runs 40-60^0C with 2^0C rise in intervals. The water in the still starts warming due to heat supplied from the bottom. Water in the system vaporizes. Temperature difference between water and glass leads to vapour condensation. The bottom of the solar still is kept at different temperatures from 40^0C to 60^0C. Due to

temperature source applied at the bottom non uniform temperature distribution is generated in the domain. To observe temperature distribution in Y-axis, (vertical direction in solar still) temperature plots have been made. Temperature distribution given by transient thermal analysis is exported (In Excel file) to plot in vertical direction (Y- axis). Information in this file is related to each node of the model mesh. It extracts complete information regarding each node i.e. node number, nodal co-ordinates and temperature generated at each node. As temperature is varying from top to bottom, the line has drawn in vertical direction in the centre of the solar still and temperature graphs are drawn with respect to Y-axis.

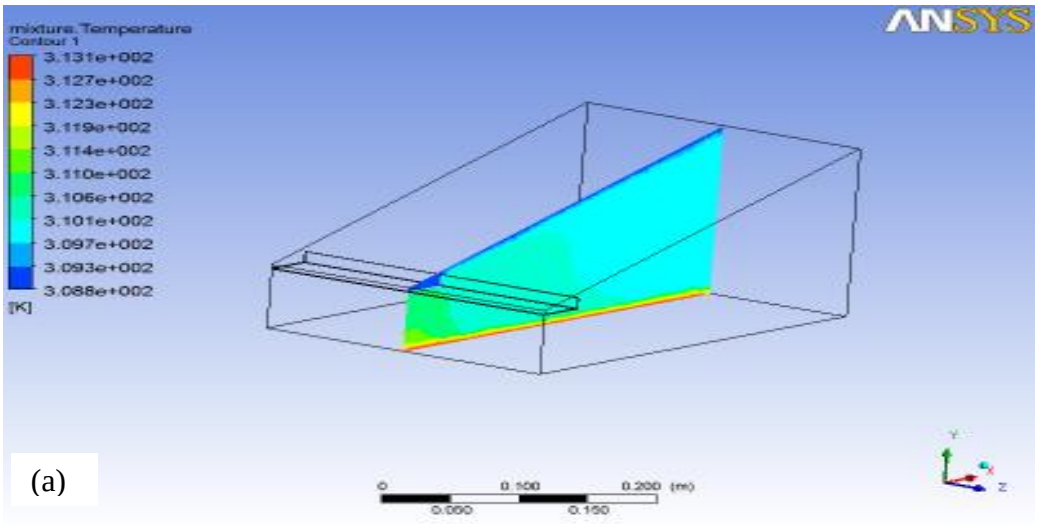

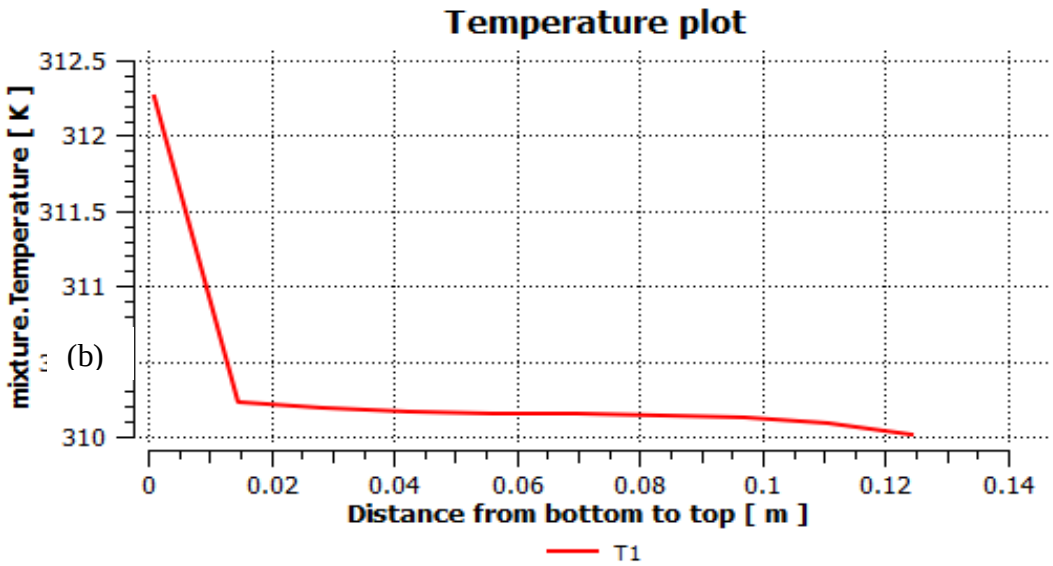

Fig. 4.1 a) Gas mixture temperature on a plane inside the solar still when bath temperature is 40^0 C for 15^0 inclination. b) Temperature Plot.

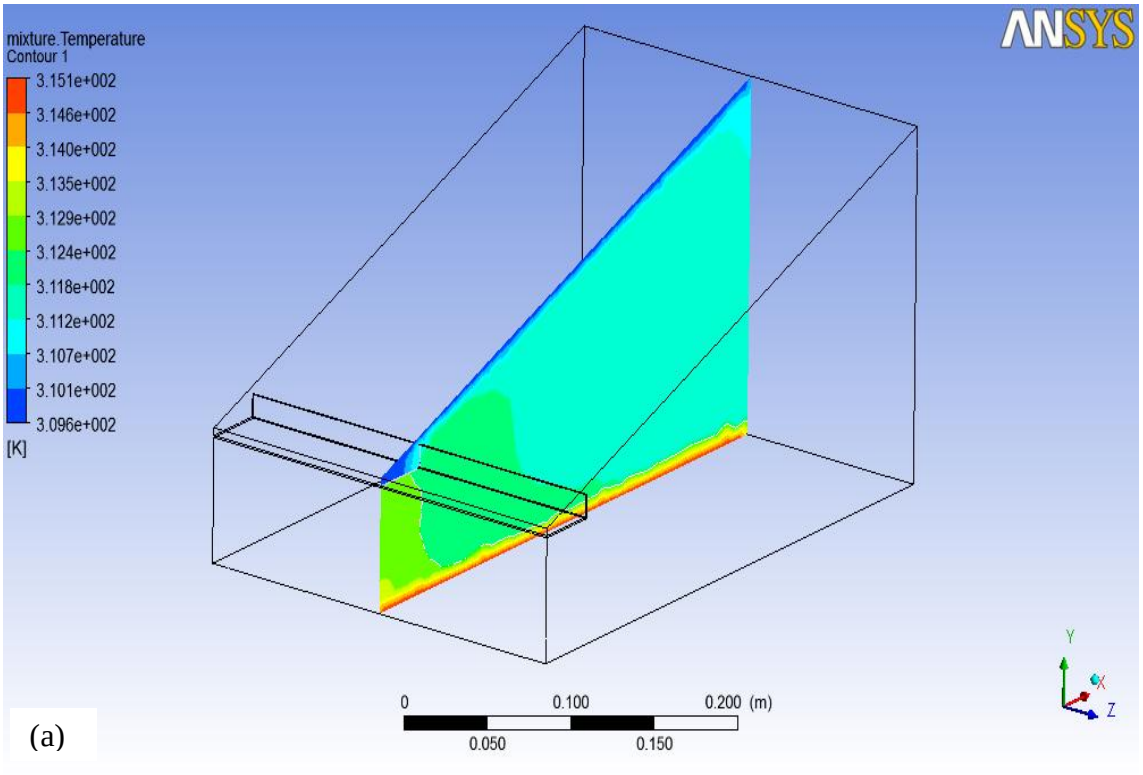

(a)

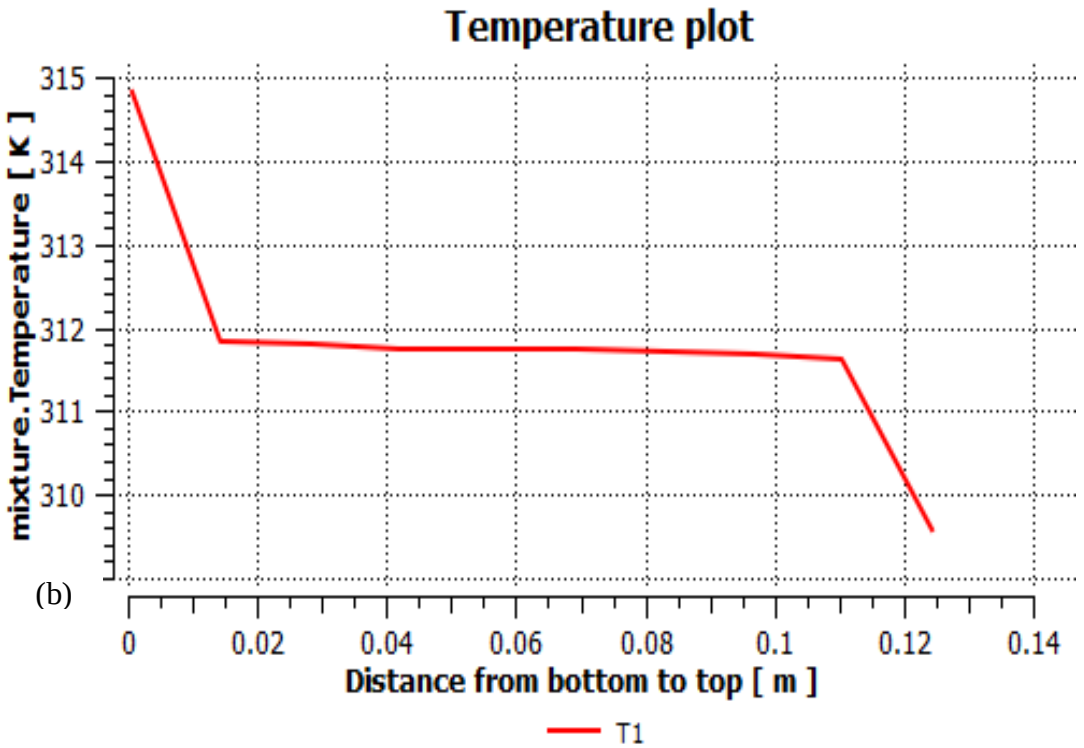

(b)

Fig. 4.2 a) Gas mixture temperature on a plane inside the solar still when bath temperature is 42^0 C for 15^0 inclination. b) Temperature Plot.

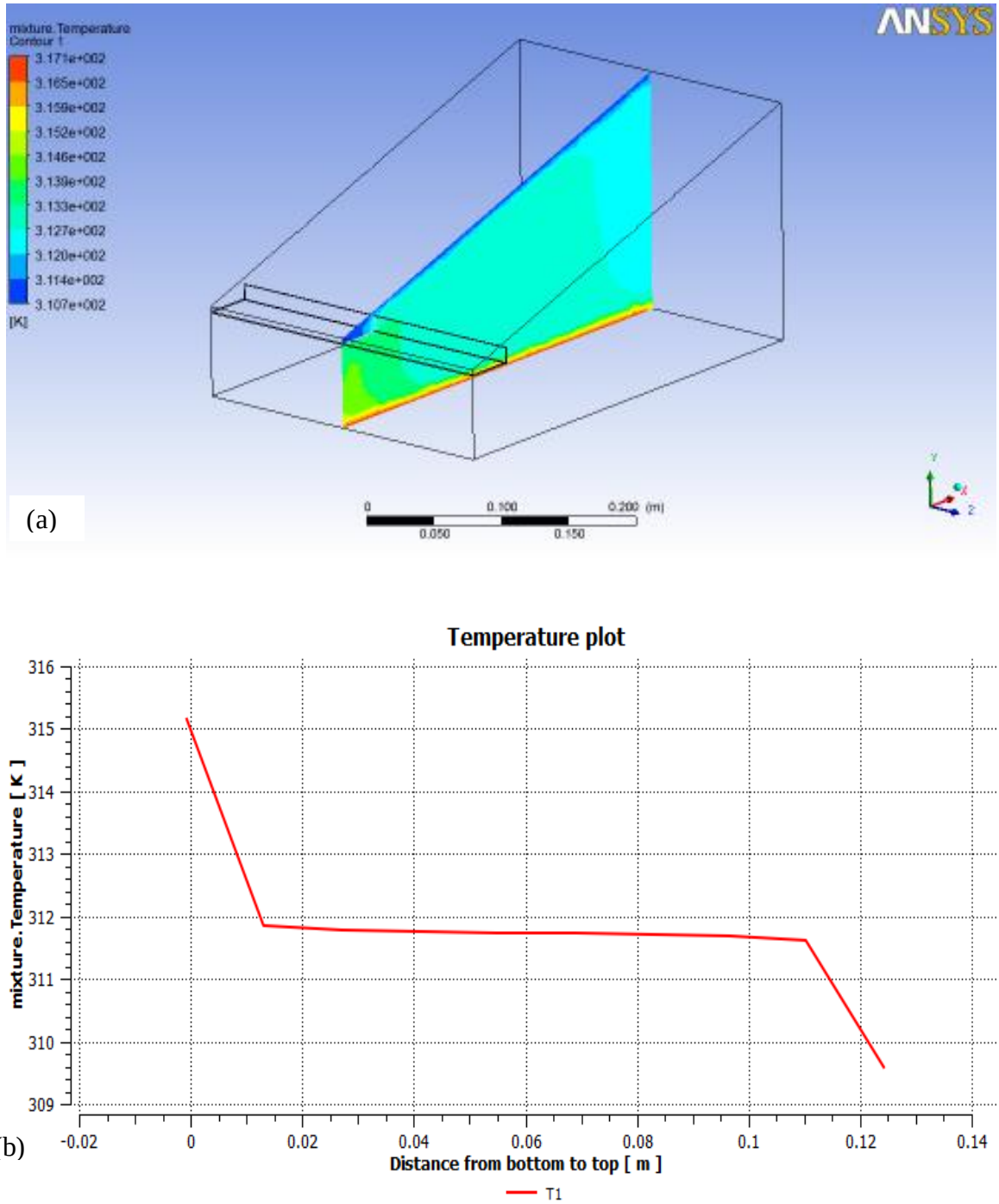

Fig. 4.3 a) Gas mixture temperature on a plane inside the solar still when bath temperature is 44^0 C for 15^0 inclination. b) Temperature Plot.

To represent results of temperature distribution in the form of 3-D colored contour plots the images have been taken for each individual simulation and few of them as sample representation are shown in Figure 4.1-4.11. Red region in the contour plots represent highest temperature and blue region represent the lowest temperature in the domain it is clearly seen in the figure due to large temperature difference between glass and water

temperature water condenses on the glass. The temperature applied at bottom result an increase in temperature of gas there is average rise in temperature about 3^0C.

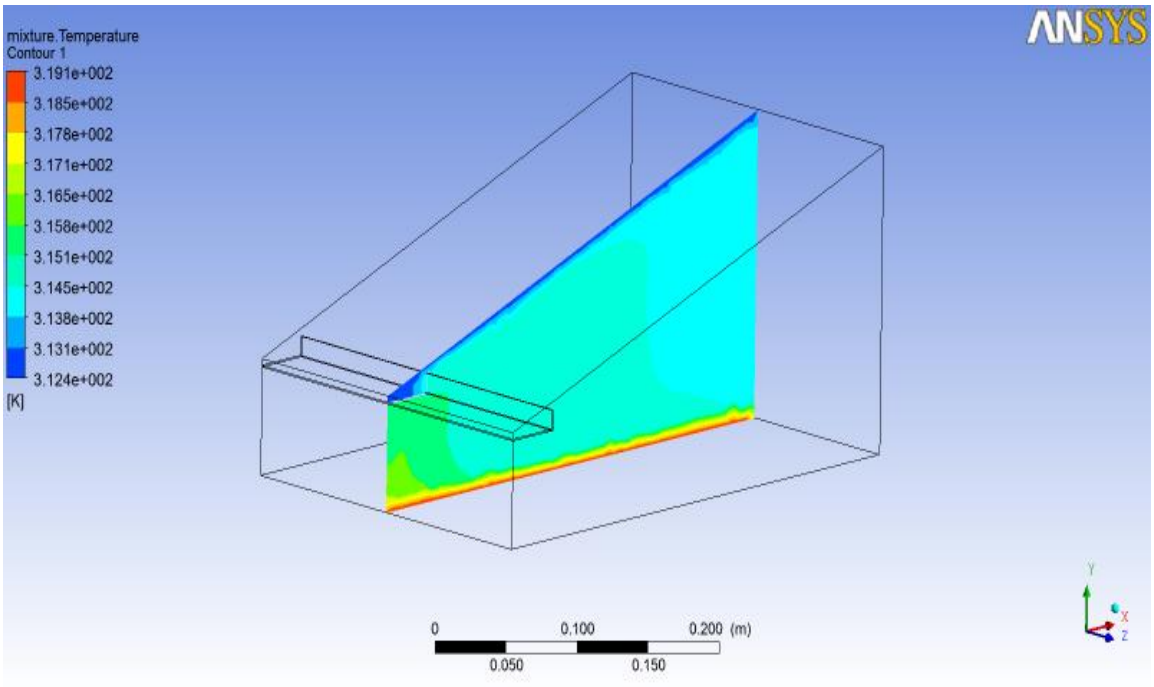

(a)

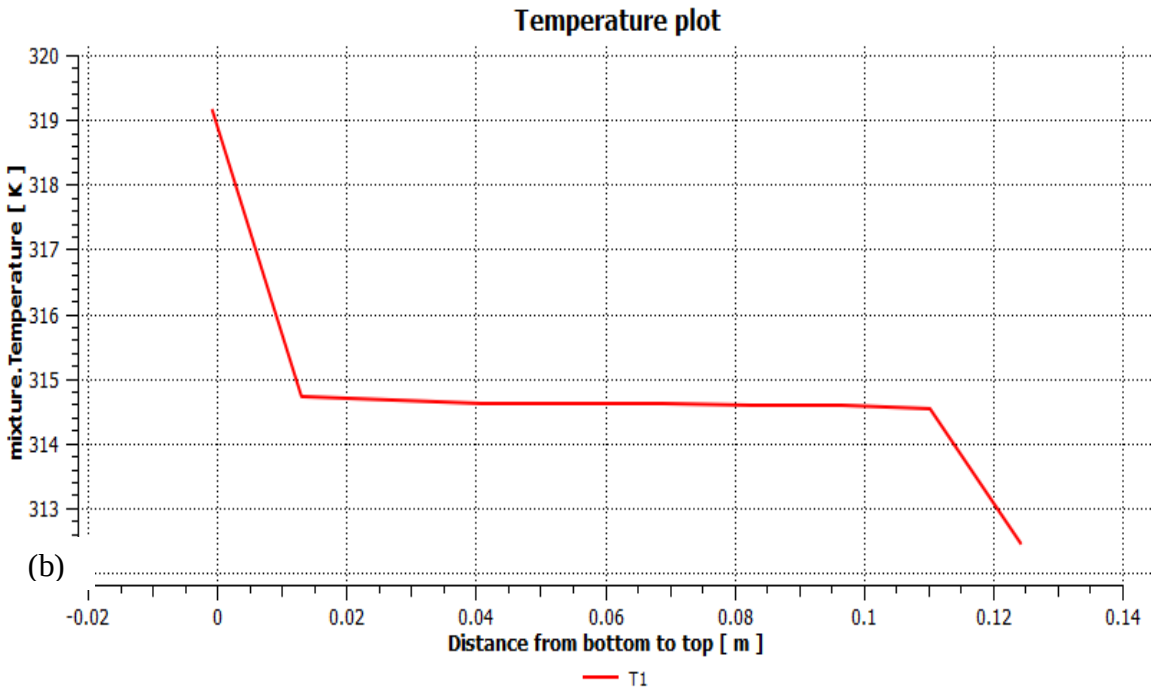

(b)

Fig. 4.4 a) Gas mixture temperature on a plane inside the solar still when bath temperature is 46^0 C for 15^0 inclination. b) Temperature Plot.

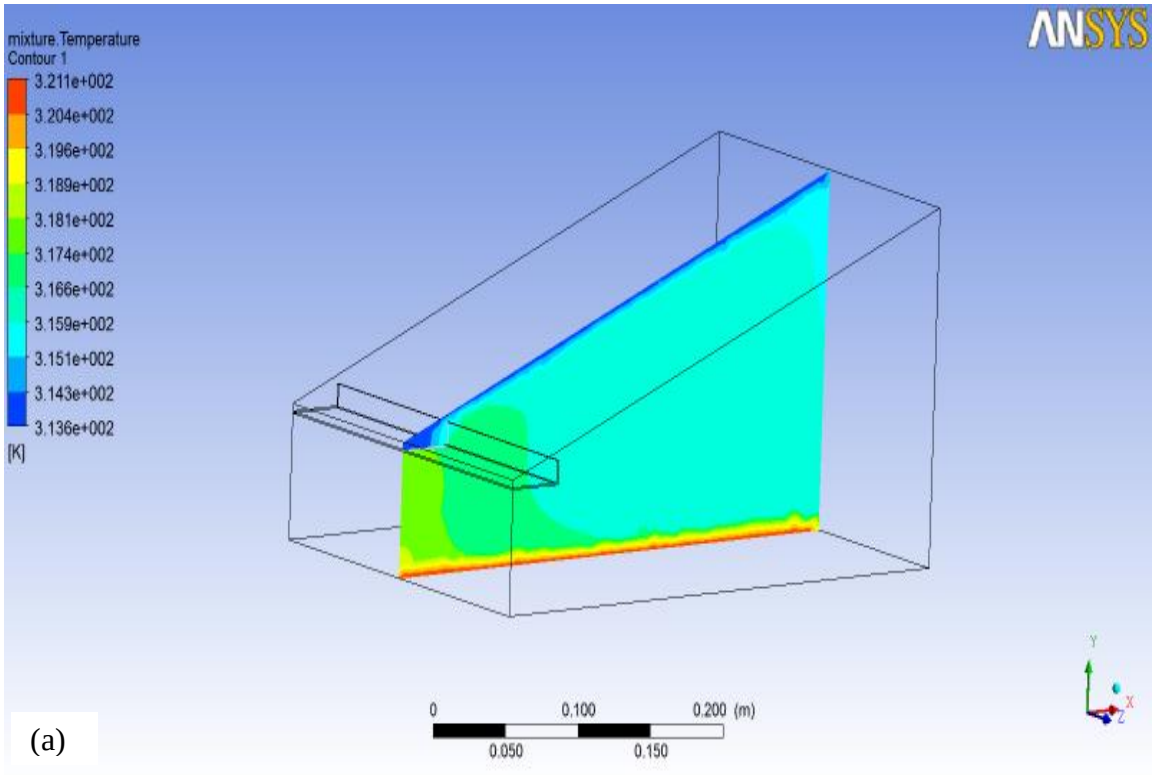

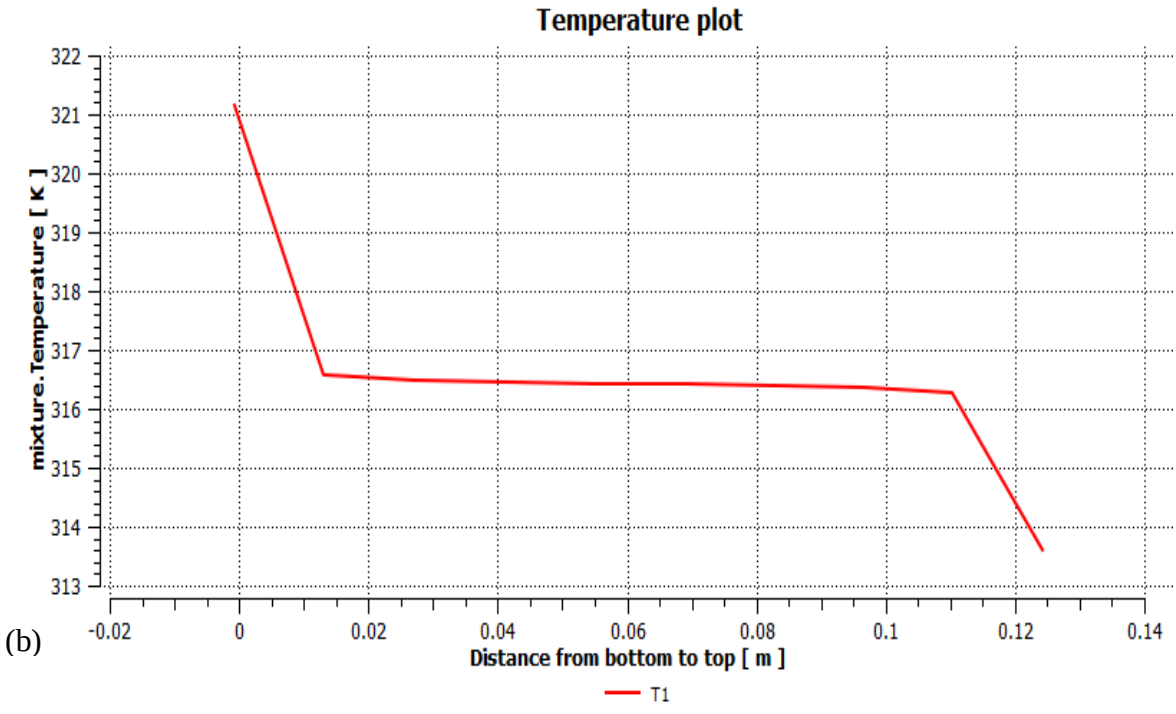

Fig. 4.5 a) Gas mixture temperature on a plane inside the solar still when bath temperature is 48^0 C for 15^0 inclination. b) Temperature Plot.

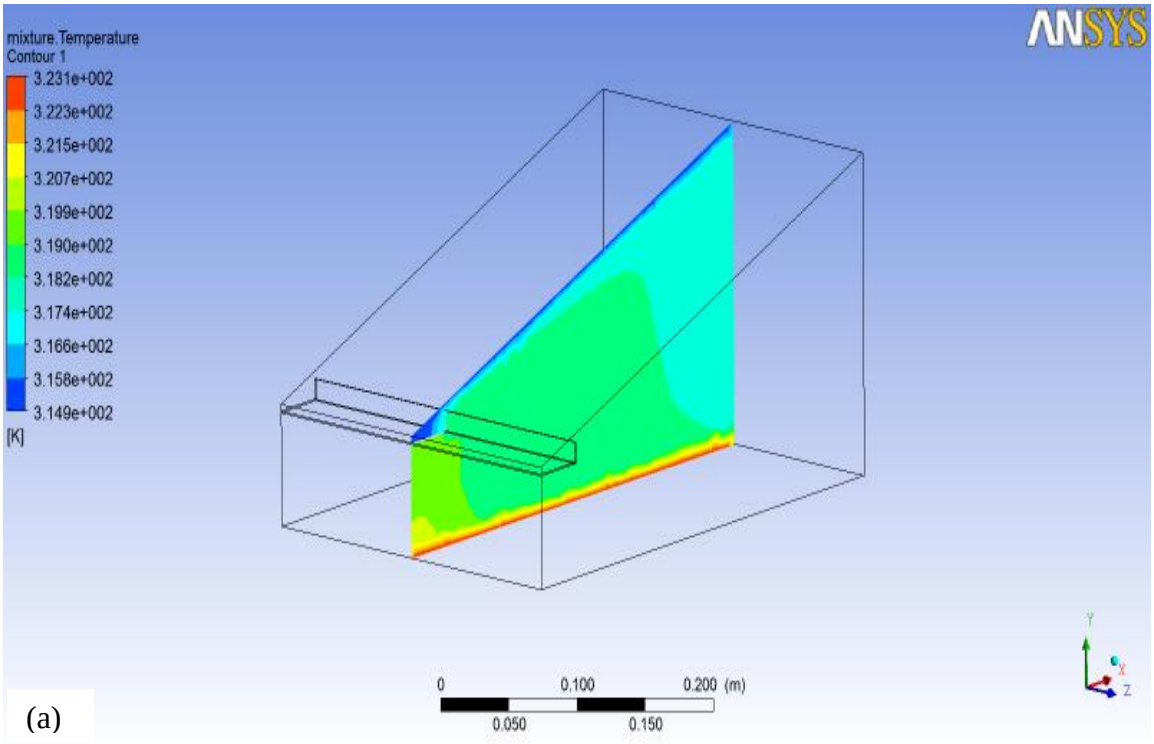

(a)

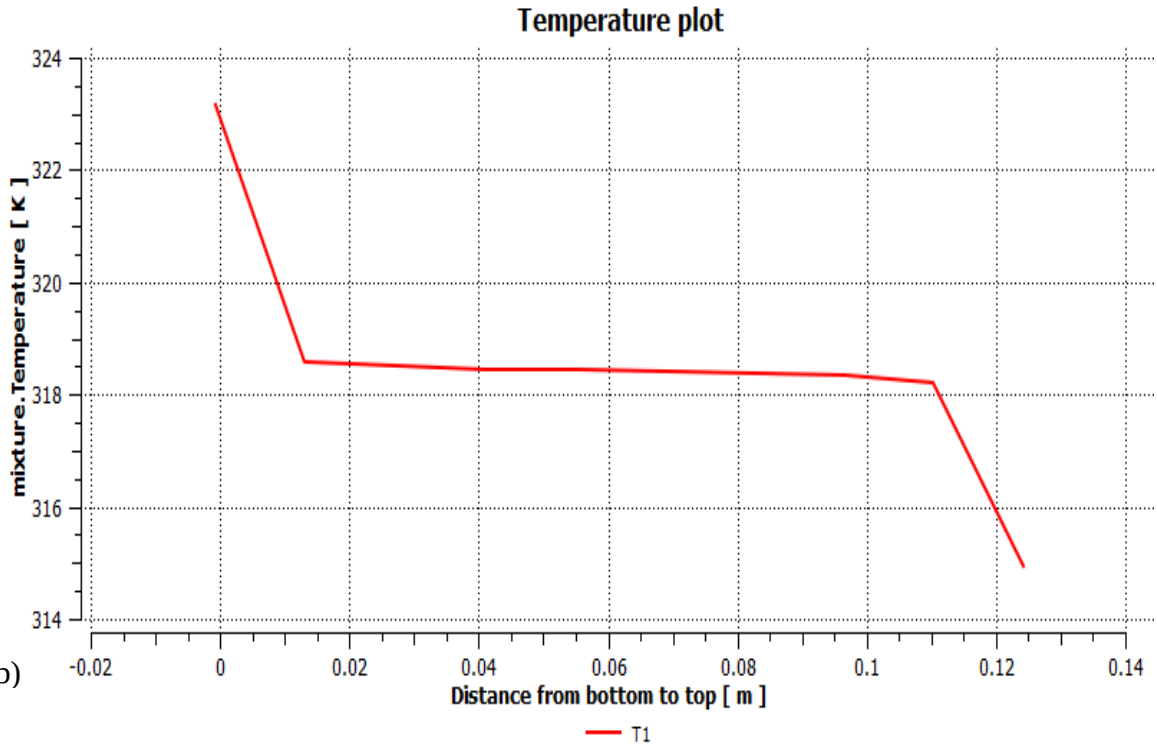

(b)

Fig. 4.6 a) Gas mixture temperature on a plane inside the solar still when bath temperature is 50^0 C for 15^0 inclination. b) Temperature Plot.

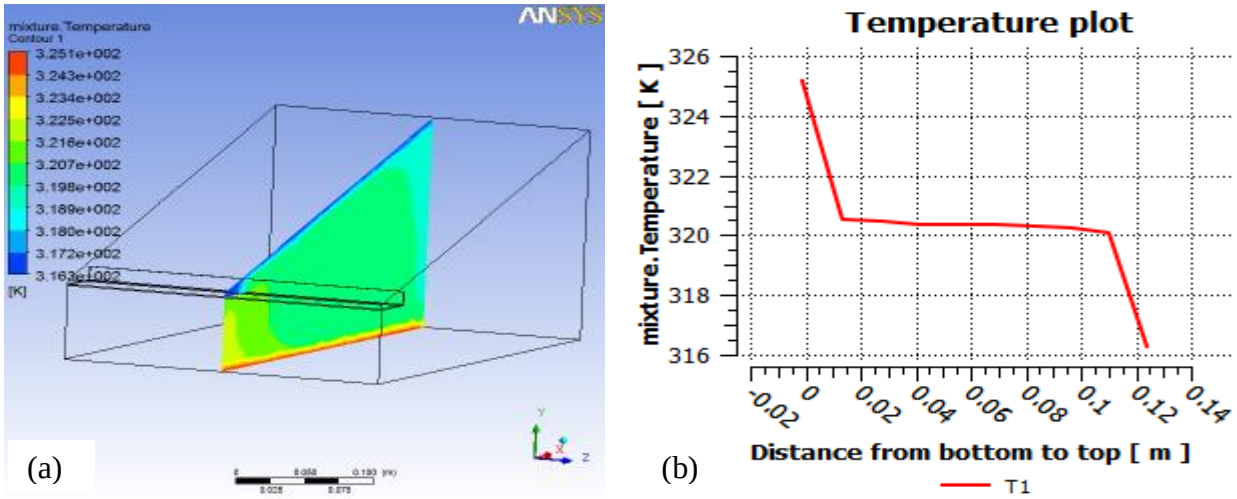

Fig. 4.7 a) Gas mixture temperature on a plane inside the solar still when bath temperature is 52^0 C for 15^0 inclination. b) Temperature Plot.

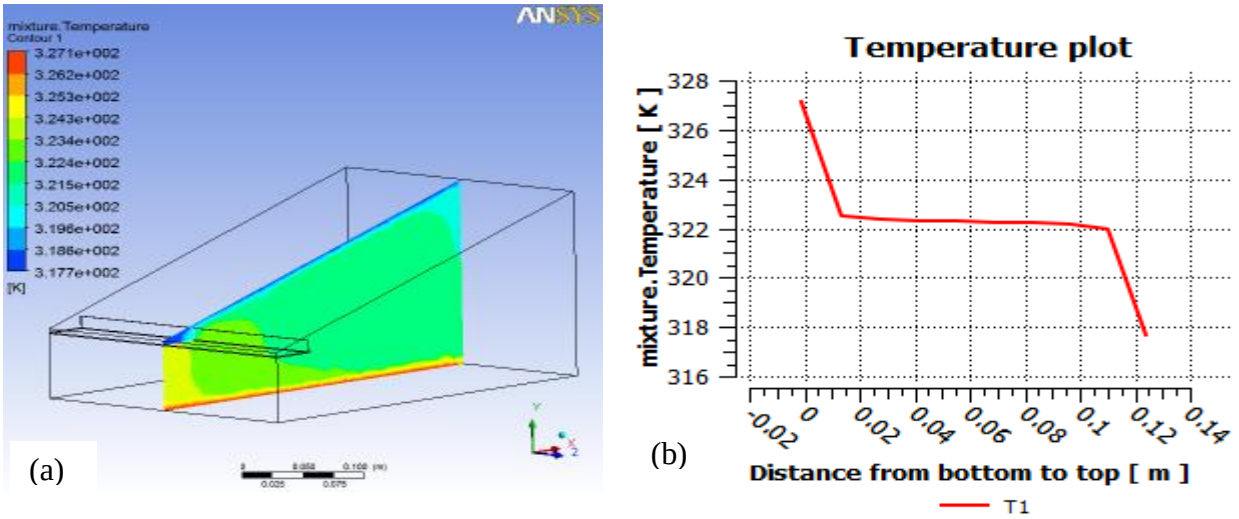

Fig. 4.8 a) Gas mixture temperature on a plane inside the solar still when bath temperature is 54^0 C for 15^0 inclination. b) Temperature Plot.

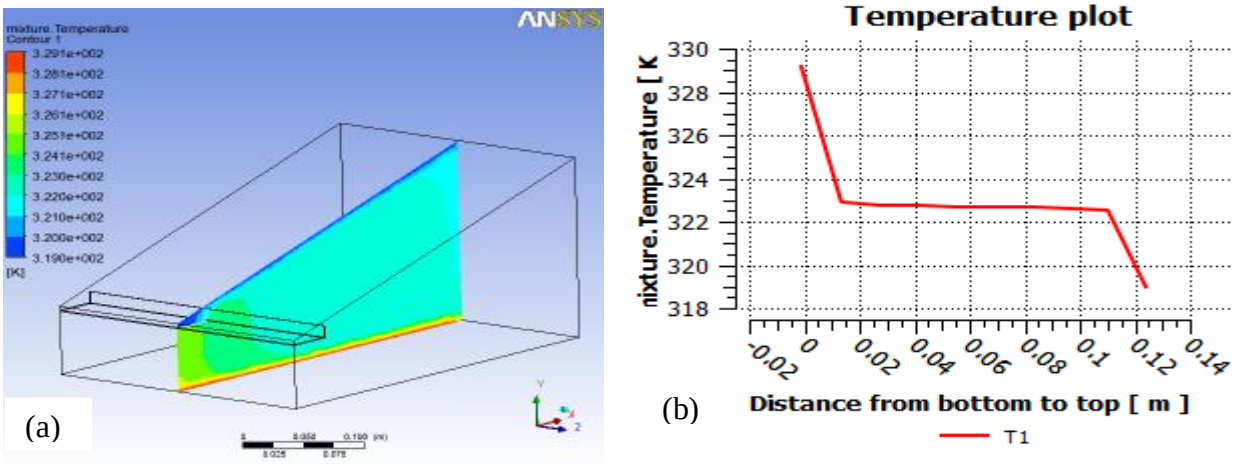

Fig. 4.9 a) Gas mixture temperature on a plane inside the solar still when bath temperature is 56^0 C for 15^0 inclination. b) Temperature Plot.

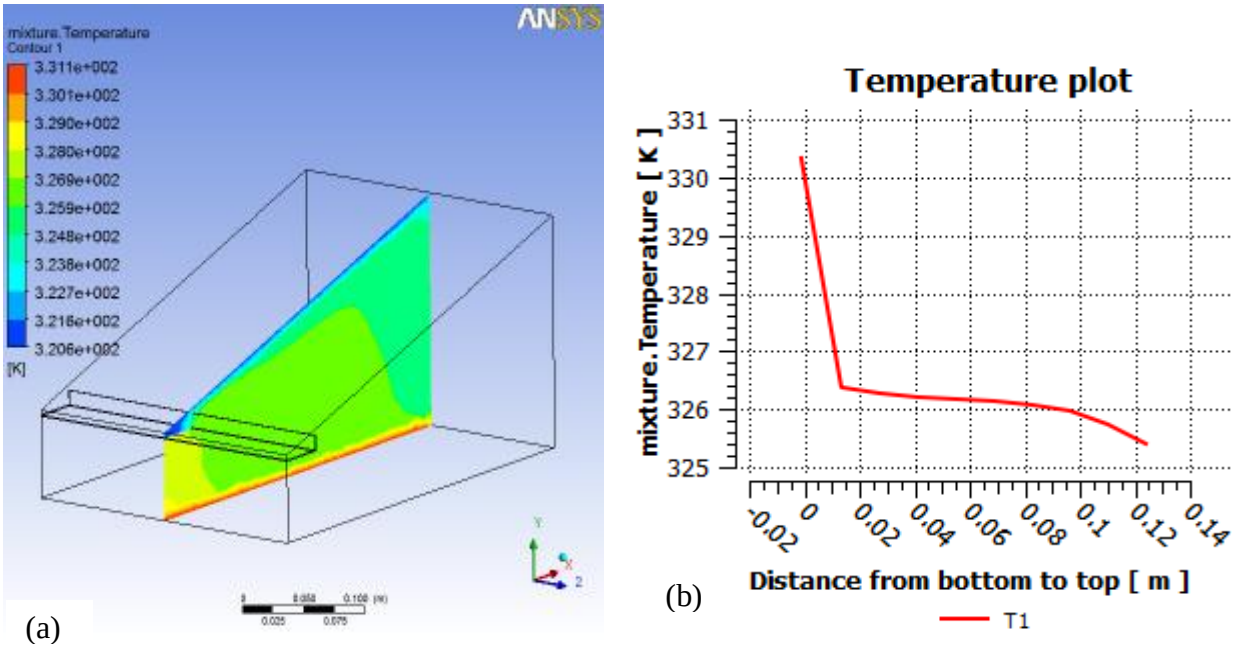

Fig. 4.10 a) Gas mixture temperature on a plane inside the solar still when bath temperature is 58^0 C for 15^0 inclination. b) Temperature Plot.

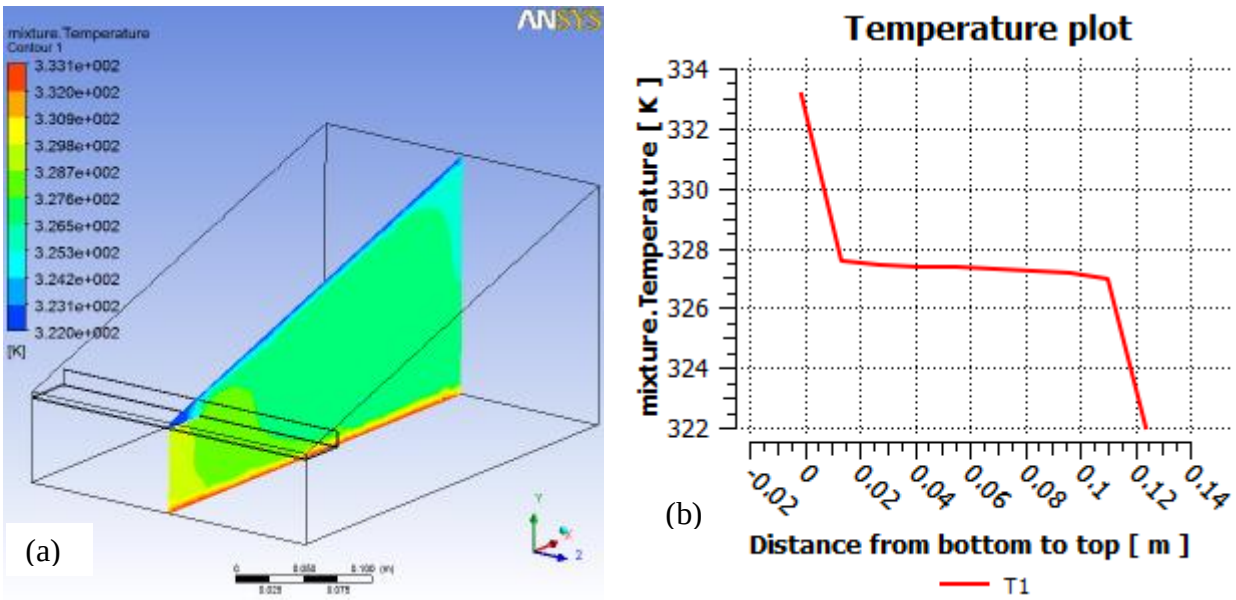

Fig. 4.11 a) Gas mixture temperature on a plane inside the solar still when bath temperature is 60^0 C for 15^0 inclination. b) Temperature Plot.

4.1.2.2 Simulation for 30^0 inclination.

To analyze the temperature variation in solar still another set of simulation is done at 30^0 inclination. The input parameter is bath temperature from 40^0 to 60^0 C with 2^0C rise in interval. The difference is only change in inclination by changing the higher height dimensions. Similarly as explained above Fig4.12-4.16shows the results of simulation runs.

Heat is applied at the bottom so the temperature is maximum at the bottom and it decreases as we are moving away from the bottom. To represent results of temperature distribution in the form of 3-D colored contour plots the images have been taken for each individual simulation and few of them as sample representation are shown in Figure 4.12-4.16. Red region in the contour plots represent highest temperature and blue region represent the lowest temperature in the domain it is clearly seen in the figure due to large temperature difference between glass and water temperature water condenses on the glass.

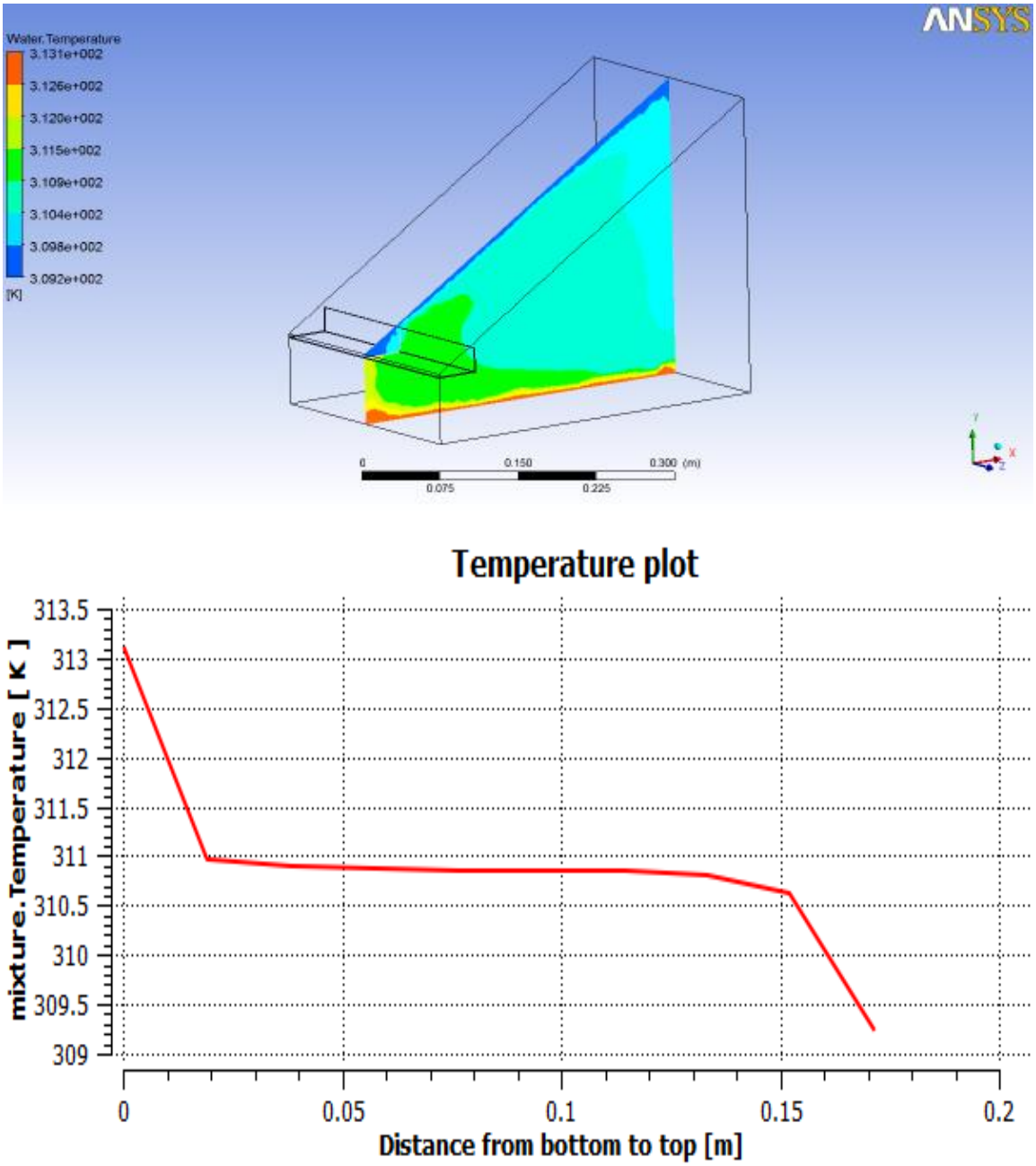

Fig. 4.12 a) Gas mixture temperature on a plane inside the solar still when bath temperature is 40^0 C for 30^0 inclination. b) Temperature Plot.

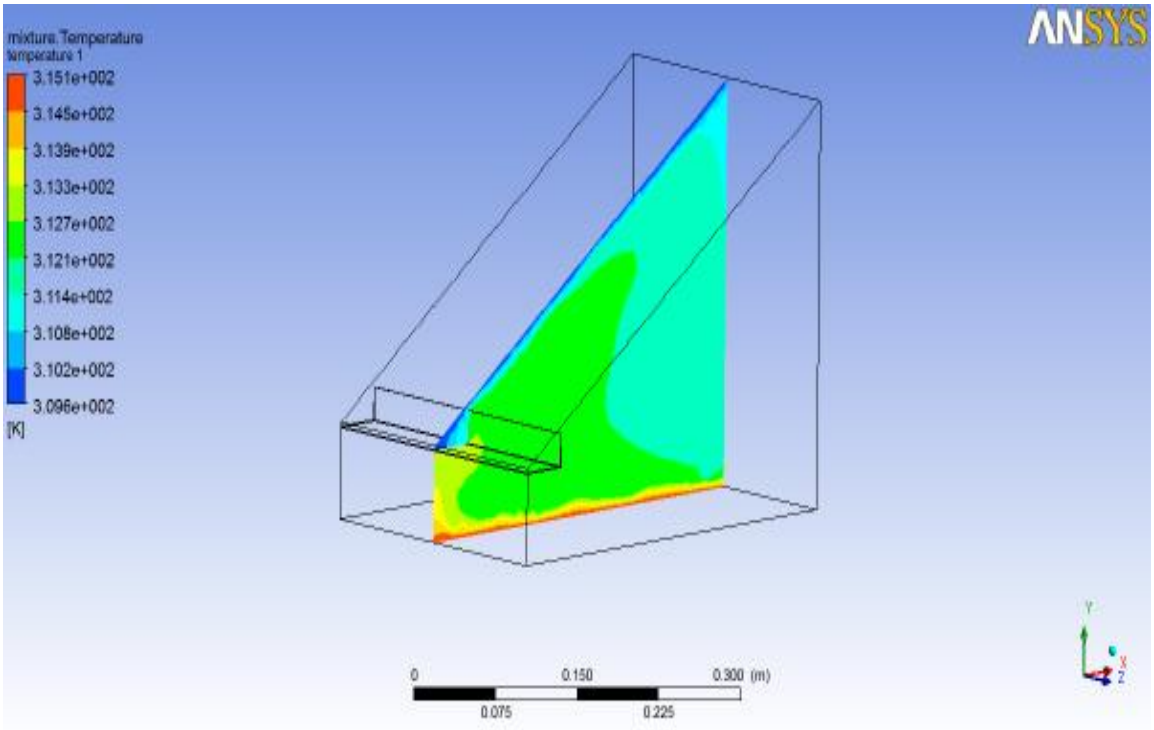

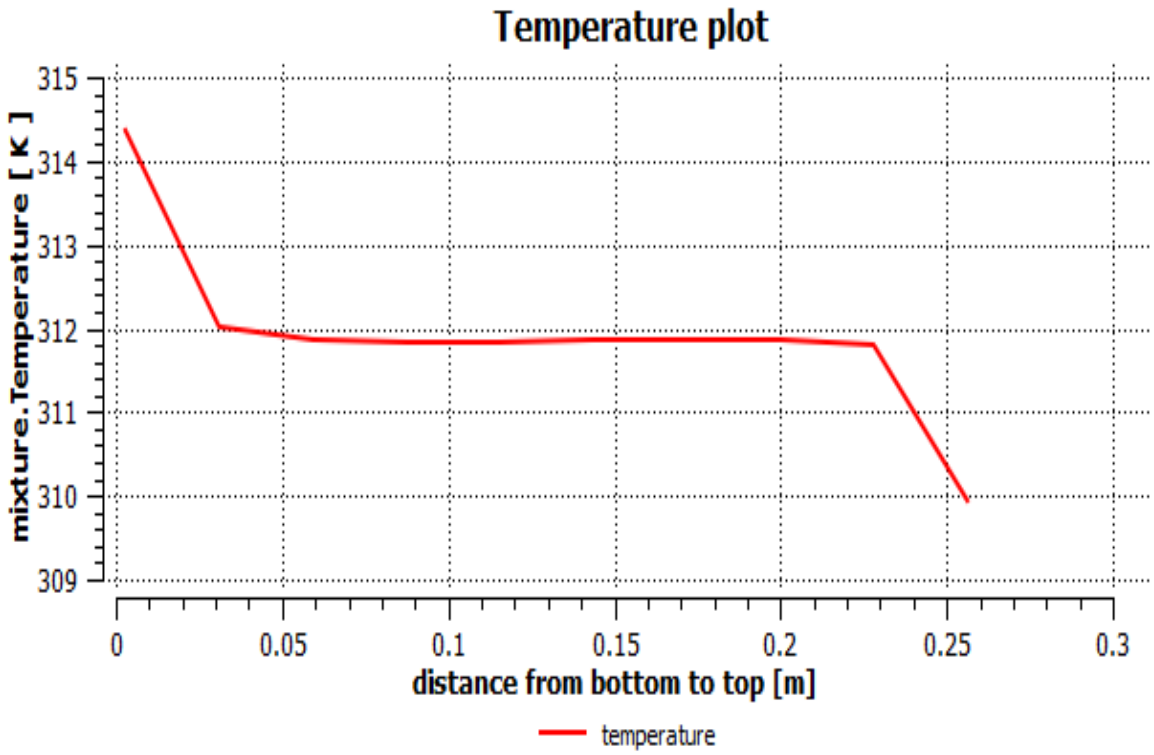

Fig. 4.13 a) Gas mixture temperature on a plane inside the solar still when bath temperature is 42^0 C for 30^0 inclination. b) Temperature Plot.

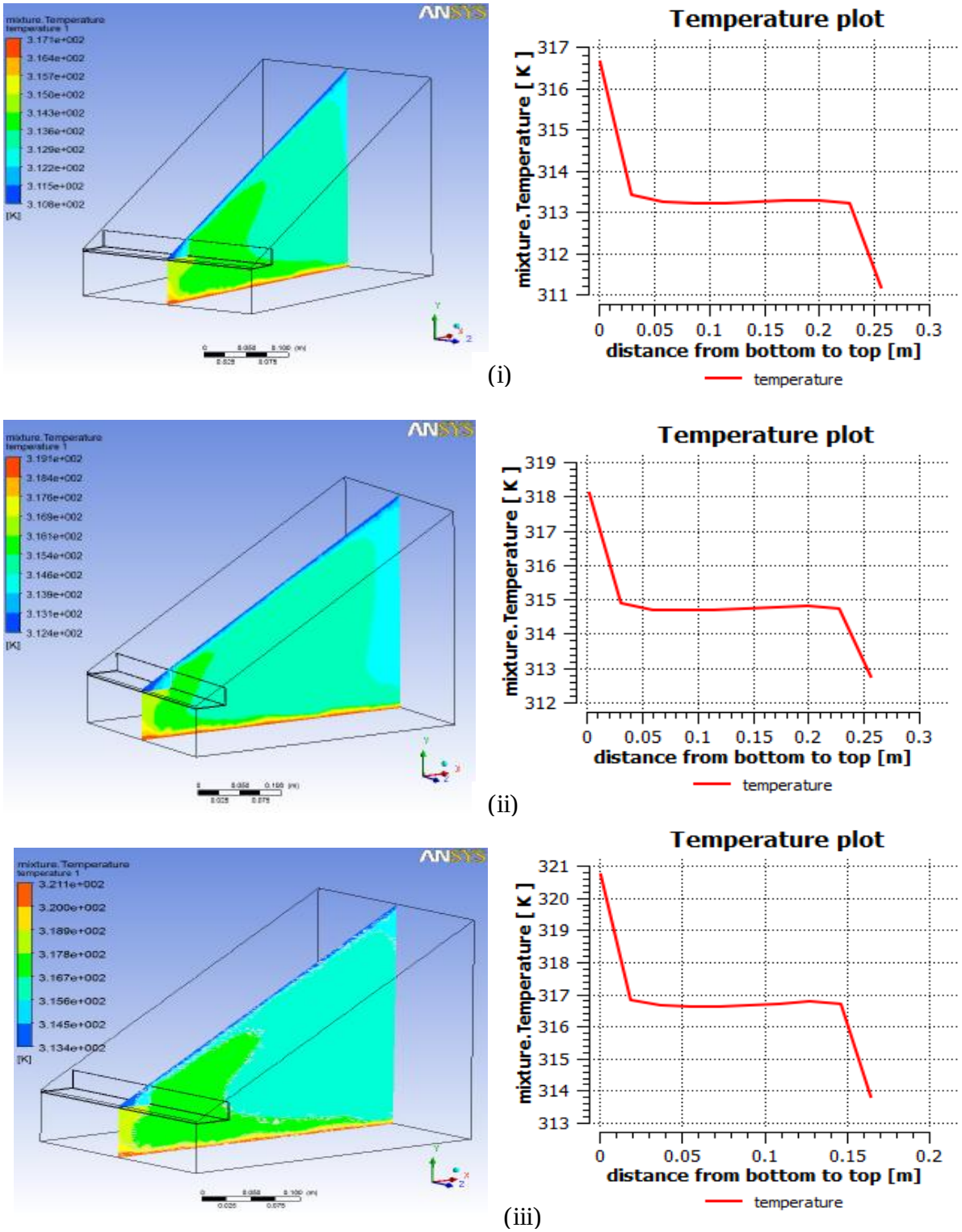

Fig. 4.14 Temperature Plot and Gas mixture temperature on a plane inside the solar still when bath temperature is (i) 44^0 (ii) 46^0 and (iii) 48^0C respectively for 30^0 inclination.

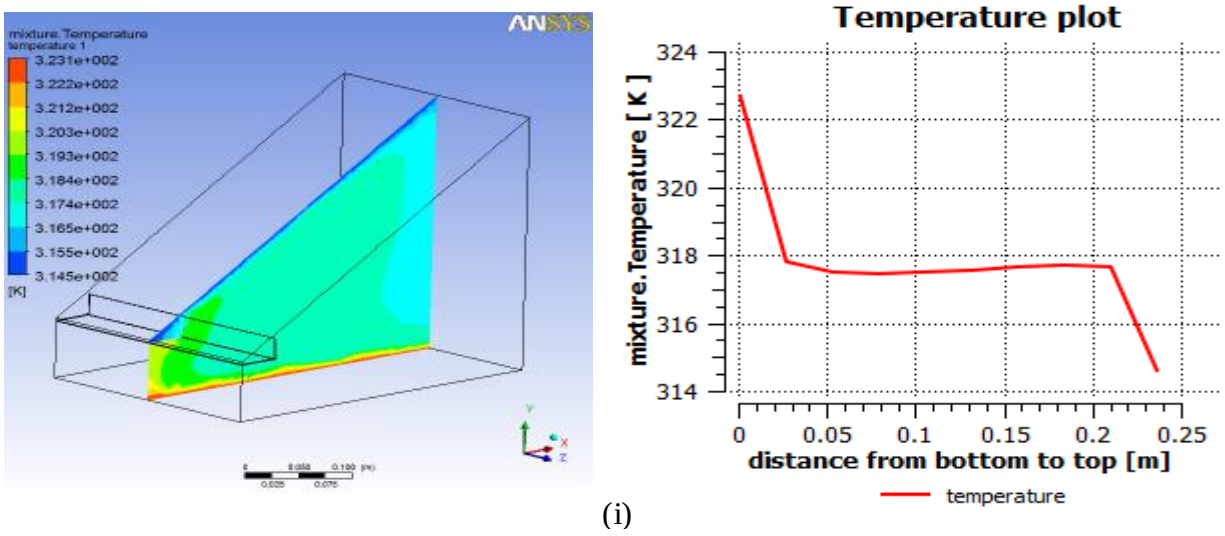

(i)

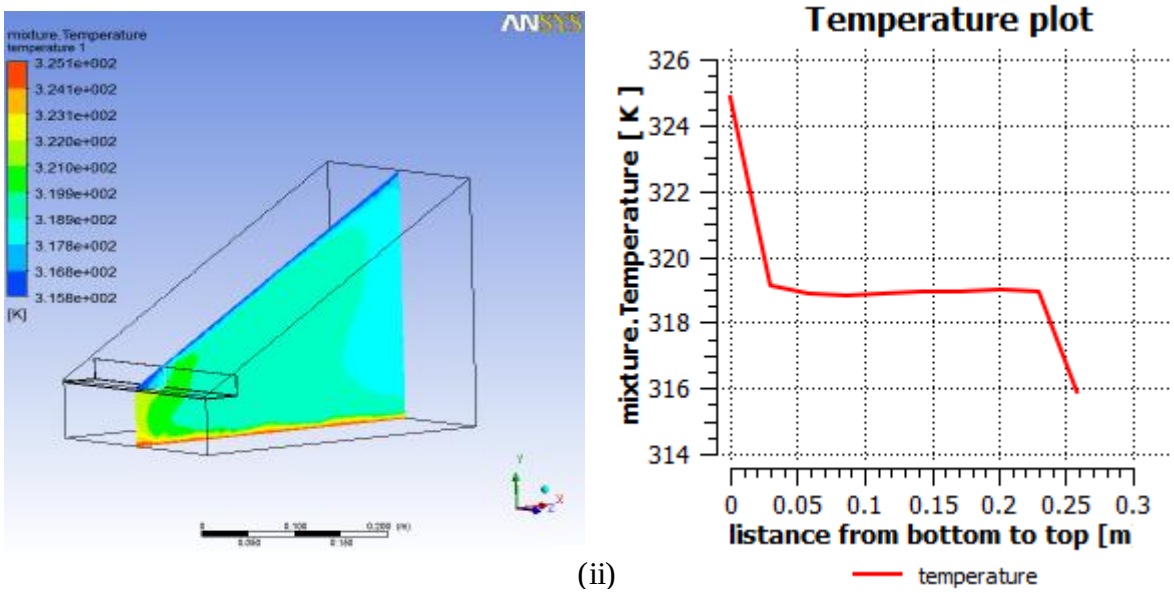

(ii)

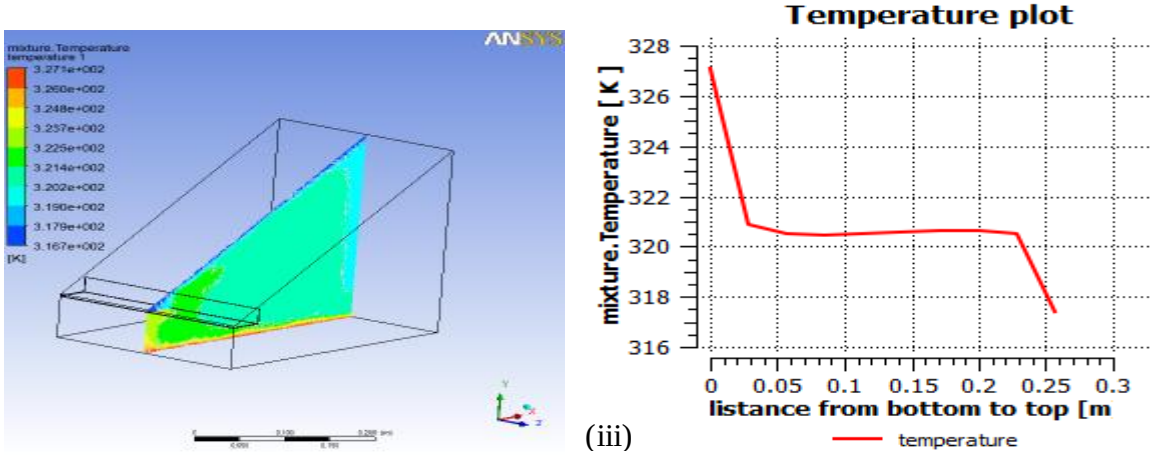

(iii)

Fig. 4.15 Temperature Plot and Gas mixture temperature on a plane inside the solar still when the bath temperature is (i) 50^0 (ii) 52^0 (iii) 54^0 C for 30^0 inclination.

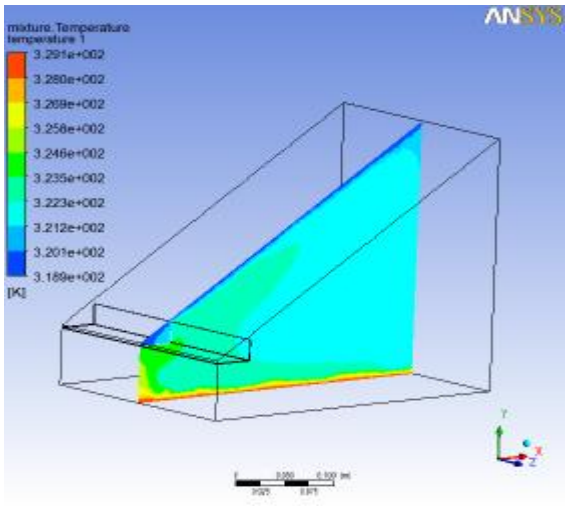

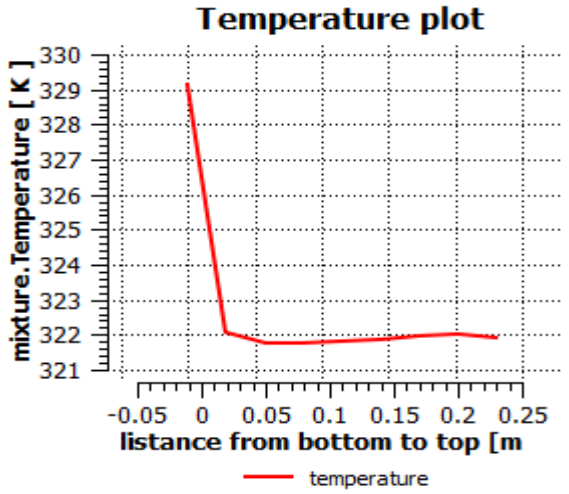

(i)

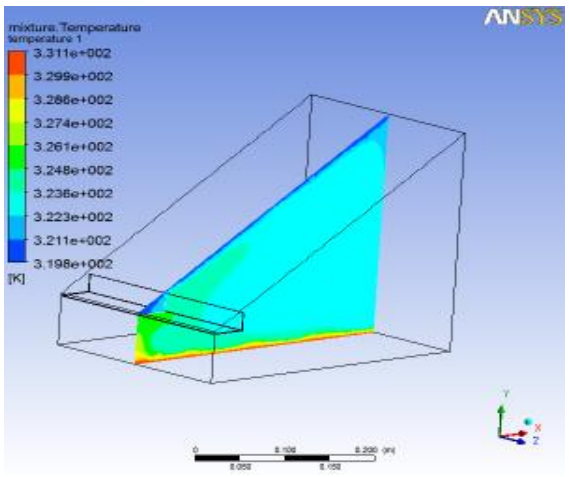

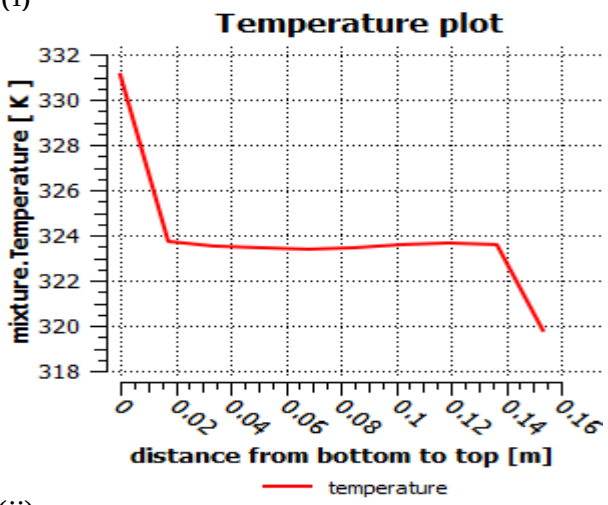

(ii)

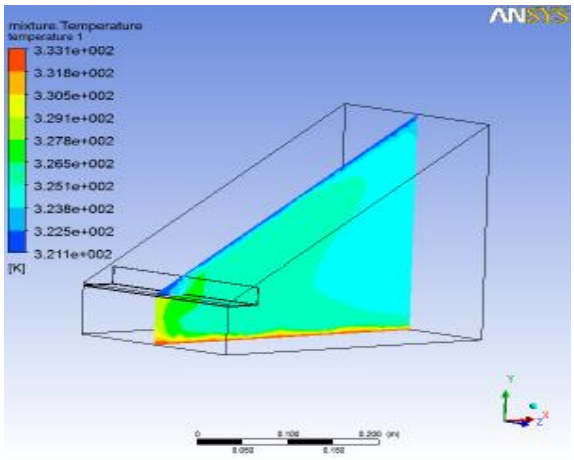

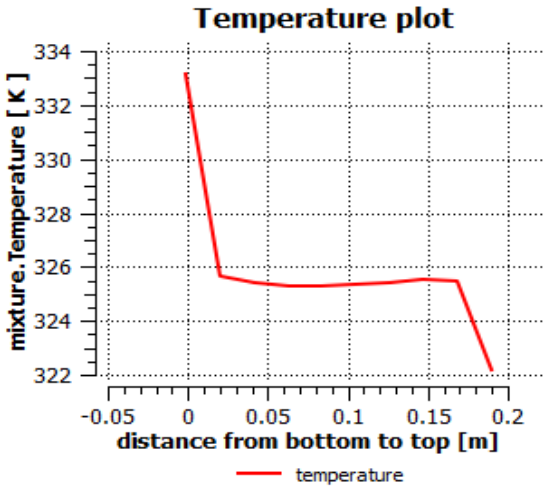

(iii)

Fig. 4.16 Temperature Plot and Gas mixture temperature on a plane inside the solar still when bath temperature is (i) 56^0 (ii) 58^0 and (iii) 60^0 C for 30^0 inclination.

4.1.2.3 Simulation result for 15^0 and 30^0 inclination for Water temperature.

To represent results of water temperature distribution in the form of 3-D colored contour plots the images have been taken for each individual simulation and few of them as sample representation are shown in Figure 4.17 and 4.19. Heat transfer occur between the bottom and the water interface water changes from liquid to gaseous phase. While evaporation some energy is carried by vapours so the temperature of water is less then the temperature of bottom.

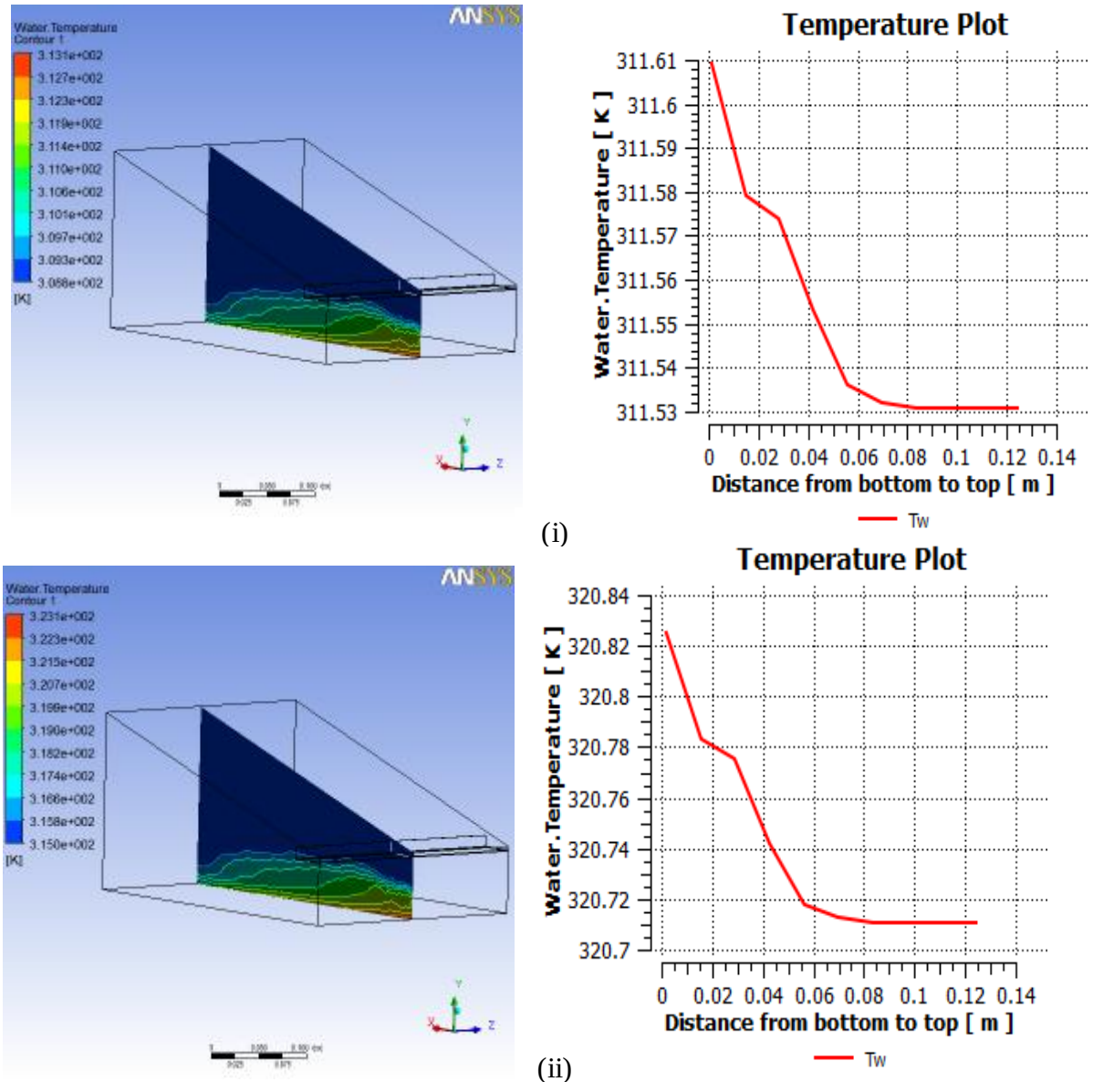

Fig. 4.17 Temperature Plot and Water temperature contours when bath temperature is (i) 40^0 and (ii) 50^0 C for 15^0 inclination.

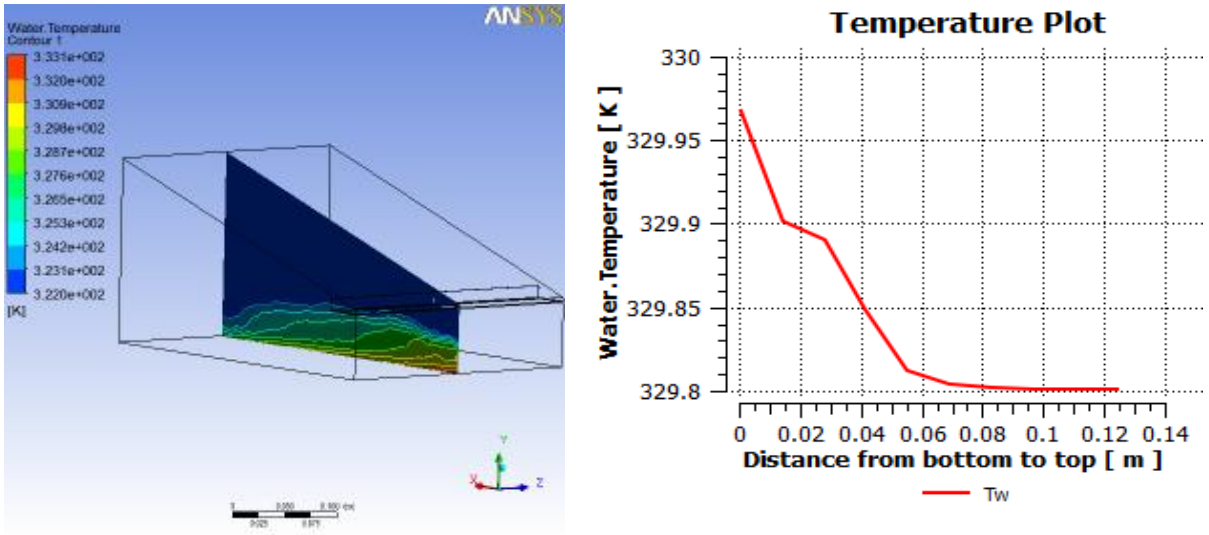

(i)

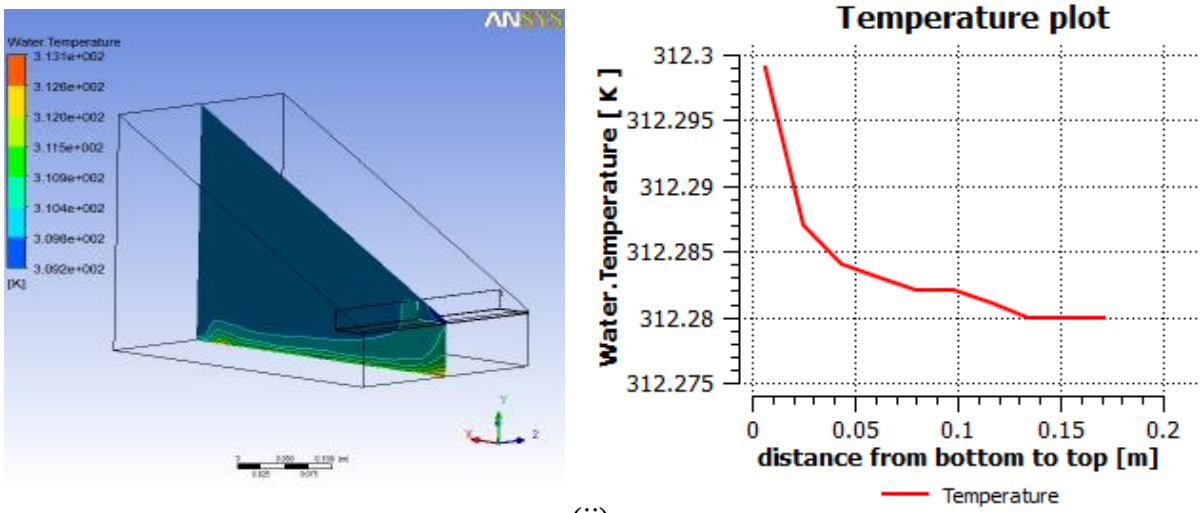

(ii)

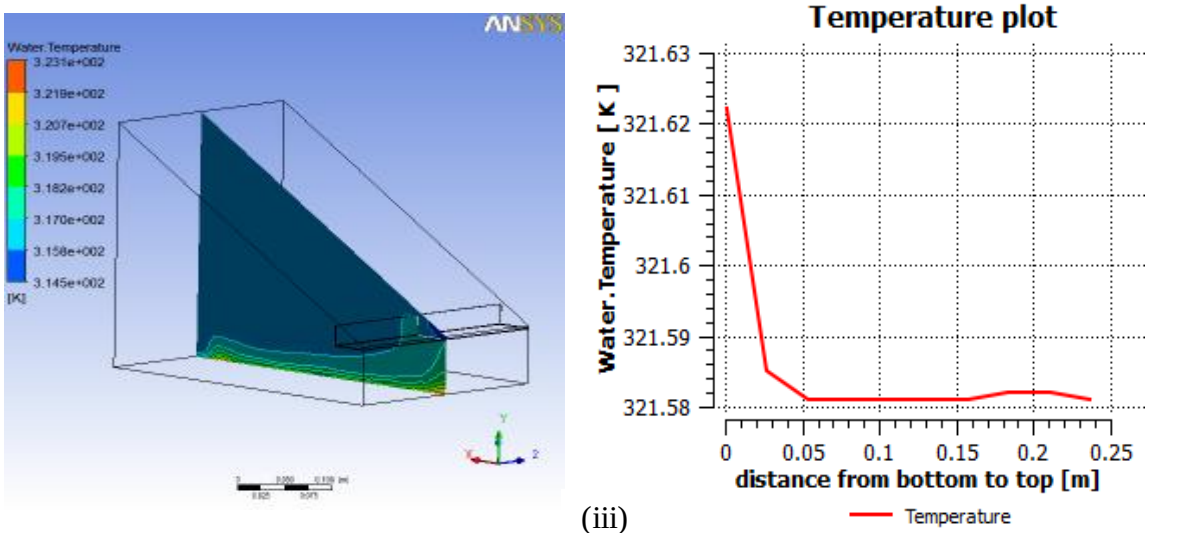

(iii)

Fig. 4.18 Temperature Plot and Water temperature contours when bath temperature is (i) 60^0 for 15^0 inclination (ii) 40^0 C and (iii) 50^0 C for 30^0 inclination.

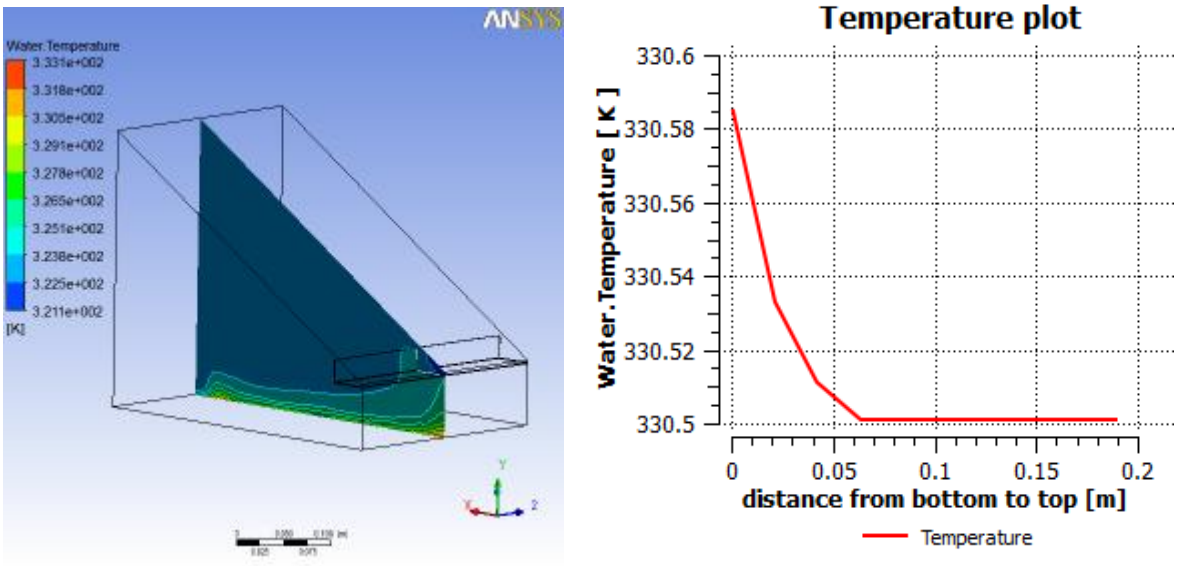

Fig. 4.19 Temperature Plot and Water temperature contour when bath temperature is 60^0 C for 30^0 inclination.

4.2 EXPERIMENTAL VALIDATION.

4.2.1 Water temperature

From the above results water temperature predicted by CFD simulation is compared with available experimental data of Kumar and Tiwari [7] for 15^0 and 30^0 inclination shown in figure 4.20. This Fig has been drawn with Water temperature as ordinate and Bath temperature as abscissa. Water temperature is in good agreement with experimental data. The average error of water temperature is 8% and 6 % respectively from 40^0 to 60^0 C with rise in bath temperature.

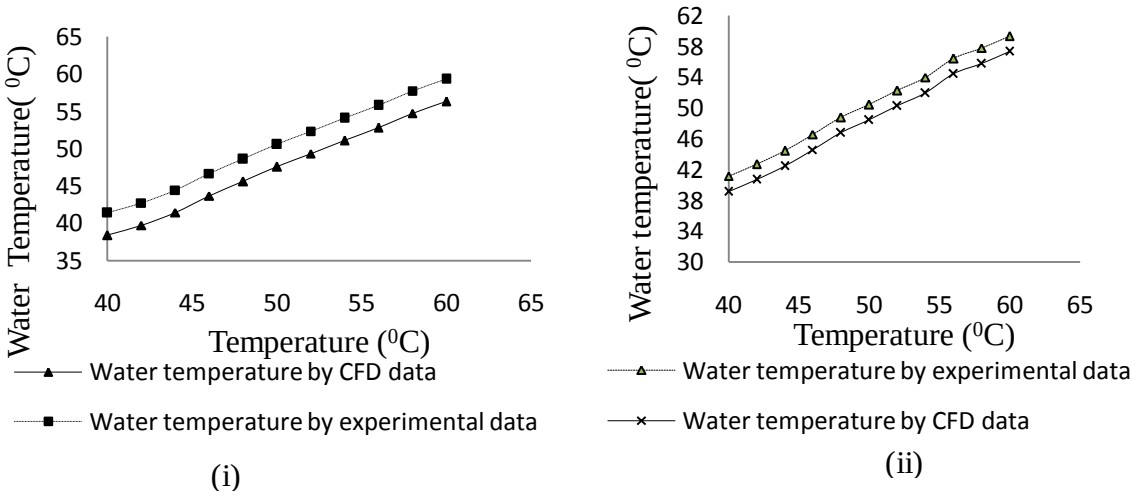

Fig 4.20: Water temperature predicted by the CFD simulation and experimental data for i) 15^0 inclination ii) 30^0 inclination

4.2.2 Production rate of water

When the salinated water is heated water gets evaporated and converted into water vapour which is condensed to obtain potable water in liquid state. ANSYS CFX gives the mass flow of gas and water in Kg/sec which is divided by evaporation area to obtain the amount of fresh water produced. It was assumed that the amount of water evaporated is equal to the rate of water production Kg/m^2 sec. In other words the amount of water evaporated is equal to the amount of water condensed. The same amount of water is collected in distillate channel. To represent the mass flow not all only two images of contours are taken as shown in fig 4.21 for 15^0 and $30^{0.}$.

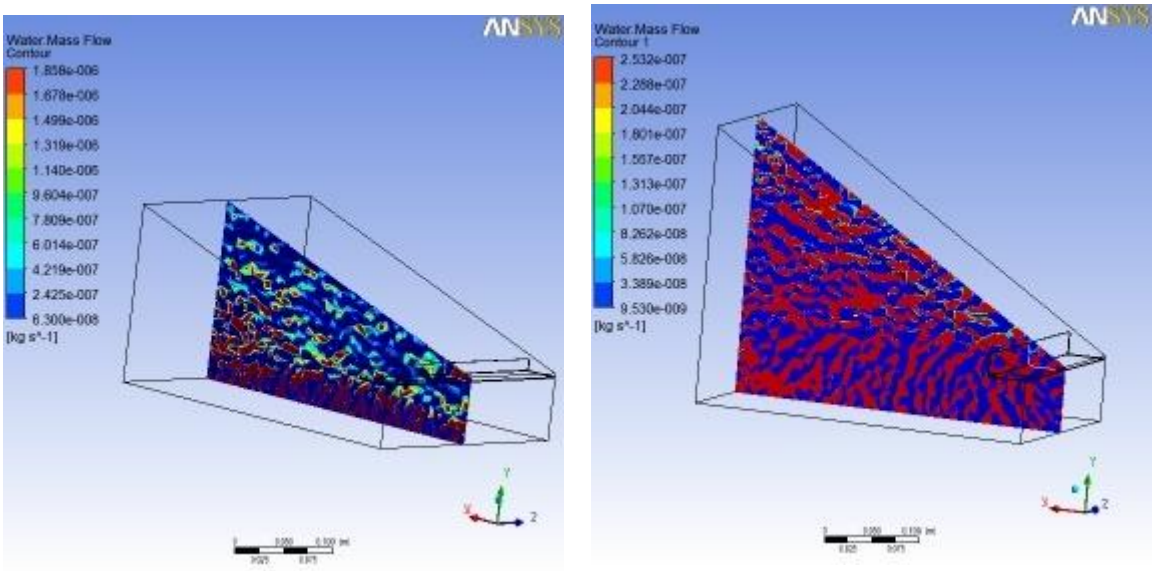

Fig 4.21: Water mass flow predicted by CFD simulation.

From the above contours the amount of fresh water produced is calculated. Figure 4.22 and 4.23 shows the results of simulation run and experimental data from 40^0 to 60^0 C with 2^0 C interval for both 15^0 and 30^0 inclination. In the figures 4.22 and 4.23 it is noted that as the process begins water in the basin is heated by supplying heat from the bottom. Water starts warming up. Gradually the still space saturates with vapour and fresh water production rate is maximum when the bath temperature is at 60^0C. It has been found that water production rate increases with increase in heat supplied. This is due to the fact that, at higher temperature evaporation rate is high. The amount of distillate output received will be higher for the higher temperature of evaporative surface and also for lower temperature of condensing surface. In other words, the higher value of evaporative surface temperature and lower value of condensing surface temperature, both leads to the rise in distillate output. A

little consideration reveals that both of this increase the temperature difference ΔT between evaporative and condensing surfaces . It plays an important role in optimizing the yield and so ultimately convective mass transfer coefficient as well. In the starting water production rate is low as the bath temperature is low. The average error for production rate is 11.8% for 15^0 slope and 7.6% for 30^0 slope.

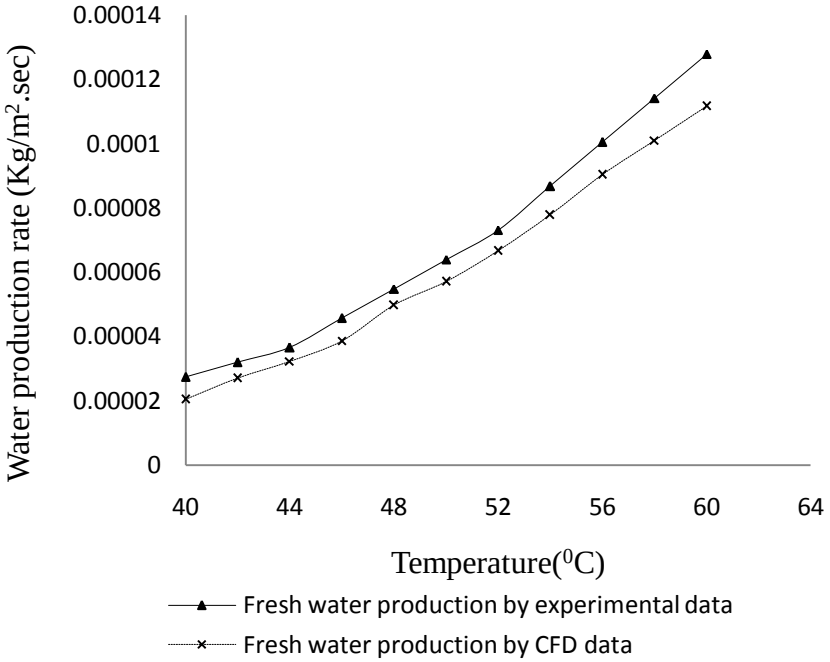

Fig 4.22: The rate of fresh water production from experimental data and simulation result for 15^0 inclination.

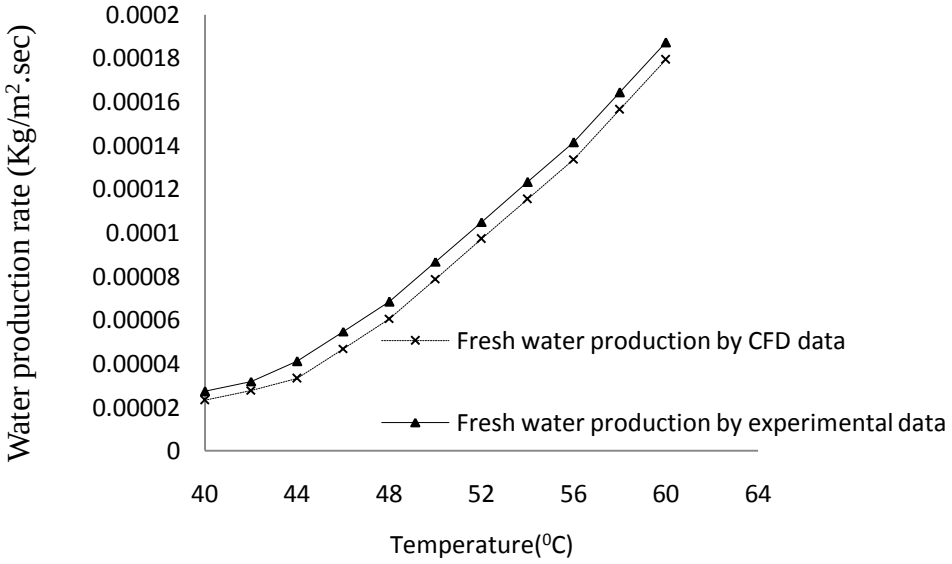

Fig 4.23: The rate of fresh water production from experimental data and simulation result for 30^0 inclination.

Figure 4.24 shows the condensed water droplets on the glass as the water heated. The water temperature is higher than glass cover temperature. Temperature difference between water vapour and glass leads to vapour condensation on the glass surface. For drop formation on condensing cover adhesion forces are taken into account. Droplets slip down and get collected in the trace as shown in figure 4.26.

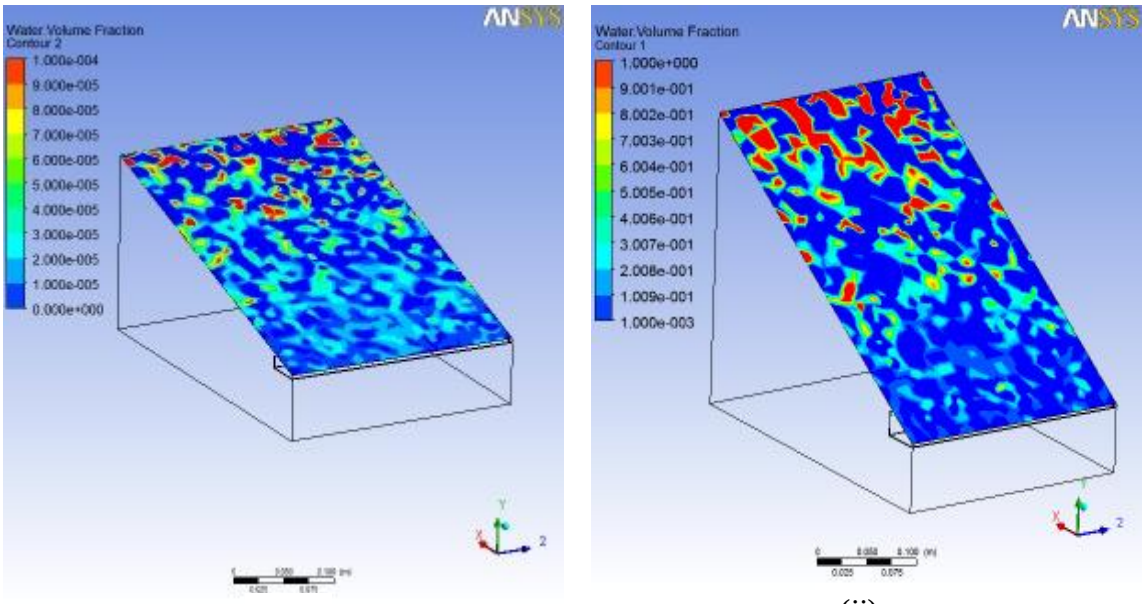

(i) (ii)

Fig 4.24: Water volume fraction on the glass for (i) 15^0 inclination and (ii) 30^0 inclination.

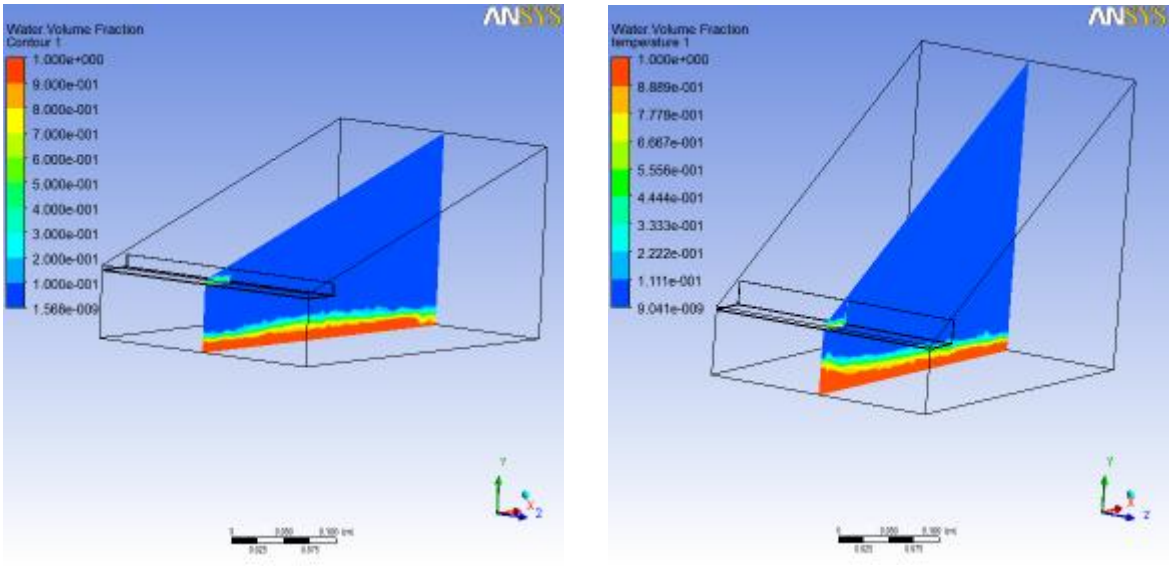

(i) (ii)

Fig 4.25: Water volume fraction contour from the side view for (i) 15^0 inclination and (ii) 30^0 inclination.

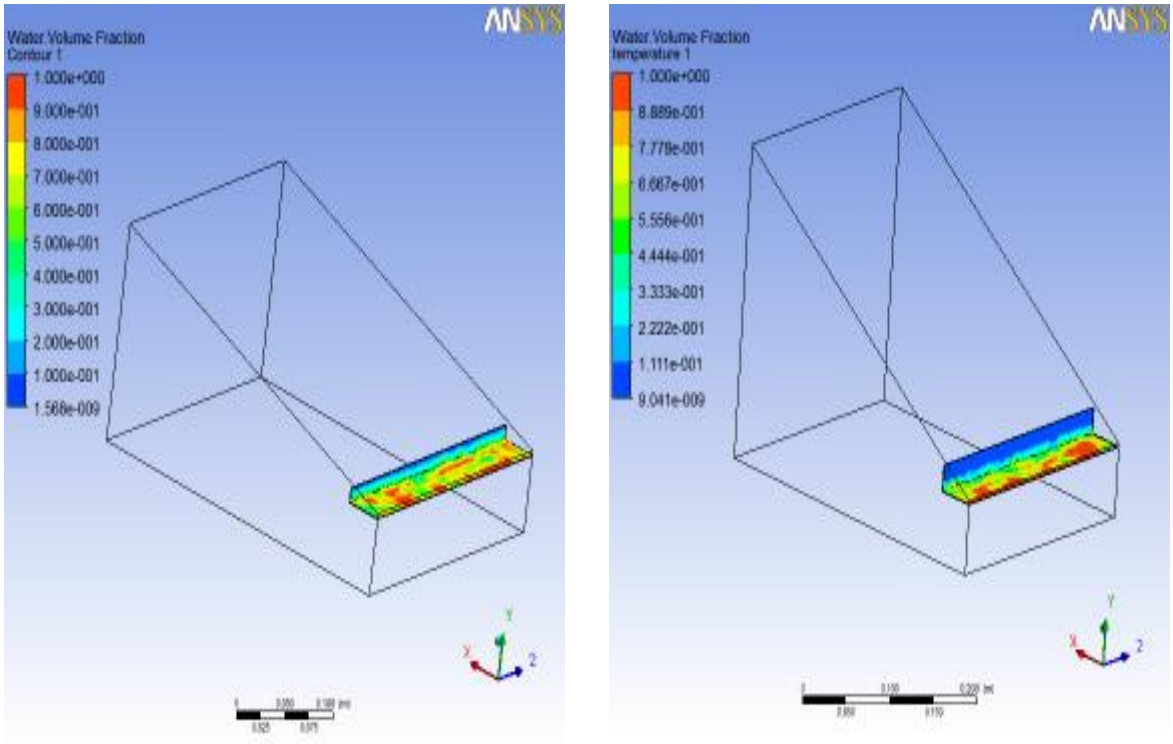

(i) (ii)

Fig 4.26: Water volume fraction contour on distillate collector for (i) 15^0 inclination and (ii) 30^0 inclination.

To show the water volume fraction a plane is inserted in the solar still. Figure 4.26 shows water volume fraction contours. It is obvious that gas and liquid phase are completely apart and their interface is distinct. As shown in Figs 4.24, 4.25 and 4.26 Liquid is seen only at the bottom, top and distillate collector.

As mentioned earlier, heat transfer is due to the buoyancy force. Gas phase moves on circular path lines between bottom and the glass. Warm water moves upward as their density decreases and the portion of vapour gets condensed on the top where it cools down and gets heavier. It forces the lighter warm vapour towards the glass and hence free convection heat transfer mechanism takes place as shown in Figs 4.27 and 4.28.

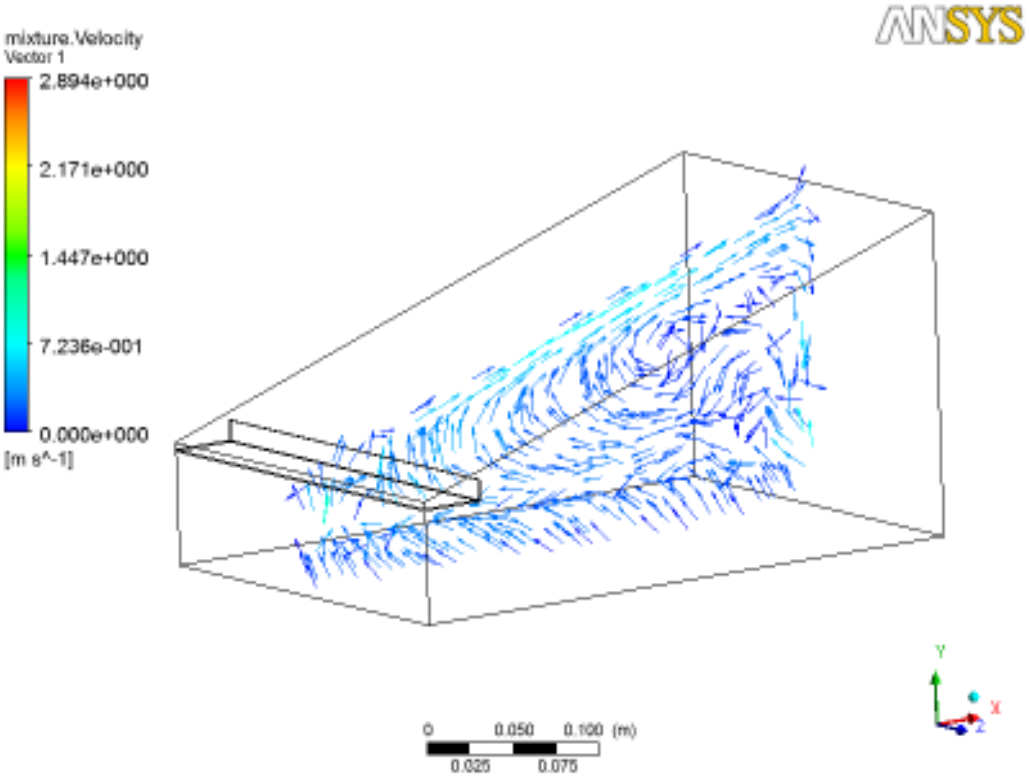

Fig 4.27: Gas mixture velocity on a plane inside the solar still for 15^0 inclination.

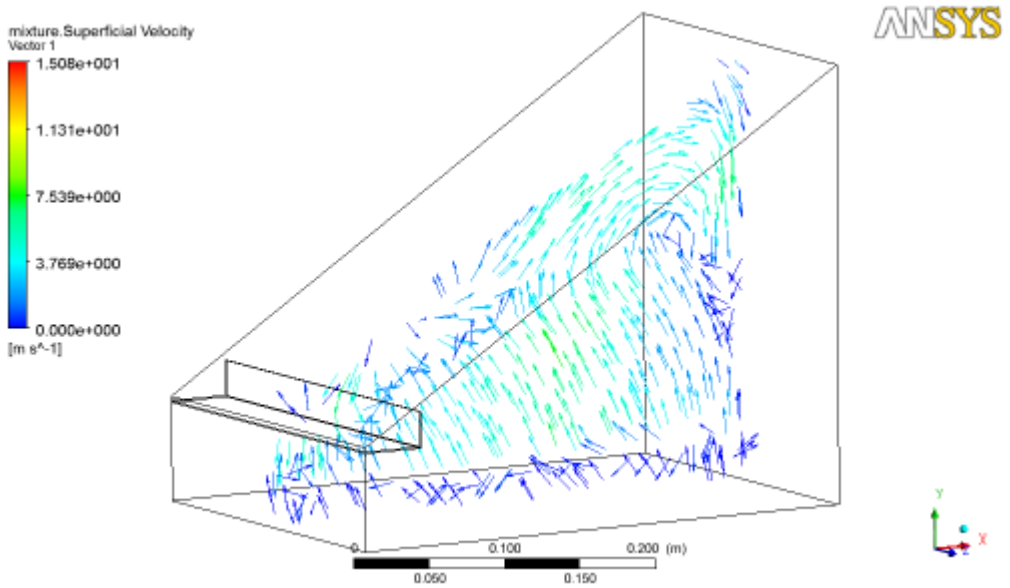

Fig 4.28: Gas mixture velocity on a plane inside the solar still for 30^0 inclination.

4.2.3 Heat transfer coefficient analysis

The equations given in Chapter 3 are used to find the convective and evaporative heat transfer coefficient. The gas phase above the liquid water is convected to the condensing

cover by the action of buoyancy force caused by density variation due to temperature difference between water surface and condensing cover temperature. This internal heat transfer process is free convection. Therefore vapour gets a circular motion in the solar still and heat transfer takes place as natural convection. Outside the solar still free or forced convection takes place depending upon the atmospheric condition.

The data from CFX is exported to excel files and equations from (3.9) to (3.22) explained in chapter 3 are solved to get the values C and n and ultimately hcw and hew. The constant C and n evaluated for CFD data of 15^0 inclination to be equal to 0.2058 and 0.2618 for experimental data of Kumar and Tiwari [7] these values would be 0.2071 and 0.2658 respectively for the temperature range of 40-60^0C. Similarly for the same temperature range the values of C and n for 30^0 inclination is 0.01 and 0.5. For experimental data of Kumar and Tiwari [7] the values are 0.01019 and 0.512.

4.2.3.1 Heat transfer coefficient for 15^0 inclination

Fig.4.30 has been drawn with convective heat transfer coefficient as ordinate and bath temperature as abscissa. From fig 4.29 it has been found that convective heat transfer coefficient rises from 2.015 to 2.532 and its percentage rise is 25.65% in the operating range of 40^0 to 60^0C. In the same temperature range the evaporative heat transfer coefficient rise is about 154.43% from 10.18 to 25.89 as shown in fig 4.30.

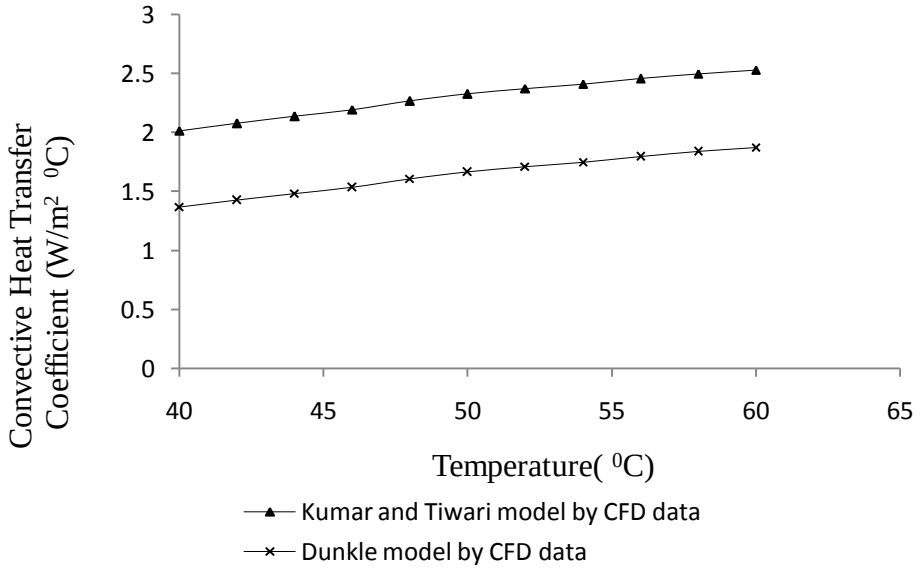

Fig 4.29: Variation of convective heat transfer coefficient (h_{cw}) within temperature range of 40-60^0C for 15^0slope of the condensing cover by using CFD data.

Figs. 4.29 and 4.30 are based on the values obtained by CFD data. By putting the Obtained values of C and n and temperature from CFD data in equations in chapter 3 it is observed that the values obtained by the Kumar and Tiwari model are very closer to the values obtained by Dunkle's model (DM) for both convective and evaporative heat transfer coefficients for water temperature range of 40-60°C, otherwise there is a significant difference between the results obtained by both models after 50^0C. The maximum deviation of 32% and 32.6% is observed for the values of hcw, and hew, respectively when the water temperature is found as low as 38°C, which is significantly lower than 50°C. Thus, the values obtained by the K &T are free from Dunkle's [13] shortcomings.

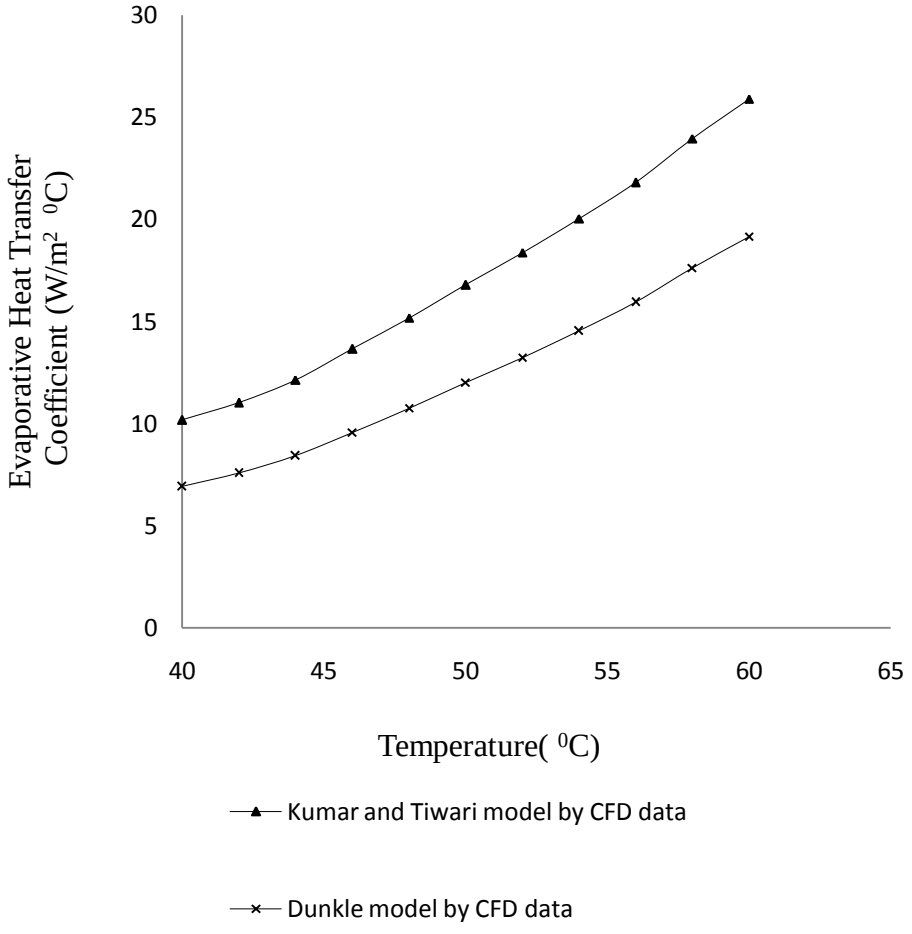

Fig 4.30: Variation of evaporative heat transfer coefficient (h_{ew}) within temperature range of 40-60^0C for 15^0slope of the condensing cover by using CFD data.

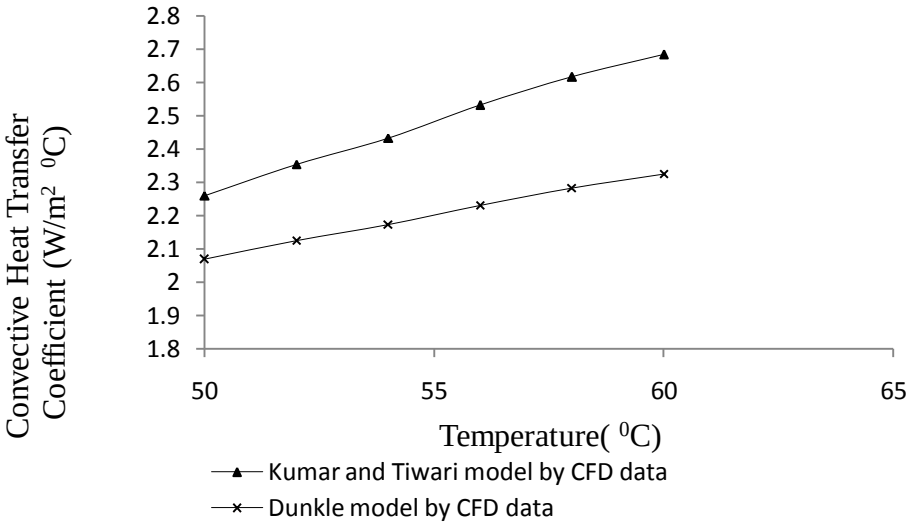

Fig. 4.31 Variation of convective heat transfer coefficient (h_{cw}) within temperature range of 50-60^{0}C for 15^0 slope of the condensing cover by using CFD data.

The convective heat transfer coefficient rise is reduced to 18.77% for temperature range of 50^0 to 60^0 C as shown in Fig 4.31. Similarly for the same temperature range the evaporative coefficient rise is reduced to 68% as shown in Fig 4.32. It is observed that if the span of the temperature range is reduced, the rise in the value of the convective and evaporative heat transfer coefficients are also reduced.

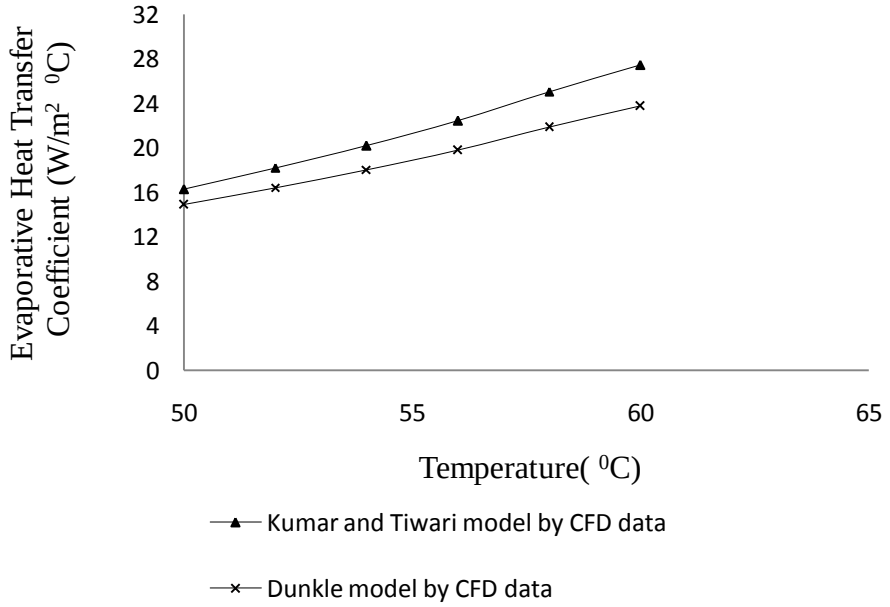

Fig. 4.32 Variation of evaporative heat transfer coefficient (h_{ew}) within temperature range of 50-60^{0}C for 15^{0}slope of the condensing cover.

4.2.3.2 Heat transfer coefficient for 30^0 inclination

From Fig 4.33 it is seen that convective heat transfer coefficient rises from 2.17 to 3.27 and its percentage rise is 50% in the operating range of 40^0 to 60^0 C. In the same temperature range the evaporative heat transfer coefficient rise is about 199% from 11.03 to 33.05 as shown in fig4.35. Again the Figs. 4.33 and 4.34 shows hcw and hew variation for small temperature range. It can be observed that the values obtained by the Kumar and Tiwari are very closer to the values obtained by Dunkle's model (DM) for both convective and evaporative heat transfer coefficients for water temperature range of 40-50°C, after 50^0C it starts deviating . The maximum deviation of 37.7% and 37.9% is observed for the values of hcw, and hew, respectively when the water temperature is found 60°C, which is significantly higher than 50°C. Thus, deviation is due to Dunkle's [13] shortcomings and assumptions at higher temperature.

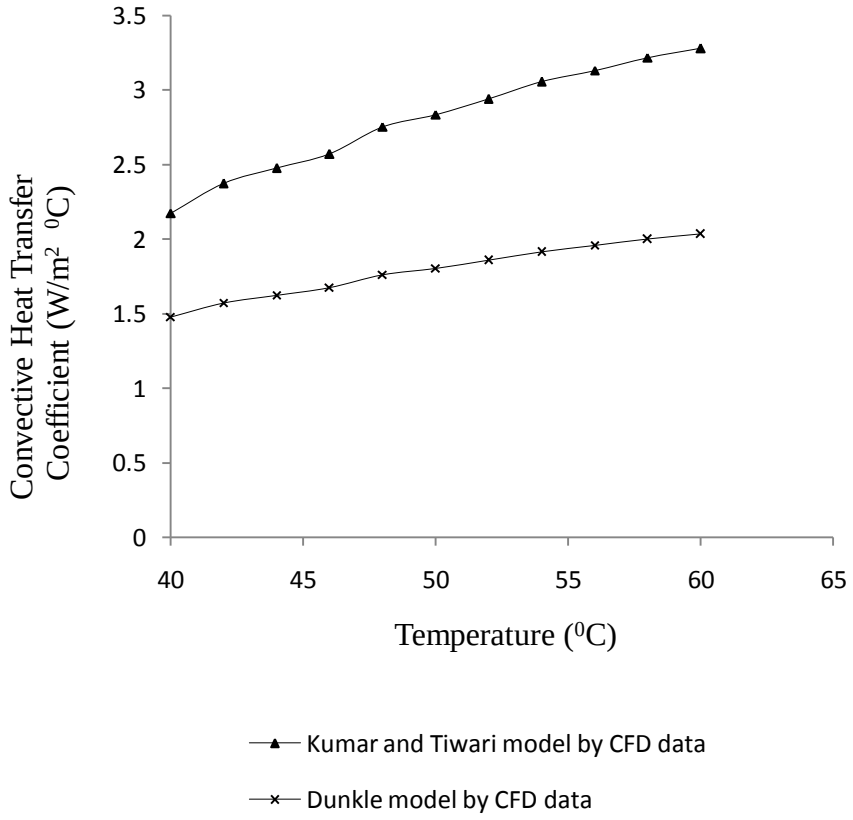

Fig 4.33 Variation of convective heat transfer coefficient (h_{cw}) within temperature range of 40^0- 60^0C for 30^0slope of the condensing cover.

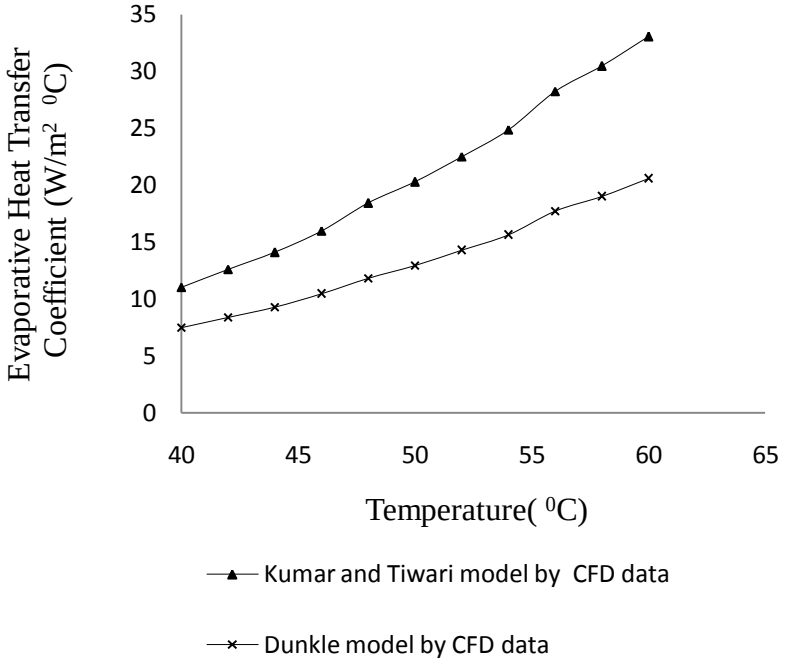

Fig. 4.34 Variation of evaporative heat transfer coefficient (h_{ew}) within temperature range of 40^0-60^0C for 30^0slope of the condensing cover.

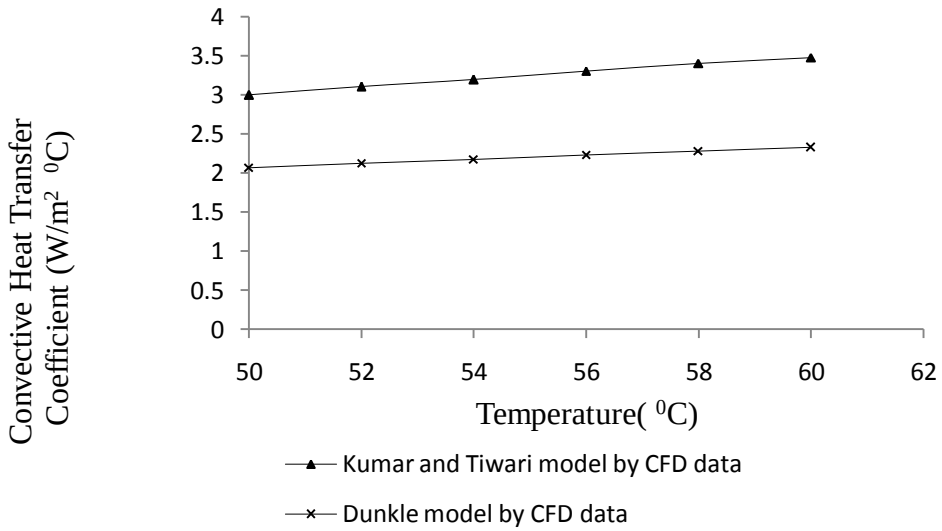

Fig. 4.35 Variation of convective heat transfer coefficient (h_{cw}) within temperature range of 50^0- 60^0C for 30^0slope of the condensing cover.

The convective heat transfer coefficient rise is reduced to 16% for temperature range of 50^0 to 60^0 C as shown in fig 4.35. Similarly for the same temperature range the evaporative coefficient rise is reduced to 64%.It is observed that if the span of the temperature range is

reduced, the rise in the value of the convective and evaporative heat transfer coefficients are also reduced as shown in fig 4.36.

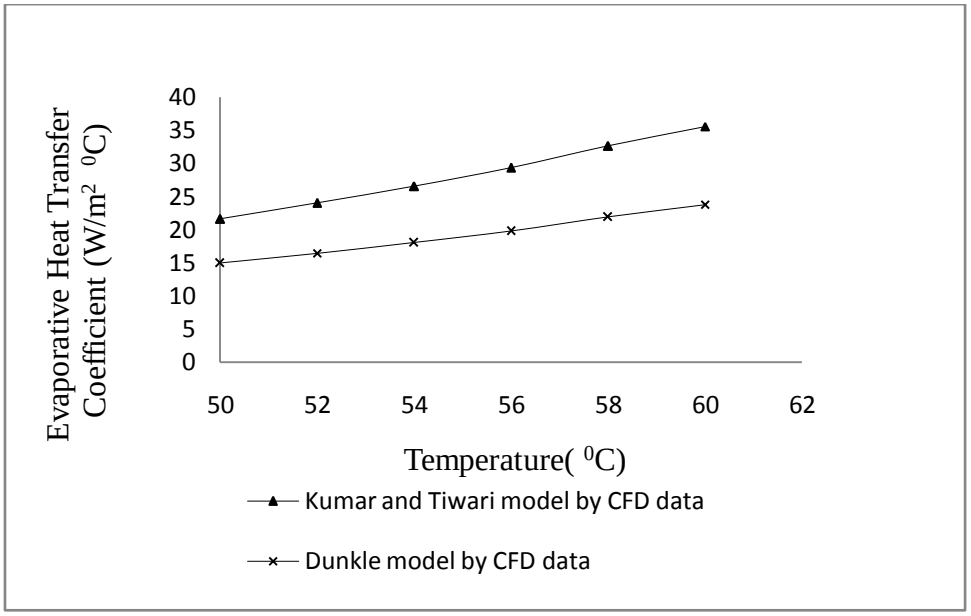

Fig. 4.36 Variation of evaporative heat transfer coefficient (h_{ew}) within temperature range of 50^0- 60^0C for 30^0slope of the condensing cover.

4.2.4 Comparison of experimental and simulation results for heat transfer coefficient.

Validation of the simulation results of heat transfer coefficient with the experimental one has been shown in Figure 4.37, 4.38, 4.39 and 4.40. Figure 4.37 compares the results for inclination of condensing cover at 15^0. From Figure 4.37 it is observed that experimental results of convective heat transfer coefficient nearly match with the heat transfer coefficient in simulation at all bath temperature from 40^0-60^0C. So the average error for convective heat transfer coefficient is 8%.

Figure 4.38 shows comparison of simulation and experimental results for evaporative heat transfer coefficient. From Figure 4.38 it is observed that the average error for evaporative heat transfer coefficient is 18.83%.

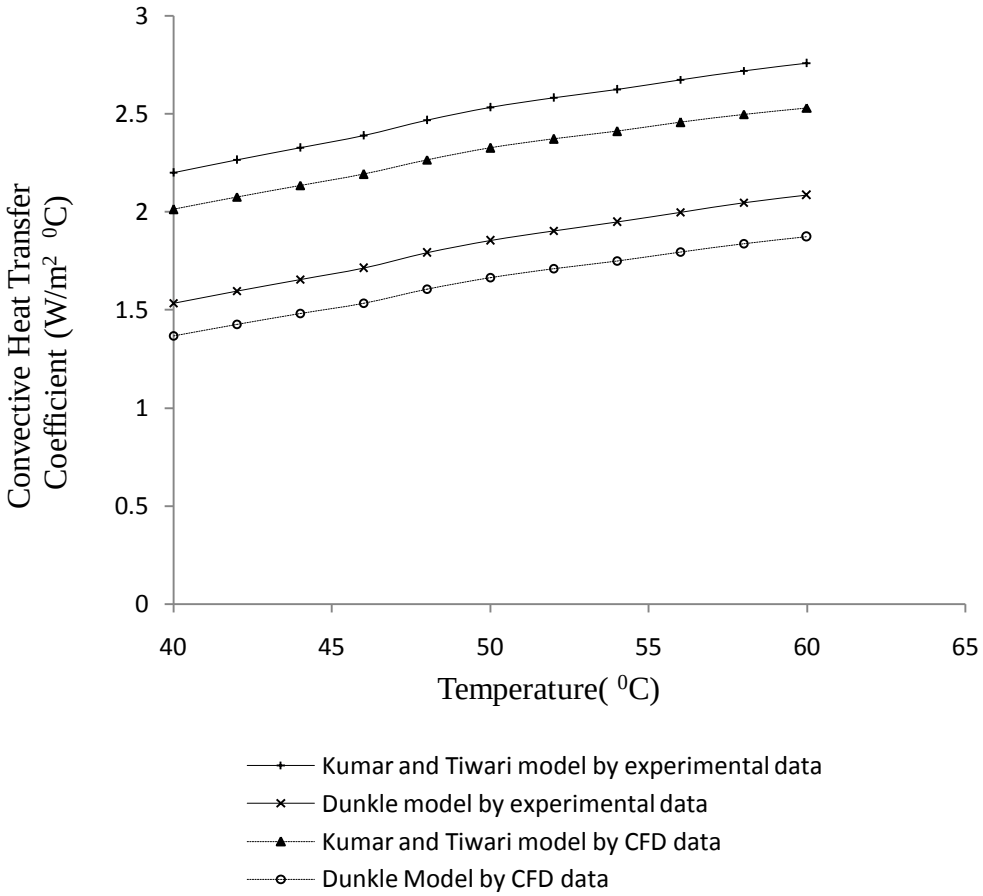

Fig. 4.37 Variation of convective heat transfer coefficient (h_{cw}) within temperature range of 40^0- 60^0C for 15^0slope of the condensing cover.

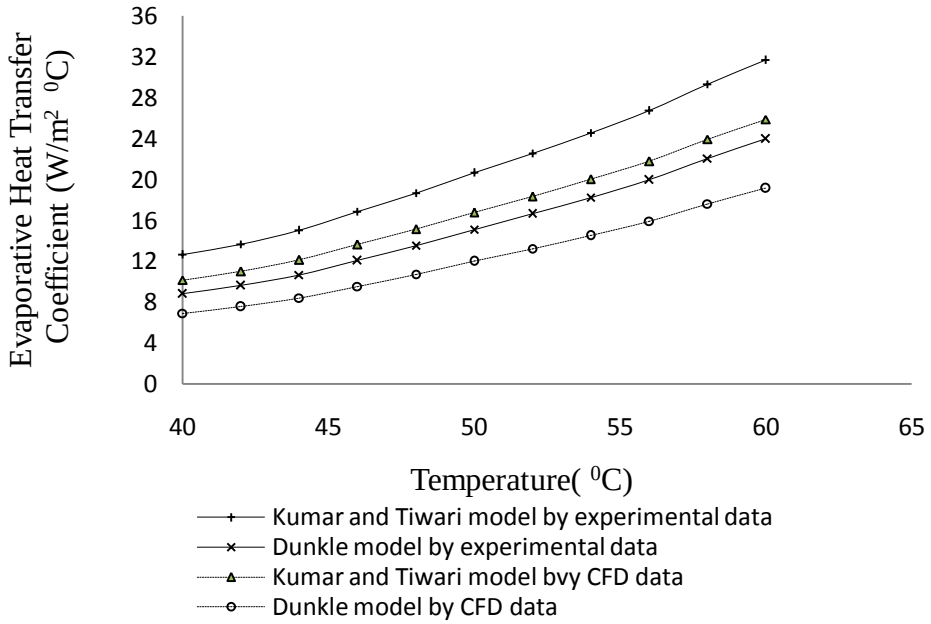

Fig. 4.38 Variation of evaporative heat transfer coefficient (h_{ew}) within temperature range of 40^0- 60^0C for 15^0 slope of the condensing cover.

Similarly as explained above from Figure 4.39 it is observed that experimental results of convective heat transfer coefficient nearly match with the heat transfer coefficient in simulation at all bath temperature from 40^0-60^0C. So the average error for convective heat transfer coefficient is 10.43%. CFD data obtained by both models underpredict as shown in figure 4.39 but the trend they are following is the same as that of experimental data.

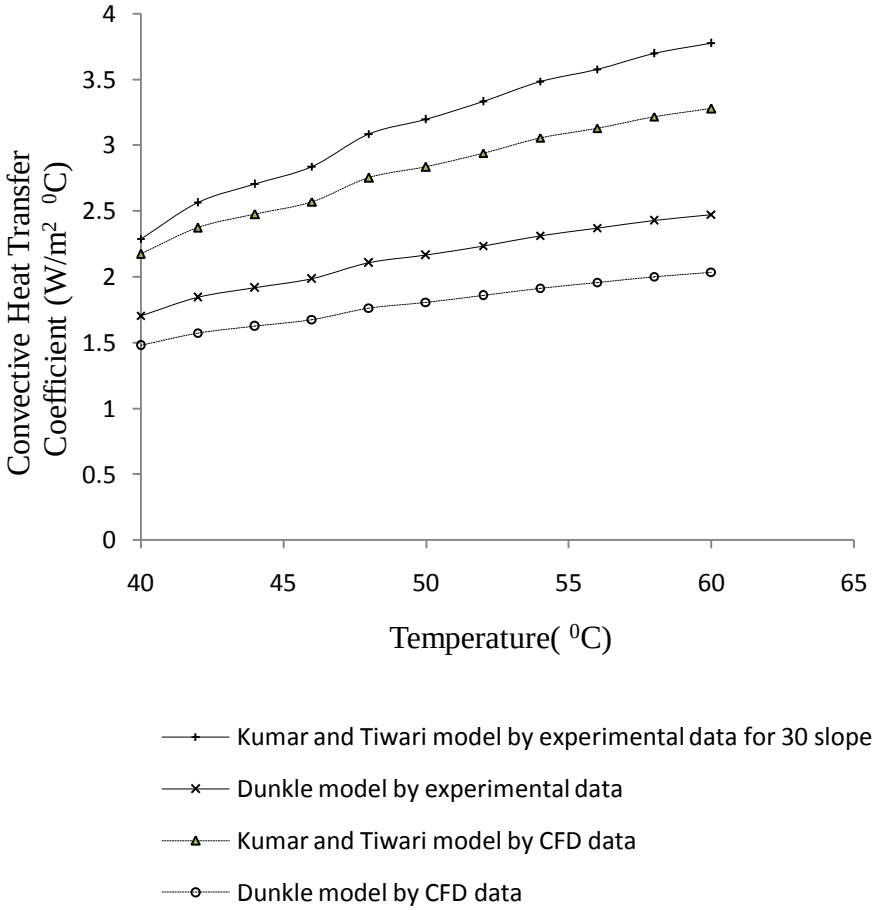

Fig. 4.39 Variation of evaporative heat transfer coefficient (h_{cw}) within temperature range of 40^0- 60^0C for 30^0 slope of the condensing cover.

Figure 4.40 shows comparison of simulation and experimental results for evaporative heat transfer coefficient. From Figure 4.40 it is observed that the average error for evaporative heat transfer coefficient is 20.63%. Data obtained by the simulation follow the same trend as of experimental data with certain error.

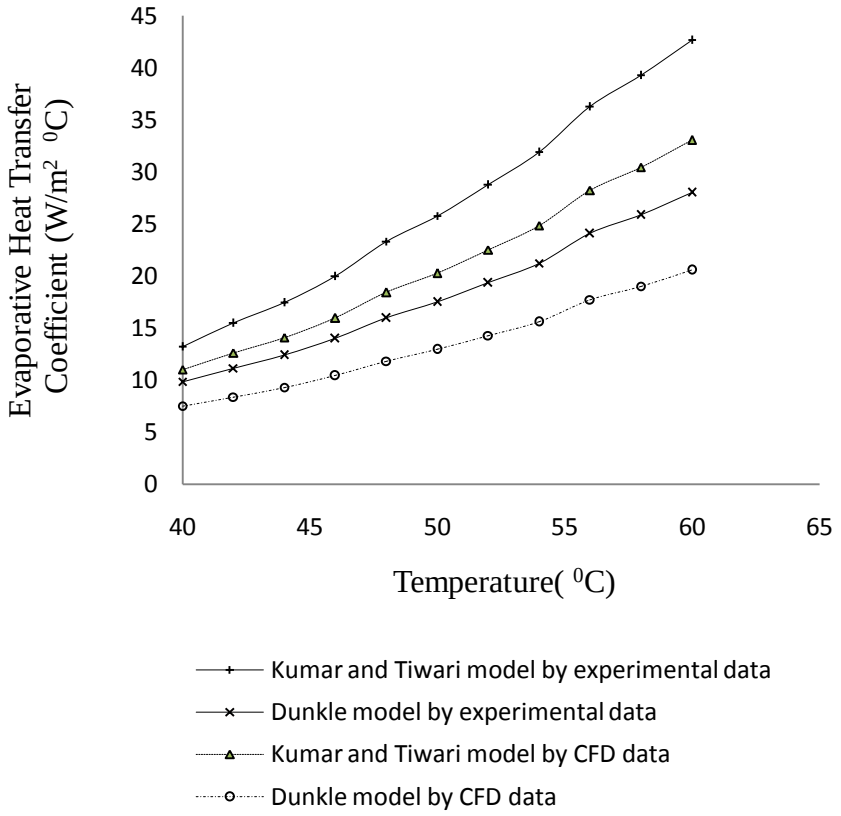

Fig. 4.40 Variation of evaporative heat transfer coefficient (h_{ew}) within temperature range of 40^0- 60^0C for 30^0 slope of the condensing cover.

Convective and evaporative heat transfer coefficients obtained from CFD simulation results and experimental data by using Kumar and Tiwari [7] and dunkle [13] model are shown in fig 4.37-4.40 it is obvious that the CFD prediction and experimental results are agreeable. The trend of variations in heat transfer coefficient is similar to Temperature variation as shown in fig 4.20 because both h_{cw} and h_{ew} are dependent to water and glass temperatures.

4.3 Optimization

From all simulation results it was observed that mass of fresh water produced and heat transfer coefficient all are in good agreement with experimental data. As simulation is done at two different inclinations now we have to observe which inclination gives more yield. Figure 4.41-4.44 shows that the values of convective and evaporative heat transfer coefficient by Dunkle model and Kumar and Tiwari model. The convective and evaporative heat transfer coefficient are higher for condensing cover at inclination 30^0 for temperature range of 40^0 to 60^0 C as compared to condensing cover at inclination 15^0.

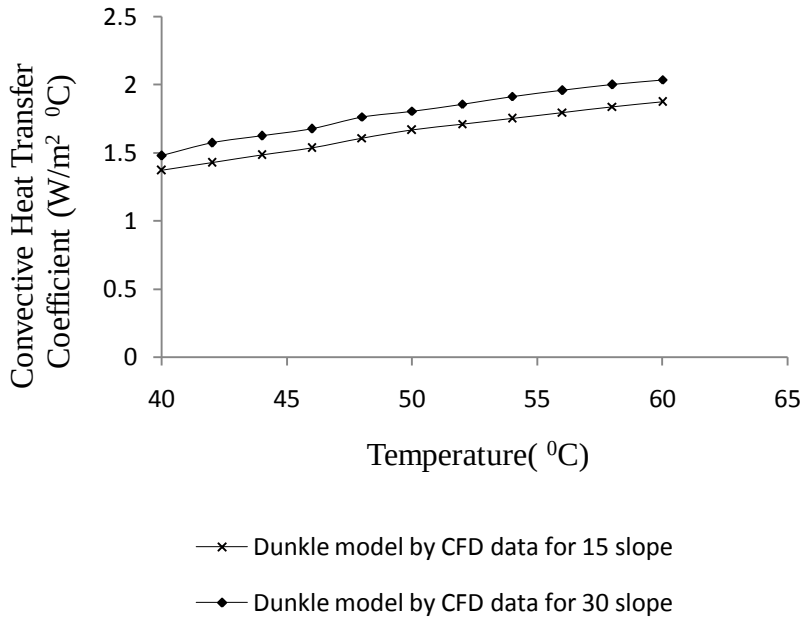

Fig. 4.41 Variation of convective heat transfer coefficient (h_{cw}) within temperature range of 40-60^{0}C for 15^{0}and 30^0 slope of the condensing cover by CFD data.

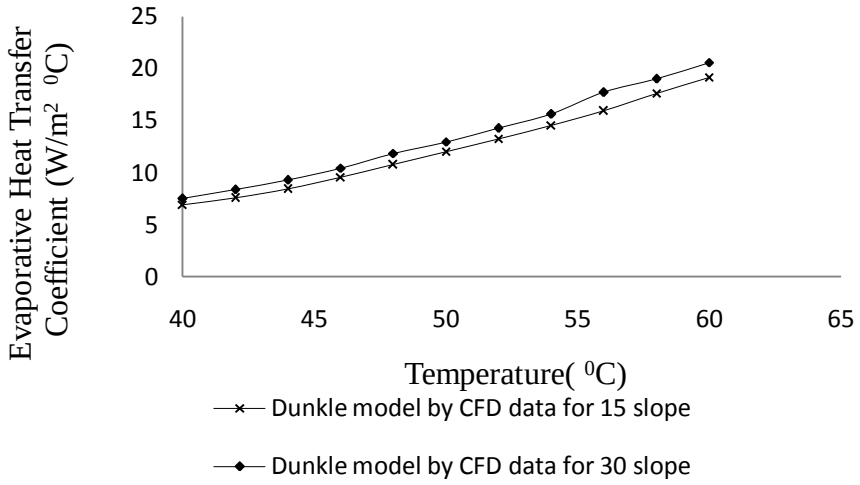

Fig. 4.42 Variation of evaporative heat transfer coefficient (h_{ew}) within temperature range of 40-60^{0}C for 15^0 and 30^0 slope of the condensing cover by CFD data.

Fig 4.41 and 4.42 shows the deviation between 15 and 30^0 inclination for convective and evaporative heat transfer coefficient by the CFD data result obtained are almost closer with little deviation.

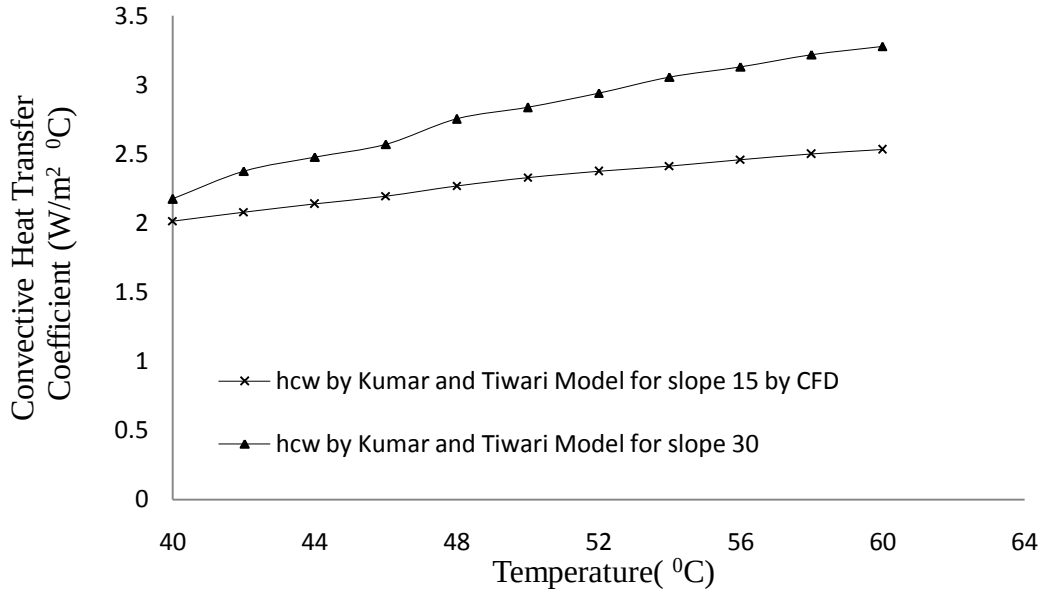

Fig. 4.43 Variation of convective heat transfer coefficient (h_{cw}) within temperature range of 40-60^{0}C for 15^0 and 30^0 slope of the condensing cover by CFD data.

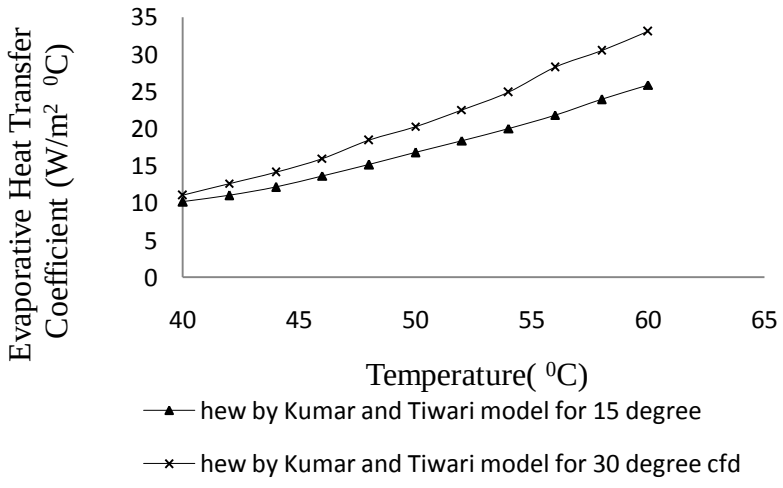

Fig. 4.44 Variation of evaporative heat transfer coefficient (h_{ew}) within temperature range of 40-60^{0}C for 15^0 and 30^0 slope of the condensing cover CFD data.

From Fig 4.43 and 4.44 it has been observed that there is some deviation between both convective and evaporative heat transfer coefficient and the deviation is about 17.91 and 18.3%. so it is observed that slope at 30 degree have high heat transfer in humid air then 15^0 inclination.

Similarly figure 4.45 shows the variation of distillate collected from 40^0 to 60^0 C for inclination 15^0 and 30^0. Yield is again highe for 30^0 inclination compared to 15^0 inclination. The average deviation is found 29.4%. Which is significant higher then 15^0 so it is concluded that at higher inclination the yield is high.

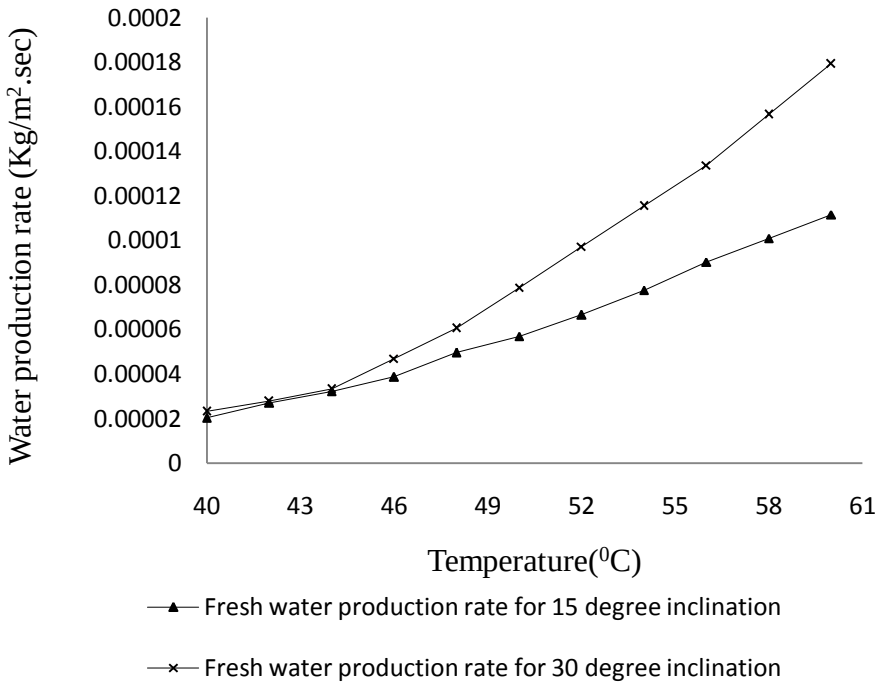

Fig 4.45 Fresh water production rate for different inclination for bath temperature from 40-60^0C by CFD data.

CHAPTER 5
CONCLUSION AND FUTURE SCOPE

5.1 FLOW OF WORK DONE

In present thesis work modeling of evaporation and condensation process is done for different inclination of condensing covers to optimize the mass yield and heat transfer coefficient to improve the performance of distillation unit under indoor conditions. Performance of solar still is evaluated by varying the temperature at the bottom of solar still from $40^0 – 60^0$ C at inclinations 15^0 and 30^0 .

First of all simulation work is done on ANSYS CFX. Simulation of evaporation process is done on a single slope solar still. Different sets of simulation are done by varying the temperature of top and bottom according to experimental data. The behavior of phase change and temperature distribution is observed due to evaporation. The temperature of water obtained by CFX and mass yield is compared with the available experimental data. Two inclination of condensing cover at 15^0 and 30^0 are taken for simulation. By plotting the curves of mass of water produced, convective and evaporative heat transfer coefficient it is optimized that which condensing cover gives best performance.

Based on the results of the present work, following conclusions are drawn:

1. Selecting best inclination

i) Two condensing covers at inclination 15^0 and 30^0 are investigated by plotting the curves, it is observed that condensing cover at 30^0 inclination gives higher yield as compared to condensing cover at 15^0 inclination. The condensing cover at 30^0 inclination gives about 29.4% higher yield than 15^0 inclination.

ii) Curves for convective and evaporative heat transfer coefficient are plotted. It is observed that condensing cover at inclination 30^0 obtain the high convective and evaporative heat transfer coefficient. By comparing the result of convective and evaporative heat transfer coefficient it has been found that the average rise is 17.91% and 18.3%. which is significantly high so it is concluded that at 30^0 inclination of condensing cover both yield and heat transfer is high.

2. Effect of the span of temperature range: It is concluded that if the temperature is reduced, rise in the value of convective and evaporative heat transfer are also reduced.

3. Effect of input parameter on yield: In the previous chapter it is shown that if the temperature at the bottom is increasing, the yield is also increased. So temperature applied at the bottom is the most significant factor.

4. Comparison of Dunkle model and Kumar and Tiwari model: Convective and evaporative heat transfer coefficients based on Dunkle's correlation and Kumar and Tiwari model are calculated. The results are obtained with accuracy upto 50^0 C. At higher operating temperature range the convective and evaporative heat transfer coefficient do not agree with Kumar and Tiwari model. There is large deviation from 50-60^0C. This is due to Dunkle's assumptions.

5. Experimental validation: To validate the simulation results of mass of fresh water produced and heat transfer coefficient from 40-60^0C and water temperature with available experimental data. It was observed that the results produced by CFD simulation are good in agreement with certain error.

5.2 FUTURE SCOPE

There were several improvements that could be implemented to improve the design and performance but was not possible to do so during the course of the project due to time restrictions. These suggestions are recommended for any future work to be conducted on the solar still for desalination purposes:

1. The CFD analysis of the multiphase water evaporation process could be improved by simulating a buoyant flow due to radiation falling on the condensing cover rather than heat supplied from the bottom. This could be done by applying radiation on the condensing cover.
2. Computer simulation can be used for simulating evaporation process through new solar still designs. Designs of solar still can be improved further by changing different cross-sections like rectangular or cylindrical or by changing the shapes of condensing cover.
3. A CFD analysis should be conducted on the condensation process by considering separate condenser.

REFERENCES

[1] T Mezhar, H Fath, Z Abbas, & A Khaled (2011) Techno-economis assessment and environmental impacts of desalination technologies. Desalination, vol. 266, p.263-276

[2] A Mills (1999) Heat Transfer, Prentice Hall, New Jersey.

[3] M Telkes (1956) Research on methods for Solar Distillation. US Office of Saline water, Washington, DC, Res. Dev. Prog., Rep. No.13, PB 161388.

[4] HS Aybar (2007) A review of desalination by solar still. Solar Desalination, pp. 207-214.

[5] MT Chaibi and AM El-Nashar (2009) A Review of Solar Thermal Energy Technologies for Water Desalination. Seawater Desalination (131-163)

[6] R Winston (1974) Solar concentrators of novel design. Solar Energy 16, 89–95.

[7] AK Tiwari, GN Tiwari (2005) Effect of the condensing cover's slope on internal heat and mass transfer in distillation: an indoor simulation. Desalination 180 (73-88)

[8] VJ Madhav (2011), Performance of Black Granite Basin Solar Still: A Comparative Study. Int J Engg Techsci Vol 2(2), 161-168.

[9] S Kumar and GN Tiwari (1996) Estimation of convective mass transfer in solar distillation system, Solar Energy 57, 459-464.

[10] AK Tiwari, GN Tiwari (2006) Effect of water depths on heat and mass transfer in a passive solar still: in summer climatic condition. Desalination 195, 78-94.

[11] MSK Tarawneh (2007) Effect of water depth on the performance evaluation of solar still. JJMIE Volume 1, number1, p. 23-29.

[12] O Badran and M Khader (2007) Evaluating thermal performance of a single slope solar still. Heat mass transfer 43, 985-995.

[13] RV Dunkle (1961) Solar water distillation, the roof type still and a multiple effect diffusion still, International Developments in Heat Transfer, ASME, Proc. International Heat Transfer, Part V, University of Colorado, p. 895.

[14] N Setoodeh, R Rahimi, A Ameri (2011) Modeling and determination of heat transfer coefficient in a basin solar still using CFD. Desalination 268 (103-110).

[15] AJ Khalifa, AM Hamood (2009), Performance correlations for basin type solar stills, Desalination 249, 24–28

[16] S Abdallaha, M Khaderb, O Badran (2009), Effect of various absorbing materials on the thermal performance of solar stills. Desalination 242, 128–137

[17] V Belessiotis, K Voropoulos, E Delyarmis (1995), Experimental and theoretical method for the determination of the daily output of a solar still: input-output method. Desalination 100, 99-104

[18] AA El-Sebaii, AA Al-Ghamdi, FS Al-Hazmi, AS Faidah (2009), Thermal performance of a single basin solar still with PCM as a storage medium. Applied Energy 86, 1187-1195.

[19] H Tanaka, Y Nakatake (2007), Improvement of the tilted wick solar still by using a flat plate reflector, Desalination 216, 139–146.

[20] B Chaouchi, A Zrelli, S Gabsi (2007), Desalination of brackish water by means of a parabolic solar concentrator Desalination 217, 118–126.

[21] O Badran, HA Al-Tahaineh (2005), The effect of coupling a flat-plate collector on the solar still Productivity Desalination 183, 137–142

[22] K Sampathkumar, T Arjunan, P Pitchandi, P Senthilkumar (2010), Active solar distillation – A detailed review. 14, 1503–1526.

[23] R Dev, GN Tiwari (2011), Characteristic equation of the inverted absorber solar still. Desalination 269, 67-77.

[24] FP Incropera, D Witt, DP Bergman, and AS Lavine (2007), Fundamentals of heat and mass transfer. 6th edition. New Jersey: John Wiley and Sons.

[25] CFX User Manual, ANSYS, Inc. Modeling, CFX 13.0: Solver.

[26] PT Tsilingiris (2009) Analysis of the heat and mass transfer processes in solar stills. Solar Energy, 83, p 420-431.